NUREG/CR-6787
ANL-01/25

Mechanism and Estimation of Fatigue Crack Initiation in Austenitic Stainless Steels in LWR Environments

Argonne National Laboratory

U.S. Nuclear Regulatory Commission
Office of Nuclear Regulatory Research
Washington, DC 20555-0001

NUREG/CR-6787
ANL-01/25

Mechanism and Estimation of Fatigue Crack Initiation in Austenitic Stainless Steels in LWR Environments

Manuscript Completed: September 2001
Date Published: August 2002

Prepared by
O. K. Chopra

Argonne National Laboratory
9700 South Cass Avenue
Argonne, IL 60439

J. Muscara, NRC Project Manager

Prepared for
Division of Engineering Technology
Office of Nuclear Regulatory Research
U.S. Nuclear Regulatory Commission
Washington, DC 20555-0001
NRC Job Code Y6388

UNITED STATES
NUCLEAR REGULATORY COMMISSION
Washington, D.C. 20555-0001

ERRATA

May 24, 2005

Report Number: NUREG/CR-6787, ANL–01/25

Report Title: Mechanism and Estimation of Fatigue Crack Initiation in Austenitic Stainless Steels in LWR Environments

Prepared by: Division of Engineering Technology
Office of Nuclear Regulatory Research
U.S. Nuclear Regulatory Commission
Washington, DC 20555-0001

Date Published: August 2002

Instructions: Please replace the following four equations of the report:

On page 37 Eqs. 18 & 19

$$\ln(N) = 5.675 - 2.030 \ln(\varepsilon_a - 0.126) + T' \dot{\varepsilon}' O' \quad (18)$$

$$\ln(N) = 7.122 - 1.671 \ln(\varepsilon_a - 0.126) + T' \dot{\varepsilon}' O', \quad (19)$$

On page 38 Eq. 22

$$O' = 0.281 \qquad \text{(all DO levels).} \quad (22)$$

On page 45 Eq. 36

$$\ln(F_{en}) = 1.028 - T' \dot{\varepsilon}' O', \quad (36)$$

KVIL
JN 21'05
MD

Publishing Services Branch
Office of Information Services

Mechanism and Estimation of Fatigue Crack Initiation in Austenitic Stainless Steels in LWR Environments

by

O. K. Chopra

Abstract

The ASME Boiler and Pressure Vessel Code provides rules for the construction of nuclear power plant components. Figures I–9.1 through I–9.6 of Appendix I to Section III of the Code specify fatigue design curves for structural materials. However, the effects of light water reactor (LWR) coolant environments are not explicitly addressed by the Code design curves. Existing fatigue strain–vs.–life (ε–N) data illustrate potentially significant effects of LWR coolant environments on the fatigue resistance of pressure vessel and piping steels. This report provides an overview of fatigue crack initiation in austenitic stainless steels in LWR coolant environments. The existing fatigue ε–N data have been evaluated to establish the effects of key material, loading, and environmental parameters (such as steel type, strain range, strain rate, temperature, dissolved–oxygen level in water, and flow rate) on the fatigue lives of these steels. Statistical models are presented for estimating the fatigue ε–N curves for austenitic stainless steels as a function of the material, loading, and environmental parameters. Two methods for incorporating environmental effects into the ASME Code fatigue evaluations are presented. The influence of reactor environments on the mechanism of fatigue crack initiation in these steels is also discussed.

Contents

Abstract iii

Executive Summary xi

Acknowledgments xv

1 Introduction 1

2 Overview of Fatigue ε–N Data 5

2.1 Air Environment 5

2.1.1 Fatigue Life 5

2.1.2 Cyclic Hardening Behavior 7

2.2 LWR Environments 9

2.2.1 Strain Amplitude 9

2.2.2 Hold–Time Effects 10

2.2.3 Strain Rate 11

2.2.4 Dissolved Oxygen 11

2.2.5 Temperature 13

2.2.6 Sensitization Annealing 15

2.2.7 Flow Rate 16

2.2.8 Cast Stainless Steels 16

3 Mechanism of Fatigue Crack Initiation 19

3.1 Formation of Engineering–Size Cracks 19

3.2 Growth of Small Cracks in LWR Environments 20

3.3 Fracture Morphology 25

3.4 Surface Oxide Film 29

3.5 Exploratory Fatigue Tests 31

4 Operating Experience in the Nuclear Power Industry 33

5 Statistical Model 35

5.1 Least–Squares Fit 35

5.2 The ANL Statistical Model 35
5.2.1 Air Environment 35
5.2.2 LWR Environments 36
5.3 Japanese MITI Guidelines 38
5.4 Model Developed by the Bettis Laboratory 38
5.5 Comparison of Various Estimation Schemes 40
6 Incorporating Environmental Effects into Fatigue Evaluations 43
6.1 Fatigue Design Curves 43
6.2 Fatigue Life Correction Factor 45
7 Conservatism in Fatigue Design Curves 47
8 Summary 53
References 55

Figures

1. Fatigue ε–N data for carbon steels and austenitic stainless steels in water 2

2. Fatigue ε–N behavior for Types 304, 316, and 316NG austenitic stainless steels in air at various temperatures 6

3. Influence of specimen geometry on fatigue life of Types 304 and 316 stainless steel 6

4. Influence of temperature on fatigue life of Types 304 and 316 stainless steel in air 7

5. Effect of strain range and strain rate on cyclic–hardening of Type 316NG stainless steel in air at room temperature and 288°C 8

6. Effect of strain range and strain rate on cyclic hardening of Type 304 stainless steel in air at 288°C 8

7. Results of strain rate change tests on Type 316 SS in low–DO water at 325°C 10

8. Fatigue life of Type 304 stainless steel tested in high–DO water at 260–288°C with trapezoidal or triangular waveform but with comparable tensile strain rates... 11

9. Dependence of fatigue lives of austenitic stainless steels on strain rate in low– and high–DO water 11

10. Dependence of fatigue life of Types 304 and 316NG stainless steel on strain rate in high– and low–DO water at 288°C 12

11. Effects of conductivity of water and soaking period on fatigue lives of Type 304 SS in high–DO water 13

12. Change in fatigue lives of austenitic stainless steels in low–DO water with temperature..... 14

13. Waveforms for change in temperature during exploratory fatigue tests 14

14. Fatigue life of Type 316 stainless steel under constant and varying test temperature..... 15

15. Effect of sensitization annealing on fatigue life of Types 304 and 316 stainless steel in low–DO water at 325°C 15

16. Effect of sensitization anneal on the fatigue lives of Types 304 and 316NG stainless steel in high–DO water 16

17. Fatigue strain amplitude–vs.–life data for CF–8M cast SSs in air..... 17

18. Effect of strain rate on cyclic–hardening behavior of wrought and cast SSs in air at 288°C 17

19. Fatigue strain amplitude–vs.–life data for CF–8M cast SSs in water 18

20. Dependence of fatigue lives of CF–8M cast SSs on strain rate in low–DO water at various strain amplitudes 18

21. Schematic illustration of growth of short cracks in smooth specimens as a function of fatigue life fraction and crack velocity as a function of crack length 19

22. Schematic illustration of film rupture/slip dissolution process 21

23. Depth of largest crack plotted as a function of fatigue cycles for austenitic stainless steels in air and water 21

24. Crack growth rates plotted as a function of crack length for austenitic stainless steels in air and water environments 22

25. Corrosion fatigue data for Type 316NG and sensitized Type 304 SS in high–DO water at 289°C 23

26. Crack growth rate data for Type 304 SS determined from fatigue ε–N tests in PWR and high–DO water at 289°C 24

27. Photomicrographs of fatigue cracks on gauge surfaces and along longitudinal sections of Type 304 stainless steel tested in air, high–DO water, and low–DO simulated PWR environment at 288°C, ≈0.75% strain range, and 0.004%/s strain rate 26

28. Photomicrographs of surface cracks along longitudinal sections of Type 316NG stainless steel at 288°C, ≈0.75% strain range, and two strain rates in air, high–DO water, and low–DO simulated PWR environment 27

29. Photomicrographs of fracture surfaces of Types 304 and 316NG SS specimens tested at 288°C, ≈0.75% strain range, and 0.004%/s strain rate in air, high–DO water, and low–DO simulated PWR water 28

30. Photomicrographs of gauge surfaces of Type 316NG SS specimens tested in air, simulated PWR water, and high–DO water 29

31. Higher–magnification photomicrographs of oxide films that formed on Type 316NG stainless steel in simulated PWR water and high–DO water 30

32. Schematic of the corrosion oxide film formed on austenitic stainless steels in LWR environments 30

33. Effects of environment on formation of fatigue cracks in Type 316NG SS in air and low–DO water environments at 288°C 31

34. Experimental and predicted ε–N behavior for Type 304 SS in low–DO water at 289°C and 0.4 and 0.004%/s strain rate 40

35. Experimental and predicted ε–N behavior for Type 316NG SS at 289°C in high–DO water and 0.4%/s strain rate and low–DO water and 0.005%/s strain rate 40

36. Experimental and predicted ε–N behavior for Types 304 and 316 SS in low–DO water at 325°C and 0.4, 0.01, and 0.001%/s strain rate 41

37. Experimental and predicted change in the fatigue lives of Type 304 SS with temperature in low–DO water at 0.3 and 0.6% strain amplitudes and 0.4 and 0.01%/s strain rates 42

38. Experimental and predicted change in the fatigue lives of austenitic SS with strain rate in low–DO water at 325°C 42

39. Fatigue design curves developed from statistical model for austenitic stainless steels in air at room temperature 44

40. Fatigue design curves developed from statistical models for austenitic stainless steels in water with <0.05 ppm DO at 250°C, 289°C, and 325°C 44

41. Experimental data adjusted for environmental effects and best–fit fatigue ε–N curve in room–temperature air for austenitic stainless steels 46

42. Fatigue data for carbon and low–alloy steel vessels tested in room–temperature water 48

43. Surface roughness profile of the fatigue test specimen 50

44. Effect of surface roughness on fatigue life of Type 304 stainless steel in air and low–DO water at 289°C 51

Tables

1. Fatigue test results for Type 304 austenitic SS at 288°C..... 13

2. Fatigue test results for Type 316NG austenitic stainless steel at 288°C and ≈0.5% strain range..... 31

3. Factors on cycles and strain to be applied to mean ε–N curve..... 52

Executive Summary

Section III, Subsection NB, of the ASME Boiler and Pressure Vessel Code contains rules for the design of Class 1 components of nuclear power plants. Figures I–9.1 through I–9.6 of Appendix I to Section III specify the Code design fatigue curves for applicable structural materials. However, Section III, Subsection NB–3121, of the Code states that effects of the coolant environment on fatigue resistance of a material were not intended to be addressed in these design curves. Therefore, the effects of environment on fatigue resistance of materials used in operating pressurized water reactor (PWR) and boiling water reactor (BWR) plants, whose primary–coolant pressure boundary components were designed in accordance with the Code, are uncertain.

The current Section–III design fatigue curves of the ASME Code were based primarily on strain–controlled fatigue tests of small polished specimens at room temperature in air. Best–fit curves to the experimental test data were first adjusted to account for the effects of mean stress and then lowered by a factor of 2 on stress and 20 on cycles (whichever was more conservative) to obtain the design fatigue curves. These factors are not safety margins but rather adjustment factors that must be applied to experimental data to obtain estimates of the lives of components. They were not intended to address the effects of the coolant environment on fatigue life. Recent fatigue–strain–vs.–life (ε–N) data obtained in the U.S. and Japan demonstrate that light water reactor (LWR) environments can have potentially significant effects on the fatigue resistance of materials. Specimen lives obtained from tests in simulated LWR environments can be much shorter than those obtained from corresponding tests in air.

This report provides an overview of fatigue crack initiation in austenitic stainless steels (SSs) in LWR coolant environments. The existing fatigue ε–N data are analyzed to define key material, loading, and environmental parameters that influence the fatigue lives of these steels. Statistical models are presented for estimating the fatigue ε–N curves as a function of material, loading, and environmental parameters. Effects of reactor coolant environment on the mechanism of fatigue crack initiation in austenitic SSs are discussed. A detailed metallographic examination of fatigue test specimens was performed to investigate the role of coolant environments on the formation and growth of small cracks. Two methods for incorporating the effects of LWR coolant environments into the ASME Code fatigue evaluations are presented.

Overview of Fatigue ε–N Data

In air, the fatigue lives of Types 304 and 316 SS are comparable; those of Type 316NG are superior at high strain amplitudes. The fatigue ε–N behavior of cast CF–8 and CF–8M SSs is similar to that of wrought austenitic SSs. The fatigue lives of all steels are independent of temperature in the range from room temperature to 427°C. Also, strain rate has no effect on fatigue life at temperatures up to 400°C.

The fatigue lives of cast and wrought austenitic SSs are decreased in LWR environments. The reduction in life depends on strain rate, dissolved–oxygen (DO) level in water, and temperature. A minimum threshold strain is required to produce an environmentally assisted decrease in the fatigue lives of these steels. The threshold strain appears to be independent of material type and temperature, but tends to decrease as the strain amplitude is decreased.

The effects of environment on fatigue life occur primarily during the tensile–loading cycle and at strain levels greater than the threshold value. Consequently, loading and environmental conditions (e.g., strain rate, temperature, and DO level) during the tensile–loading cycle are important parameters for environmentally assisted reduction of fatigue lives of these steels. Strain rate and temperature have a strong effect on fatigue life in LWR environments. Fatigue life decreases logarithmically with decreasing strain rate below 0.4%/s; the effect saturates at 0.0004%/s. Similarly, the fatigue ε–N data suggest a threshold temperature of 150°C; in the range of 150–325°C, life decreases with temperature.

The fatigue lives of wrought and cast austenitic SSs are decreased significantly in low–DO (i.e., <0.01 ppm DO) water. However, environmental effects on the fatigue lives of these steels in high–DO water are not well known. In high–DO water the magnitude of environmental effects may be influenced by the composition or heat treatment of the steel. The existing fatigue ε–N data indicate that the fatigue lives of cast SSs are approximately the same in low– and high–DO water and are comparable to those observed for wrought SSs in low–DO water. The fatigue lives of wrought SSs in high–DO water are comparable for some steels and higher for other steels than the lives in low–DO water. Also, environmental effects on fatigue life are greater for sensitized than solution–annealed steels in high–DO water, whereas in low–DO water, a sensitization anneal has no effect on fatigue life.

Mechanism of Fatigue Crack Initiation

The fatigue life of a material is defined as the number of cycles necessary to form an "engineering" crack, i.e., a 3–mm–deep crack. During cyclic loading, surface cracks, 10 μm or more in length, form quite early in life, i.e., <10% of life, even at low strain amplitudes. Fatigue crack initiation has been divided into two stages: an initiation stage that involves the growth of microstructurally small cracks (i.e., cracks smaller than ≈200 μm), and a propagation stage that involves the growth of mechanically small cracks. Crack lengths as a function of fatigue cycles have been determined in air and LWR environments. The results indicate that decreases in the fatigue lives of these steels are caused primarily by the effects of environment on the growth of microstructurally small cracks and, to a less extent, on enhanced growth rates of mechanically small cracks.

A detailed metallographic examination of fatigue test specimens was performed to investigate the role of LWR environments on the formation and growth of fatigue cracks. The crack morphology of the specimen surface is somewhat different in air or high–DO water than in low–DO water. In low–DO water, fatigue cracks are always straight and normal to the stress axis, whereas in air or high–DO water they follow certain crystallographic features. However, the morphology of crack growth into the material is similar in both air and water.

Austenitic SSs exposed to LWR environments develop a surface oxide film consisting of a dark, fine–grained, tightly–adherent, chromium–rich inner layer that forms by solid–state growth, and a crystalline nickel–rich outer layer composed of large– and intermediate–size particles that form by precipitation or deposition from the solution. The characteristics of the surface oxide films can influence the mechanism and kinetics of corrosion processes and thereby influence fatigue crack initiation. Exploratory fatigue tests were conducted on austenitic SS specimens that were preexposed to either low– or high–DO water and then tested in air or water environments in an effort to understand the effects of surface micropits or minor differences in the surface oxide on fatigue crack initiation. The results indicate that the

presence of a surface oxide film or any difference in the characteristics of the oxide film has no effect on fatigue crack initiation in austenitic SSs in LWR environments.

The different morphology of surface cracks in low–DO water indicate that the mechanism of crack initiation is different in low–DO PWR environment than in air or high–DO water. The presence of well–defined striations indicates that mechanical factors are important; environmentally assisted reduction in the fatigue life of austenitic SSs is most likely caused by mechanisms such as hydrogen–enhanced crack growth.

Incorporating Environmental Effects into ASME Code Fatigue Evaluations

Statistical models are presented for estimating the fatigue life of austenitic SSs as a function of material, loading, and environmental parameters. Functional form and bounding values of these parameters were based on experimental observations and data trends. The models are recommended for predicted fatigue lives $\leq 10^6$ cycles. The results indicate that the ASME mean curve for SSs is not consistent with the experimental data; the current ASME mean curve is nonconservative.

The design fatigue curves for austenitic SSs in LWR environments were obtained by the procedure that was used to develop the current ASME Code design fatigue curves. Environmentally adjusted fatigue design curves have been developed by adjusting the best–fit experimental curve for the effect of mean stress and by setting margins of 20 on cycles and 2 on strain to account for the uncertainties in life associated with material and loading conditions. These curves provide allowable cycles for fatigue crack initiation in LWR coolant environments. The use of a fatigue life correction factor to incorporate the effects of environment into the ASME Code fatigue evaluations is also discussed. Data available in the literature have been reviewed to evaluate the conservatism in the existing ASME Code fatigue design curves. The results suggest that the current ASME Code requirements of a factor of 2 on stress and 20 on life are quite reasonable.

Acknowledgments

The authors thank T. M. Galvin, J. Tezak, and E. J. Listwan for their contributions to the experimental effort. This work is sponsored by the Office of Nuclear Regulatory Research, U.S. Nuclear Regulatory Commission, under Job Code Y6388; Task Manager: J. Muscara; Program Manager: W. H. Cullen, Jr.

1 Introduction

Cyclic loadings on a structural component occur because of changes in mechanical and thermal loadings as the system goes from one load set (e.g., pressure, temperature, moment, and force loading) to any other load set. For each load set, an individual fatigue usage factor is determined by the ratio of the number of cycles anticipated during the lifetime of the component to the allowable cycles. Figures I–9.1 through I–9.6 of Appendix I to Section III of the ASME Boiler and Pressure Vessel Code specify fatigue design curves that define the allowable number of cycles as a function of applied stress amplitude. The cumulative usage factor (CUF) is the sum of the individual usage factors, and the ASME Code Section III requires that the CUF at each location must not exceed 1.

The ASME Code fatigue design curves, given in Appendix I of Section III, are based on strain–controlled tests of small polished specimens at room temperature in air. The design curves have been developed from the best–fit curves to the experimental fatigue–strain–vs.–life (ε–N) data that are expressed in terms of the Langer equation[1] of the form

$$\varepsilon_a = A1(N)^{-n1} + A2, \tag{1}$$

where ε_a is the applied strain amplitude, N is the fatigue life, and A1, A2, and n1 are coefficients of the model. Equation 1 may be written in terms of stress amplitude S_a instead of ε_a, in which case stress amplitude is the product of ε_a and elastic modulus E, i.e., $S_a = E\ \varepsilon_a$. The fatigue design curves were obtained from the best–fit curves by first adjusting for the effects of mean stress on fatigue life and then reducing the fatigue life at each point on the adjusted curve by a factor of 2 on strain or 20 on cycles. However, the best–fit fatigue curve used to develop the current Code fatigue design curve for austenitic stainless steels (SSs) does not accurately represent the available experimental data.[2,3] The current Code design curve for SSs includes a reduction of only ≈1.5 and 15 from the mean curve for the SS data, not the 2 and 20 originally intended. Also, because, for the current Code mean curve, the fatigue strength at 10^6 cycles is greater than the monotonic yield strength of austenitic SSs, the current Code design curve for austenitic SSs does not include a mean stress correction. The current ASME Code mean curve for austenitic SSs is given by

$$S_a = 58020\ (N)^{-0.5} + 299.92. \tag{2}$$

The factors of 2 and 20 are not safety margins but rather conversion factors that must be applied to the experimental data to obtain reasonable estimates of the lives of actual reactor components. Although the Section III criteria document[4] states that these factors were intended to cover such effects as environment, size effect, and scatter of data, Subsection NB–3121 of Section III of the Code explicitly notes that the data used to develop the fatigue design curves (Figs. I–9.1 through I–9.6 of Appendix I to Section III) did not include tests in the presence of corrosive environments that might accelerate fatigue failure. Article B–2131 in Appendix B to Section III states that the owner's design specifications should provide information about any reduction to fatigue design curves that has been necessitated by environmental conditions.

Existing fatigue ε–N data illustrate potentially significant effects of light water reactor (LWR) coolant environments on the fatigue resistance of carbon and low–alloy steels,[5,6] as well

as of austenitic SSs[3,6] (Fig. 1). Under certain environmental and loading conditions, fatigue lives of carbon steels can be a factor of 70 lower in high–DO water than in air.[5] Therefore, the margins in the ASME Code may be less conservative than originally intended. The activities of various organizations in addressing the issue of environmental effects on fatigue life of pressure vessel and piping steels are summarized below.

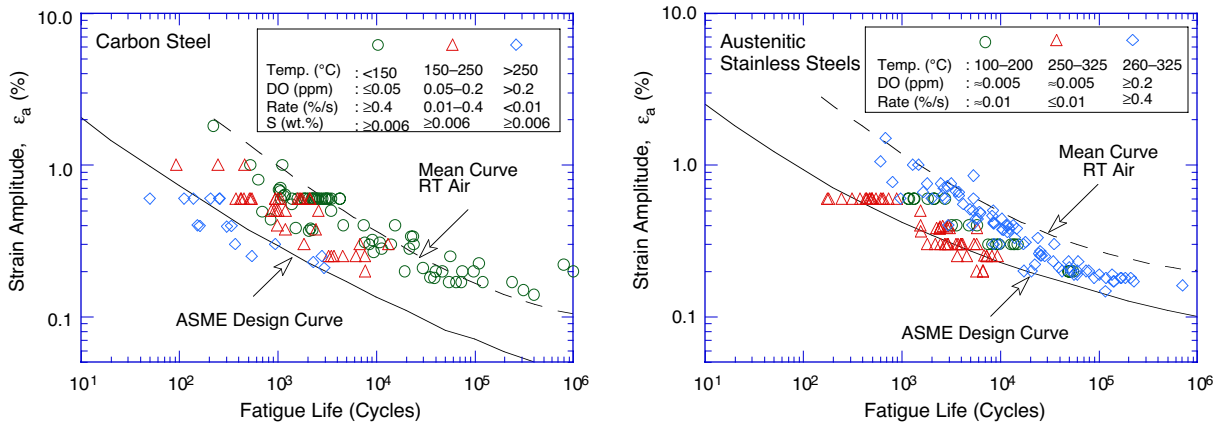

(a) (b)

Figure 1. Fatigue ε–N data for (a) carbon steels and (b) austenitic stainless steels in water; RT = room temperature

In 1986, a program was initiated at Argonne National Laboratory (ANL) to provide data and models for predicting environmental effects on fatigue design curves and to assess the validity of fatigue damage summation in piping and vessel steels under load histories typical of LWR components. The existing fatigue ε–N data, both foreign and domestic, have been compiled and evaluated to establish the effects of key material, loading, and environmental parameters on the fatigue lives of carbon and low–alloy steels, wrought and cast austenitic SSs, and Alloy 600. Experimental data were obtained under conditions in which information was lacking in the existing fatigue database. As data have become available, correlations for the best–fit fatigue ε–N curves have been developed and updated to include the effects of various parameters on fatigue life.

Based on the ε-N data available at that time, interim fatigue design curves that address environmental effects on fatigue life of carbon and low–alloy steels and austenitic SSs have been proposed by Majumdar et al.[7] More rigorous statistical models have been developed by Keisler et al.,[8,9] based on a larger database than that available when the interim design curves were developed. Results of the statistical analysis have also been used to interpret ε–N curves in terms of the probability of fatigue cracking. The work performed at ANL on fatigue of pressure vessel and piping steels in LWR coolant environments has been summarized in NUREG/CR-6583[5] for carbon and low–alloy steels and NUREG/CR-5704[3] for austenitic SSs; the results have been updated in NUREG/CR-6717.[6]

Two approaches have been proposed for incorporating the effects of LWR environments into ASME Section III fatigue evaluations: (a) develop new fatigue design curves for LWR applications, and (b) use an environmental correction factor to account for the effects of the coolant environment. Both approaches are based on the existing fatigue ε–N data in LWR

environments, i.e., the best–fit curves to the experimental fatigue ε–N data in LWR environments are used to obtain the design curves or environmental correction factor.

Environmentally adjusted fatigue design curves have been developed from the best fit to the experimental data in LWR environments by using the same procedure used to develop the current ASME Code fatigue design curves. These curves provide allowable cycles for fatigue crack initiation in LWR coolant environments. The second approach, proposed initially by Higuchi and Iida,[10] considers the effects of reactor coolant environments on fatigue life in terms of an environmental correction factor F_{en}, which is the ratio of fatigue life in air at room temperature to that in water under reactor operating conditions. To incorporate environmental effects into the ASME Code fatigue evaluations, a fatigue usage for a specific load set, based on the current Code design curves, is multiplied by the correction factor. Specific expressions for F_{en}, based on statistical models[6,11–13] and on the correlations developed by the Environmental Fatigue Data Committee of the Thermal and Nuclear Power Engineering Society of Japan,[14] have been proposed.

In 1991, the U.S. Nuclear Regulatory Commission (NRC) issued a draft Branch Technical Position (BTP) for fatigue evaluation of nuclear plant components for license renewal. The BTP raised a concern about the adequacy of the ASME Code in addressing environmental effects on fatigue resistance of materials for operating pressurized water reactors (PWRs) and boiling water reactors (BWRs), whose primary–coolant pressure boundary components are constructed as specified in Section III of the Code. In 1993, the Commission directed the NRC staff to treat fatigue as a potential safety issue within the existing regulatory process for operating reactors. The staff developed a Fatigue Action Plan (FAP) to resolve three principal issues: (a) adequacy of fatigue resistance of older vintage plants designed to the United States of America Standard B31.1 Code that did not require an explicit fatigue analysis of components, (b) effect of LWR environments on the fatigue resistance of primary pressure boundary materials, and (c) appropriate corrective action required when the Code fatigue allowable limits have been exceeded, i.e., when the CUF is >1.

The Idaho National Engineering Laboratory (INEL) assessed the significance of the ANL–developed interim fatigue design curves, by performing fatigue evaluations of a sample of components in the reactor coolant pressure boundary.[15] In all, six locations were evaluated from facilities designed by each of the four U.S. nuclear steam supply system vendors. Selected components from older vintage plants designed according to the B31.1 Code were also included in the evaluation. Conservatism in the original fatigue evaluations, e.g., actual cycles instead of assumed cycles, were removed, and fatigue usage was evaluated with a fatigue design curve that considered the effects of the coolant environment. The results indicated that most of the locations would have a CUF of less than the ASME Code limit of 1.0 for 40 years. The risk to reactor–coolant pressure boundary components from failure due to fatigue was assessed under Generic Safety Issue (GSI) 78, "Monitoring of Fatigue Transient Limits for the Reactor Coolant System," and GSI–166, "Adequacy of Fatigue Life of Metal Components." On the basis of these studies, it was concluded* that no immediate action is necessary to address fatigue issues specified in the FAP. The risk study indicated that fatigue failure of piping is not a significant contributor to core damage frequency. On the basis of the risk assessment, a backfit to incorporate environmental effects in the analysis of fatigue in operating plants could not be justified.

---

*Policy Issue, SECY–95–245, Completion of the Fatigue Action Plan, Sept. 25, 1995.

However, because these studies were less certain that the conservatism in the original fatigue calculations could be used to account for an additional 20–years of operation, the NRC staff recommended that environmental effects be considered when the samples in the INEL study[15] are evaluated during the license renewal period. These concerns were addressed in GSI-190, "Fatigue Evaluation of Metal Components for 60-year Plant Life." Based on probabilistic analyses and sensitivity studies, interactions with the industry, and various programs available to licensees to manage the effects of aging, it was concluded that no generic regulatory action is required. For some components, although cumulative probabilities of crack initiation and through-wall growth approach 1.0 within the renewal period, the maximum failure rate was in the range of 10^{-2} through-wall cracks per year. Also, these failures were generally associated with high CUF locations and components with thin walls; in most cases, the leakage from these through-wall cracks is small and not likely to lead to core damage. However, the calculations that support the resolution of this issue indicated the potential for an increase in the frequency of pipe leaks as plants continue to operate. Thus, consistent with the requirements of 10 CFR 54.2, the NRC staff recommended that aging–management programs for license renewal should address component fatigue, including the effects of the reactor coolant environment.

In 1991, the ASME Board on Nuclear Codes and Standards (BNCS) requested the Pressure Vessel Research Council (PVRC) to examine the existing worldwide ε–N data and develop recommendations for the ASME. The PVRC has been compiling and evaluating fatigue ε–N data related to the effects of LWR coolant environments on the fatigue life of pressure boundary materials; some of the results have been summarized by Van Der Sluys and Yukawa.[16] The steering committee on cyclic life and environmental effects (CLEE), at its June 15, 1999, meeting in Columbus, OH,* endorsed the environmental–correction–factor approach for incorporating the effects of LWR coolant environments into the ASME Code fatigue evaluations. The recommendations and approach to implement environmental fatigue procedures were transmitted to the ASME BNCS by letter from Hollinger to Ferguson dated October 31, 1999.

This report provides an overview of fatigue crack initiation in austenitic SSs in LWR coolant environments. The existing fatigue ε–N data are analyzed to define key material, loading, and environmental parameters that influence the fatigue lives of these steels. Statistical models are presented for estimating the fatigue ε–N curves as a function of material, loading, and environmental parameters. Effects of reactor coolant environment on the mechanism of fatigue crack initiation in austenitic SSs are discussed. A detailed metallographic examination of fatigue test specimens was performed to investigate the role of coolant environments in the formation and growth of small cracks. The two methods for incorporating the effects of LWR coolant environments into the ASME Code fatigue evaluations are presented. Data available in the literature have been reviewed to evaluate the conservatism in the existing ASME Code fatigue design curves.

---

*Welding Research Council Progress Report, Vol. LIX No. 5/6, May/June 1999.

2 Overview of Fatigue ε–N Data

The relevant fatigue ε–N data for austenitic SSs in air include the data compiled by Jaske and O'Donnell[2] for developing fatigue design criteria for pressure vessel alloys, the JNUFAD* database from Japan, and the results of Conway et al.[17] and Keller.[18] In water, the existing fatigue ε–N data include the tests performed by General Electric Co. (GE) in a test loop at the Dresden 1 reactor,[19] the JNUFAD database, studies at Mitsubishi Heavy Industries, Ltd. (MHI),[20–25] Ishikawajima–Harima Heavy Industries Co. (IHI),[26,27] and Hitachi[28,29] in Japan, and the present work at ANL.[3,6,30–33] In these studies, various criteria are used to define fatigue life of a test specimen. In the present study, fatigue life N for strain–controlled tests is defined as the number of cycles for tensile stress to decrease by 25% from its peak or steady–state value. Fatigue lives defined by other criteria, e.g., a 50% decrease in peak tensile stress or complete failure, have been converted by solving the equation

$$N = N_X \,/\, (0.947 + 0.00212\, X), \tag{3}$$

where X represents the failure criteria, i.e., 25, 50, or 100% decrease in peak tensile stress.

In air, the database for austenitic SSs is composed of 500 tests; 240 tests on 26 heats of Type 304 SS, 170 tests on 15 heats of Type 316 SS, and 90 tests on 4 heats of Type 316NG. Most of the tests have been conducted on cylindrical gauge specimens with fully reversed axial loading; ≈75 tests were on hourglass specimens, and ≈40 data points are from bending tests on flat-sheet specimens with rectangular cross section. Nearly 60% of the tests in air were conducted at room temperature, 20% at 250–325°C, and 20% at 350–450°C.

In water, the existing fatigue ε–N database consists of 310 tests; 150 tests on 9 heats of Type 304 SS, 60 tests on 3 heats of Type 316 SS, and 100 tests on 4 heats of Type 316NG. Nearly 90% of the tests in water were conducted at temperatures between 260 and 325°C. The data on Type 316NG in water have been obtained primarily at dissolved–oxygen (DO) levels ≥0.2 ppm and those on Type 316 SS, at ≤0.005 ppm DO; half of the tests on Type 304 SS were at low–DO levels and the remaining half at high–DO levels. The existing ε–N data for cast SS are very limited, a total of 64 tests on 5 heats of CF–8M SS. Nearly 90% of the tests have been conducted in simulated PWR water at 325°C. Although fatigue ε–N data have also been obtained on SS welds in LWR environments, the results were not included in the present report.

2.1 Air Environment

2.1.1 Fatigue Life

The fatigue ε–N behavior of austenitic SSs is shown in Fig. 2, where the designated three curves are based on the current ASME mean curve, the best–fit curve developed by Jaske and O'Donnell,[2] and the updated statistical model that is discussed later in this report. The results indicate that the fatigue lives of Types 304 and 316 SS are comparable; those of Type 316NG are slightly higher at high strain amplitudes. At temperatures up to 300°C, specimen geometry

* M. Higuchi, Ishikawajima–Harima Heavy Industries Co., Japan, private communication to M. Prager of the Pressure Vessel Research Council, 1992.

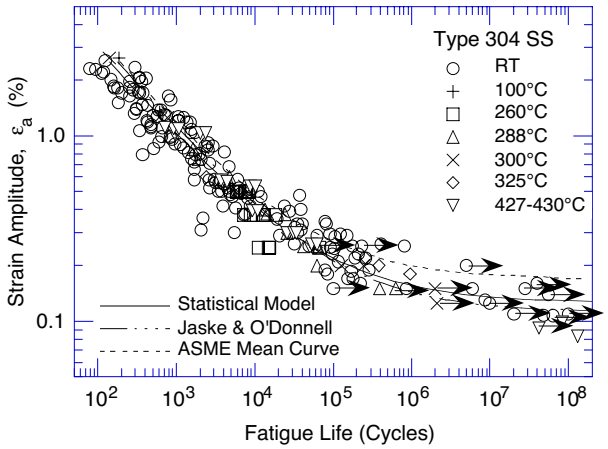

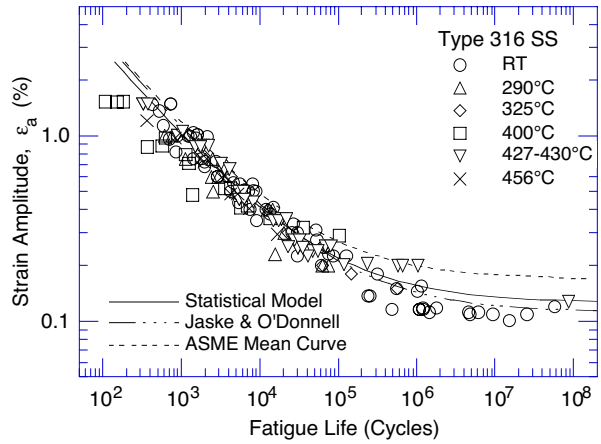

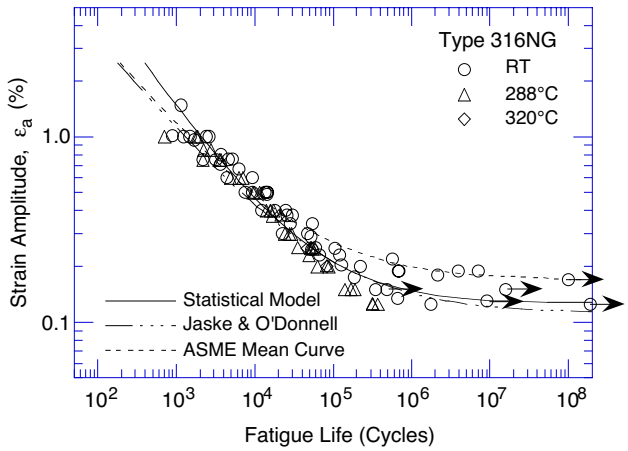

Figure 2.
Fatigue ε–N behavior for Types 304, 316, and 316NG austenitic stainless steels in air at various temperatures (Refs. 2,3,6,17,18,JNUFAD data)

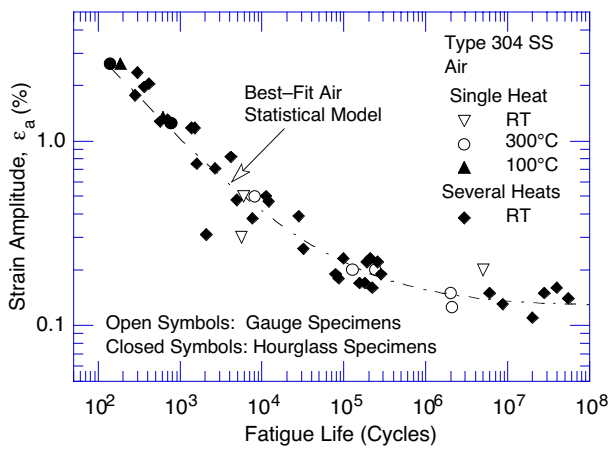

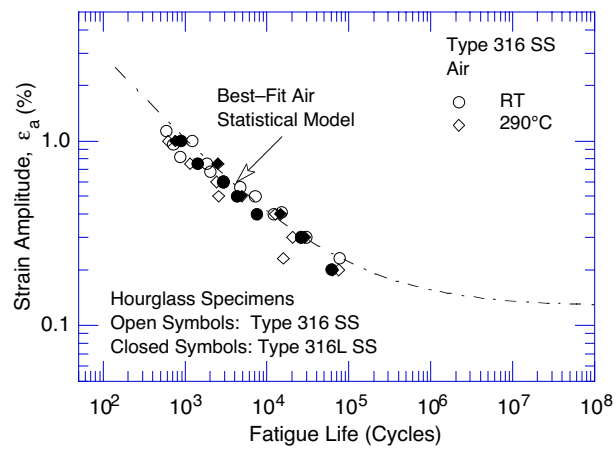

Figure 3. Influence of specimen geometry on fatigue life of Types 304 and 316 stainless steel (from JNUFAD data)

has little or no effect on the fatigue life of austenitic SSs (Fig. 3); the fatigue lives of hourglass specimens are comparable to those of gauge specimens.

Some of the tests on Type 316 SS in room–temperature air have been conducted in load–control mode at stress levels in the range of 190–230 MPa. For these tests, the strain

amplitude was calculated only as elastic strain. The data are shown as circles in Fig. 2, with strain amplitudes 0.1–0.12% and fatigue lives of 4×10^5–3×10^7. Based on cyclic stress–vs.–strain correlations for Type 316 SS,[3] actual strain amplitudes for these tests should be 0.23–0.32%. These data were excluded from the analysis in NUREG/CR–5704[3] for updating the statistical model for estimating the fatigue life of austenitic SSs in air.

Figure 2 also indicates that the ASME mean curve is not consistent with the existing fatigue ε–N data for austenitic SSs. At strain amplitudes <0.5%, the mean curve predicts significantly longer fatigue lives than those observed experimentally. At high strain amplitudes, the difference in fatigue lives between the statistical model and the ASME mean curve is primarily due to the definition of fatigue life. For example, in the latter, fatigue life is defined as complete failure of a test specimen, whereas in the statistical model, it is defined as number of cycles for tensile stress to decrease by 25% from its peak or steady–state value.

The existing fatigue ε–N data indicate that the fatigue life of austenitic SSs in air is independent of temperature in the range from room temperature to 427°C. Also, although the effect of strain rate on fatigue life seems to be significant at temperatures above 400°C, variation in strain rate in the range of 0.4–0.008%/s has no effect on the fatigue lives of SSs at temperatures up to 400°C.[34] The fatigue ε–N behavior of cast CF–8 and CF–8M SSs is similar to that of wrought austenitic SSs.[3]

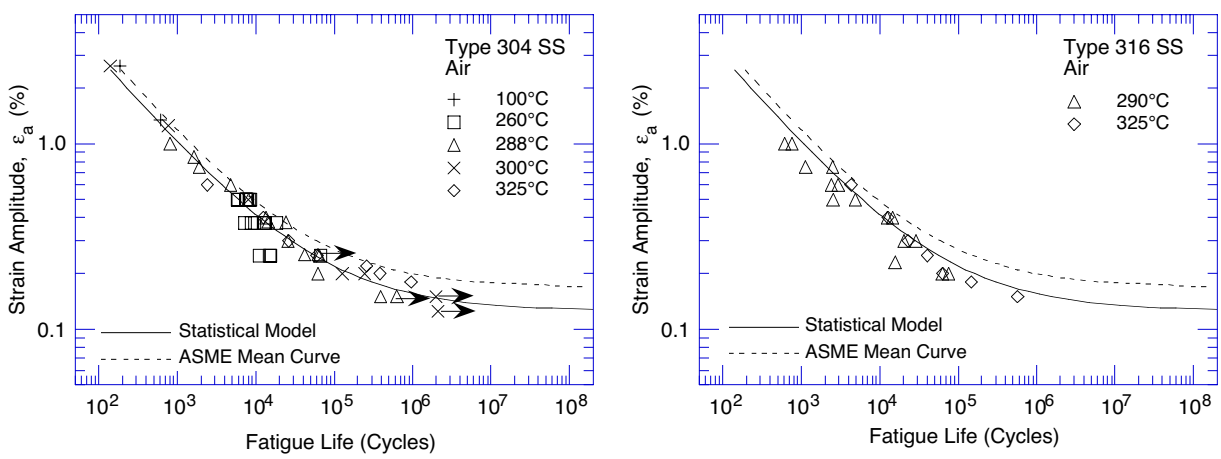

Figure 4. Influence of temperature on fatigue life of Types 304 and 316 stainless steel in air (Refs. 2,3,6,22,JNUFAD data)

2.1.2 Cyclic Hardening Behavior

During cyclic loading, austenitic SSs exhibit rapid hardening during the first 50–100 cycles; the extent of hardening increases with increasing strain amplitude and decreasing temperature and strain rate.[3,34] The cyclic strain hardening of Type 316NG tested in air at room temperature and 288°C is shown in Fig. 5; that of Type 304 SS in air at 288°C is shown in Fig. 6. In these figures, cyclic stress corresponds to the value at half life. The initial hardening is followed by softening and a saturation stage at 288°C, and by continuous softening at room temperature. For both Types 316NG and 304 SS, cyclic hardening at 288°C is greater at low strain rates, e.g., cyclic stresses are higher at 0.004%/s than at 0.4%/s.

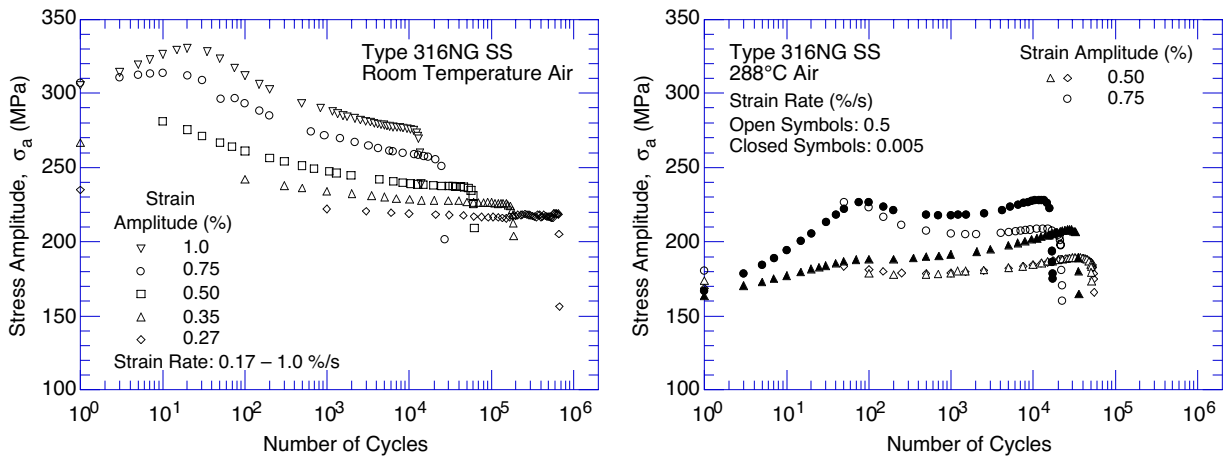

Figure 5. Effect of strain range and strain rate on cyclic–hardening of Type 316NG stainless steel in air at room temperature and 288°C (Refs. 3,6)

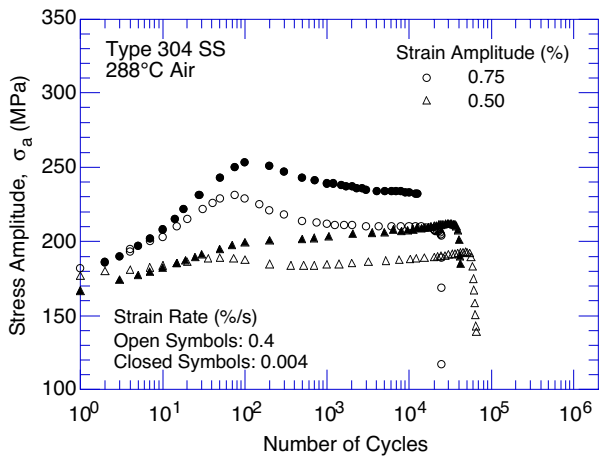

Figure 6.
Effect of strain range and strain rate on cyclic hardening of Type 304 stainless steel in air at 288°C

For the various steels, cyclic stresses increase in magnitude in the following order: Types 316NG, 304, and 316. At room temperature, the strain amplitude ε_a(%) for Type 316 SS can be expressed in terms of the cyclic stress amplitude σ_a (MPa) by the equation

$$\varepsilon_a = \frac{\sigma_a}{1950} + \left(\frac{\sigma_a}{588.5}\right)^{1.94}, \tag{4}$$

for Type 304 SS, by

$$\varepsilon_a = \frac{\sigma_a}{1950} + \left(\frac{\sigma_a}{503.2}\right)^{2.19}, \tag{5}$$

and for Type 316NG, by

$$\varepsilon_a = \frac{\sigma_a}{1950} + \left(\frac{\sigma_a}{447.0}\right)^{2.59}. \tag{6}$$

At 288–430°C, the cyclic stress–vs.–strain curve for Type 316 SS can be expressed by

$$\varepsilon_a = \frac{\sigma_a}{1760} + \left(\frac{\sigma_a}{496.8}\right)^{2.19}, \tag{7}$$

for Type 304 SS, by

$$\varepsilon_a = \frac{\sigma_a}{1760} + \left(\frac{\sigma_a}{373.9}\right)^{2.31}, \tag{8}$$

and for Type 316NG, by

$$\varepsilon_a = \frac{\sigma_a}{1760} + \left(\frac{\sigma_a}{330.1}\right)^{3.24}. \tag{9}$$

2.2 LWR Environments

The fatigue lives of austenitic SSs are decreased in LWR environments; the reduction depends primarily on strain rate and temperature; DO content in the water and material heat treatment may also influence fatigue life.[3,6,20–33] The critical parameters that influence fatigue life and the threshold values of these parameters for environmental effects to be significant are summarized below.

2.2.1 Strain Amplitude

A slow strain rate applied during the tensile–loading cycle (i.e., up–ramp with increasing strain) is primarily responsible for environmentally assisted reduction in fatigue life. Slow rates applied during both tensile– and compressive–loading cycles (i.e., up– and down–ramps) do not cause further decrease in fatigue life than that observed for tests with only a slow tensile–loading cycle.[30–32] Nearly all of the existing fatigue ε–N data have been obtained under loading histories with constant strain rate, temperature, and strain amplitude. Actual loading histories encountered during service of nuclear power plants are far more complex. Exploratory fatigue tests have been conducted with waveforms in which the slow strain rate is applied during only a fraction of the tensile loading cycle.[23,25] The results indicate that a minimum threshold strain is required for environmentally assisted decrease in fatigue lives of SSs (Fig. 7). The threshold strain $\Delta\varepsilon_{th}$ appears to be independent of material type (weld or base metal) and temperature in the range of 250–325°C, but it tends to decrease as the strain amplitude is decreased.[25] The threshold strain may be expressed in terms of the applied strain range $\Delta\varepsilon$ by the equation

$$\Delta\varepsilon_{th}/\Delta\varepsilon = -\,0.22\ \Delta\varepsilon + 0.65. \tag{10}$$

The results suggest that the threshold strain $\Delta\varepsilon_{th}$ is related to the elastic strain range of the test, and does not correspond to the strain at which the crack closes. For fully reversed cyclic loading, the crack opening point can be identified as the point where the curvature of the load–vs.–displacement line changes before the peak compressive load. In the present study, evidence of a crack opening point was observed for cracks that had grown relatively large, i.e., only near the end of life.

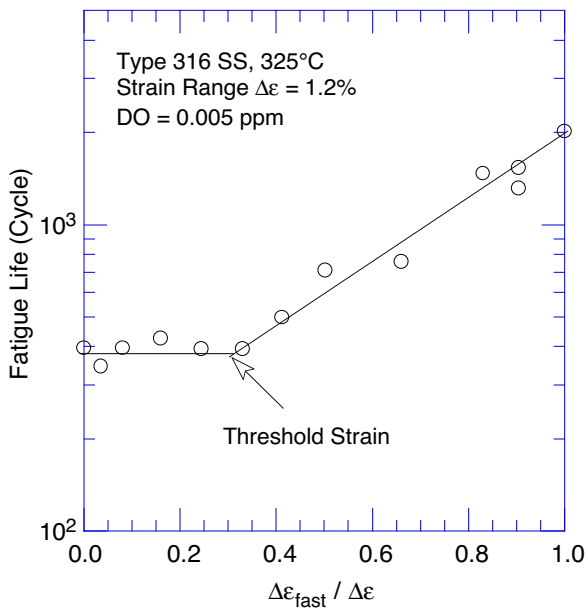

Figure 7.
Results of strain rate change tests on Type 316 SS in low–DO water at 325°C. A low strain rate was applied during only a fraction of the tensile loading cycle. Fatigue life is plotted as a function of fraction of strain at high strain rate (Refs. 23,25).

Fatigue data obtained at ANL indicate a threshold strain range of ≈0.32% for Type 304 SS.[3] For example, a specimen tested for ≈89,900 cycles at 0.15% strain amplitude and 0.01%/s strain rate failed after an additional 41,240 cycles when the strain amplitude was increased to 0.16%. Another specimen tested for ≈165,300 cycles at 0.16% strain amplitude failed after an additional 50,700 cycles at 0.17% strain amplitude.

During each fatigue cycle, relative damage due to slow strain rate is the same once the applied strain exceeds a threshold value. However, data also indicate that threshold strain does not correspond to rupture strain of the surface oxide film. The fatigue life of a Type 304 SS in low–DO water at 288°C with a 120–s hold period at zero strain during the tensile rise portion of the cycle was identical to that observed without the hold period (see Section 2.2.4 for details). If this threshold strain corresponds to the rupture strain of the surface oxide film, a hold period at the middle of each cycle should allow repassivation of the oxide film, and environmental effects on fatigue life should diminish.

2.2.2 Hold–Time Effects

Environmental effects on fatigue life occur primarily during the tensile–loading cycle and at strain levels greater than the threshold value. Consequently, loading and environmental conditions during the tensile–loading cycle, e.g., strain rate, temperature, and DO level, are important for environmentally assisted reduction of the fatigue lives of these steels. Information on the effect of hold periods on the fatigue life of austenitic SSs in water is very limited. In high–DO water, the fatigue lives of Type 304 SS tested with a trapezoidal waveform (i.e., hold periods at peak tensile and compressive strain)[19] are comparable to those tested with a triangular waveform,[26] Fig. 8. The hold–period test described in Section 2.2.4 below also indicates that hold periods should not influence the fatigue life of austenitic SSs in LWR environments. A similar behavior has been observed for carbon and low–alloy steels: the data show little or no effect of hold periods on fatigue lives of the steels in high–DO water.[5,27] A slow strain rate applied during the tensile–loading cycle is responsible for environmentally assisted reduction in fatigue life of austenitic SSs in LWR environments.

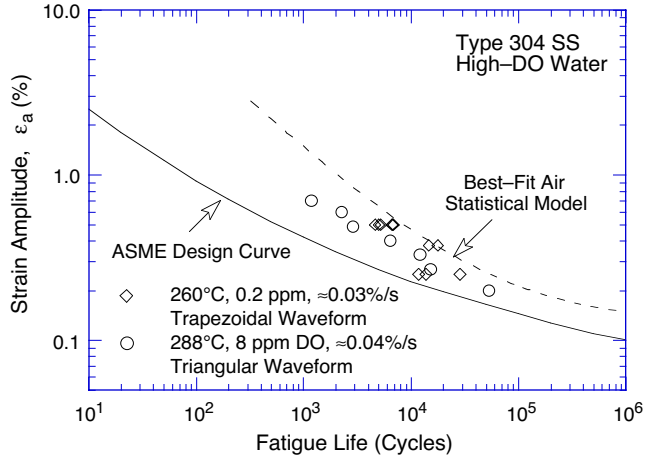

Figure 8.
Fatigue life of Type 304 stainless steel tested in high–DO water at 260–288°C with trapezoidal or triangular waveform but with comparable tensile strain rates (Refs. 19,26)

2.2.3 Strain Rate

The fatigue life of austenitic SSs in low– and high–DO water is plotted as a function of tensile strain rate in Fig. 9. In LWR environments, fatigue life decreases with decreasing strain rate. In low–DO PWR environments, fatigue life decreases logarithmically with decreasing strain rate below ≈0.4%/s; the effect of environment on life saturates at ≈0.0004%/s.[23,32] A decrease in strain rate from 0.4 to 0.0004%/s decreases the fatigue life of austenitic SSs by a factor of ≈10. For some SSs, the effect of strain rate may be less pronounced in high–DO water than in low–DO water; the effect of DO level on the fatigue life of austenitic SSs is discussed below.

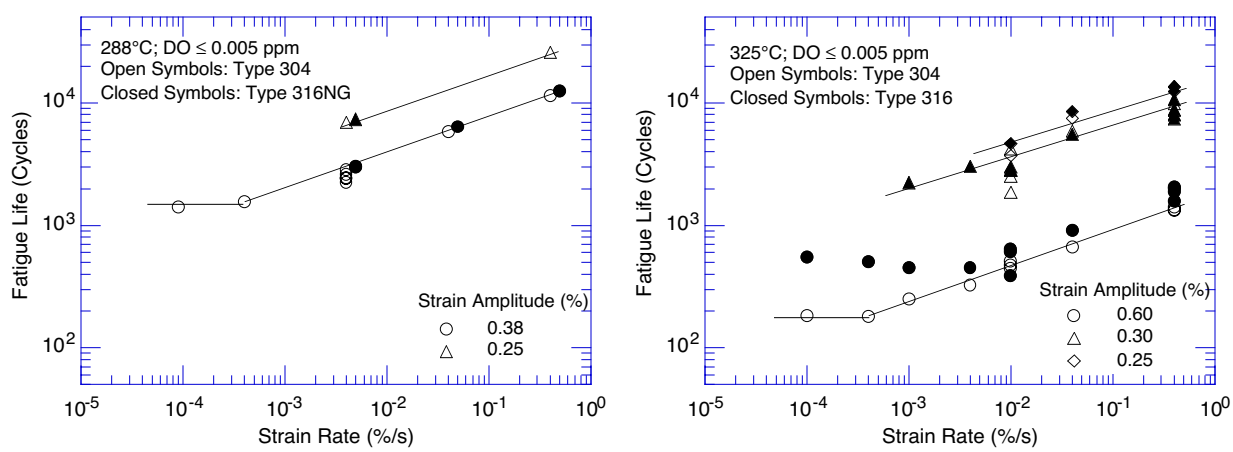

Figure 9. Dependence of fatigue lives of austenitic stainless steels on strain rate in low– and high–DO water (Refs. 3,22–26,32)

2.2.4 Dissolved Oxygen

The fatigue lives of austenitic SSs are decreased significantly in low–DO (i.e., <0.01 ppm) water; the effect is greater at low strain rates and high temperatures.[3,20–32] Environmental effects on the fatigue lives of these steels in high–DO water are not well known; the magnitude of environmental effects in high–DO water may be influenced by the composition or heat treatment of the steel. The fatigue lives of SSs in high–DO water are comparable[22,24] for some steels and higher[3] for other steels than those in low–DO water.

Only moderate environmental effects were observed for Type 304 SS when the conductivity of the water was maintained at <0.1 µS/cm and the electrochemical potential (ECP) of the steel was above 150 mV.[6] During a laboratory test, the time to reach these stable environmental conditions depends on test parameters such as the autoclave volume, flow rate, etc. In the ANL test facility, fatigue tests on austenitic SSs in high–DO water required a soaking period of 5–6 days for the ECP of the steel to stabilize. The steel ECP increased from zero or a negative value to above 150 mV during this period. The fatigue lives of Type 304 SS specimens, soaked for ≈5 days in high–DO water before testing in high–DO water at 289°C and ≈0.38 and 0.25% strain amplitude, are plotted as a function of strain rate in Fig. 10a. Similar results for Type 316NG specimens that were soaked for only one day before testing are shown in Fig. 10b. For Type 304 SS, fatigue life decreases linearly with decreasing strain rate in low–DO water, whereas in high–DO water, strain rate has no effect on fatigue life. For example, the fatigue life at ≈0.38% strain amplitude and 0.0004%/s strain rate is ≈1500 cycles in low–DO water and >7300 cycles in high–DO water. At all strain rates, the fatigue life of Type 304 SS is 30% lower in high–DO water than in air. However, the results obtained at MHI, Japan, on Types 304 and 316 SS show a different behavior; environmental effects are observed to be the same in high– and low–DO water.[22,24]

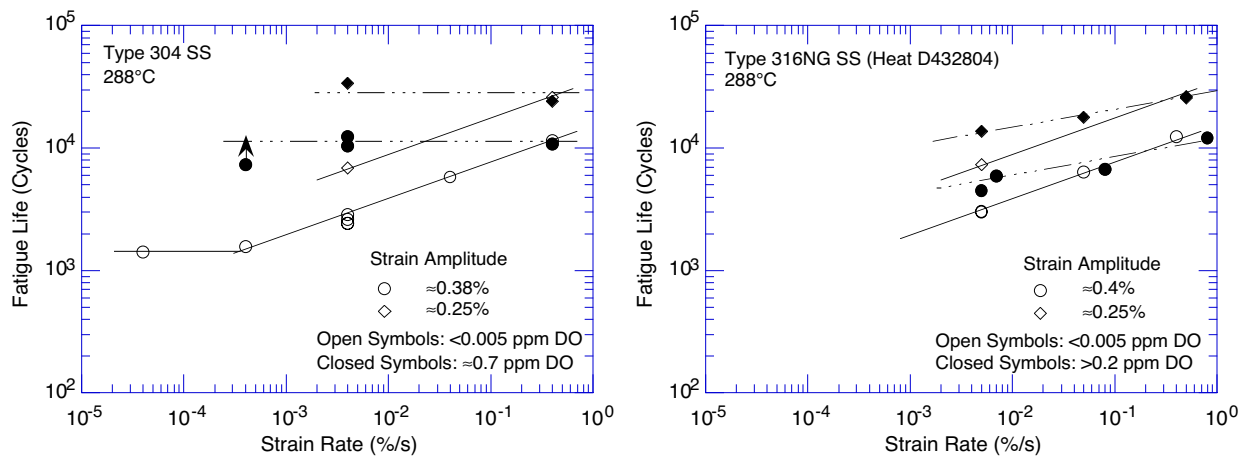

(a) (b)

Figure 10. Dependence of fatigue life of Types (a) 304 and (b) 316NG stainless steel on strain rate in high– and low–DO water at 288°C (Refs. 3,6)

For 316NG, some effect of strain rate is observed in high–DO water, although it is smaller than that in low–DO water (Fig. 10b). The different strain rate effect for the two steels may be explained on the basis of the shorter soak period for Type 316NG specimens, e.g., 24 h for Type 316NG and ≈120 h for Type 304 SS.[6] Environmental conditions may not have been stable for the tests on Type 316NG in high–DO water.

The effect of the conductivity of water and the ECP of the steel on the fatigue life of austenitic SSs is shown in Fig. 11. Environmental effects are significant for the specimens that were soaked for 24 h. For these tests, the ECP of steel was very low initially and increased during the test. Also, in high–DO water, fatigue life is decreased by a factor of ≈2 when conductivity of water is increased from ≈0.07 to 0.4 µS/cm.

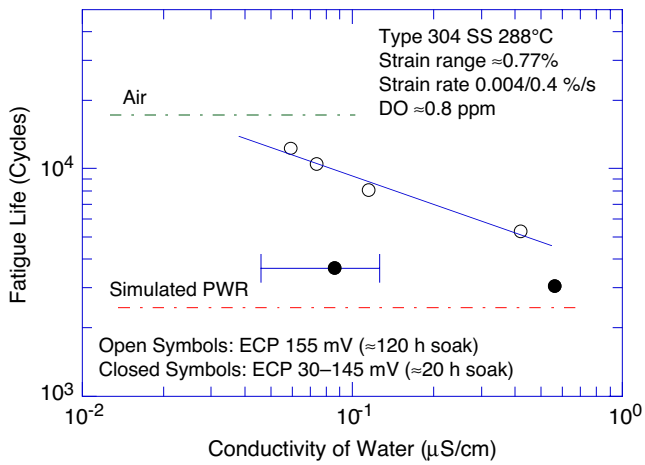

Figure 11.
Effects of conductivity of water and soaking period on fatigue lives of Type 304 SS in high–DO water (Ref. 6)

The effects of water chemistry and soaking period on the fatigue life of austenitic SSs in low–DO water have also been investigated; the results are presented in Table 1. In low–DO water, the following have no effect on the fatigue life of Type 304 SS: the addition of lithium and boron, low conductivity, soak period of ≈5 days before the test, and dissolved hydrogen.

Table 1. Fatigue test[a] results for Type 304 austenitic SS at 288°C

Test No.	Dis. Oxygen[b] (ppb)	Dis. Hydrogen (cc/kg)	Li (ppm)	Boron (ppm)	Pre–soak (days)	pH at RT	Conductivity[c] (µS/cm)	ECP SS[b] mV (SHE)	Ten. Rate (%/s)	Stress Range (MPa)	Strain Range (%)	Life N_{25} (Cycles)
1805	–	–	–	–	–	–	–	–	4.0E-3	467.9	0.76	14,410
1808	4	23	2	1000	1	6.4	18.87	–690	4.0E-3	468.3	0.77	2,850
1821	2	23	2	1000	1	6.5	22.22	–697	4.0E-3	474.3	0.76	2,420
1859	2	23	2	1000	1	6.5	18.69	–696	4.0E-3	471.7	0.77	2,420
1861	1	23	–	–	1	6.2	0.06	–614	4.0E-3	463.0	0.79	2,620
1862	2	23	–	–	5	6.2	0.06	–607	4.0E-3	466.1	0.78	2,450
1863	1	–	–	–	5	6.3	0.06	–540	4.0E-3	476.5	0.77	2,250
1871[d]	5	–	–	–	7	6.1	0.09	–609	4.0E-3	477.9	0.77	2,180

[a]Fully reversed axial fatigue tests at 288°C, ≈0.77% strain range, sawtooth waveform with 0.004/0.4%/s strain rates.
[b]Measured in effluent.
[c]Measured in feedwater supply tank.
[d]Test conducted with a 2–min hold period at zero strain.

These results suggest that the existing fatigue ε–N data on austenitic SSs in high–DO environments should be reevaluated; some of the data may have been obtained under varying environmental conditions. For example, the ECP of the steel may have been negative at the start of the test, and low–DO environment or negative ECP is known to decrease fatigue life of austenitic SSs. Also, the composition or heat treatment of the steel may have an important impact on the magnitude of environmental effects in high–DO environments. Additional data are needed to improve our insight into the effect of DO content on the fatigue life of austenitic SSs in LWR environments.

2.2.5 Temperature

The change in fatigue lives of austenitic SSs with test temperature at two strain amplitudes and two strain rates is shown in Fig. 12. The results suggest a threshold temperature of 150°C, above which the environment decreases fatigue life in low–DO water if the strain rate is below the threshold of 0.4%/s. In the range of 150–325°C, the logarithm of

fatigue life decreases linearly with temperature. Only moderate decrease in life is observed in water at temperatures below the threshold value of 150°C.

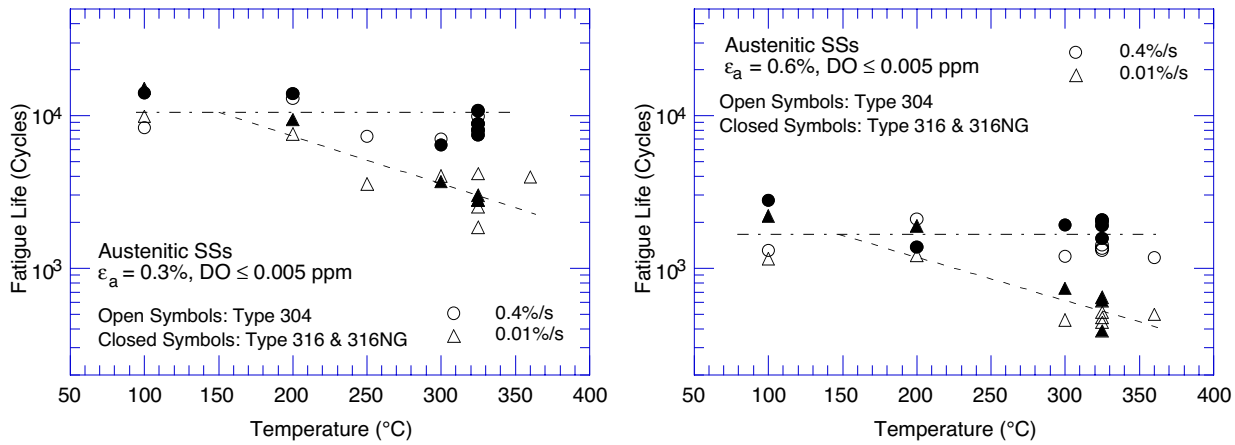

Figure 12. Change in fatigue lives of austenitic stainless steels in low–DO water with temperature (Refs. 3,6,22,24,26)

As discussed in the previous section, actual loading histories encountered during service in nuclear power plants involve variable loading and environmental conditions, whereas the existing fatigue ε–N data have been obtained under loading histories with constant strain rate, temperature, and strain amplitude. Fatigue tests have been conducted at MHI in Japan on Type 316 SS under combined mechanical and thermal cycling.[23] Triangular waveforms were used for both strain and temperature cycling. Two sequences were selected for temperature cycling (Fig. 13): an in–phase sequence, in which temperature cycling was synchronized with mechanical strain cycling; and a sequence in which temperature and strain were out of phase, i.e., maximum temperature occurred at minimum strain level and vice versa. Two temperature ranges, 100–325°C and 200–325°C, were selected for the tests.

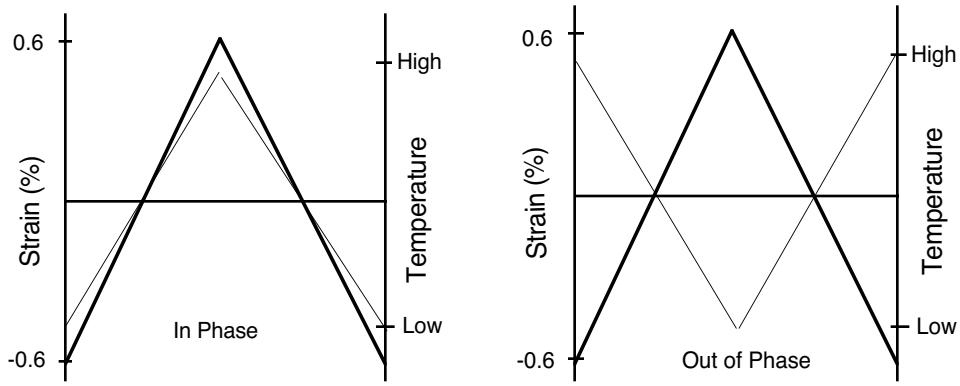

Figure 13. Waveforms for change in temperature during exploratory fatigue tests

The results are shown in Fig. 14, with the data obtained from tests at constant temperature. Note that the tensile load cycle is primarily responsible for environmentally assisted reduction in fatigue life, and that the applied strain and temperature must be above a minimum threshold value for environmental effects to occur. Thus life should be longer for out–of–phase tests than for in–phase tests, because applied strains above the threshold strain

occur at high temperatures for in–phase tests, whereas they occur at low temperatures for out–of–phase tests. An average temperature is used in Fig. 14 for the thermal cycling tests, i.e., the average of the temperature at peak strain and the temperature at threshold strain or 150°C (whichever is higher). The threshold strain for this test, from Eq. 10, is 0.46%. Thus, for the temperature range of 100–325°C, the temperature plotted in Fig. 14 is the average of 239 and 150°C for out–of–phase test and the average of 186 and 325°C for in–phase test. For the temperature range of 200–325°C, the temperature plotted in Fig. 14 is the average of 277 and 200°C for out–of–phase test and the average of 248 and 325°C for in–phase test. The results from thermal cycling tests agree well with those from constant–temperature tests (open circles in Fig. 14). The data suggest a linear decrease in the logarithm of life at temperatures above 150°C.

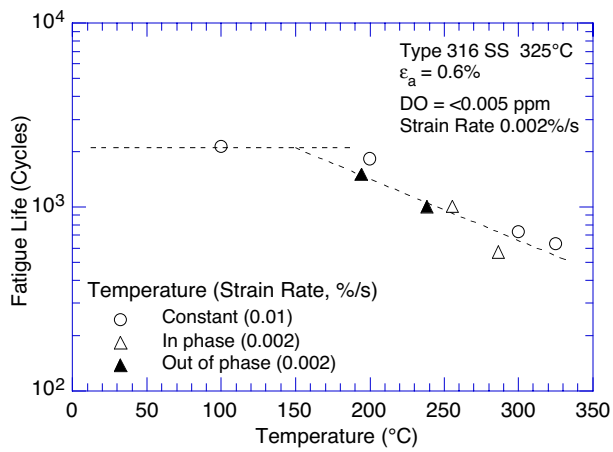

Figure 14.
Fatigue life of Type 316 stainless steel under constant and varying test temperature (Ref. 23)

2.2.6 Sensitization Annealing

The fatigue ε–N behavior of solution–annealed and sensitized Types 304, 316, and 316NG SS in low– and high–DO water are shown in Figs. 15 and 16. In low–DO (<0.005 ppm) water at 325°C, a sensitization annealing has no effect on the fatigue lives of Types 304 and 316 SS, Fig. 15. However, in high–DO (8 ppm) water at 300°C, the fatigue life of sensitized Type 304 SS

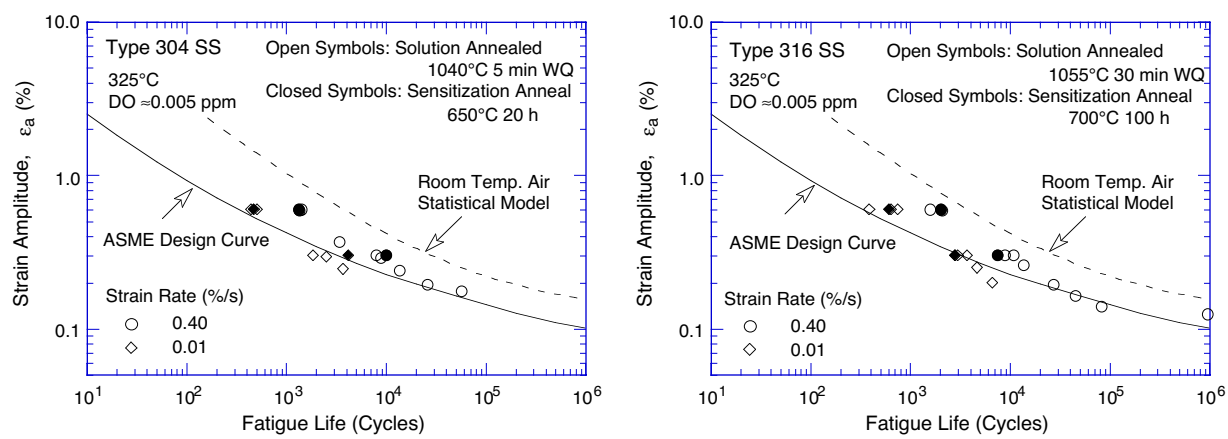

(a) (b)

Figure 15. Effect of sensitization annealing on fatigue life of Types (a) 304 and (b) 316 stainless steel in low–DO water at 325°C (Refs. 22,24). WQ = water quenched.

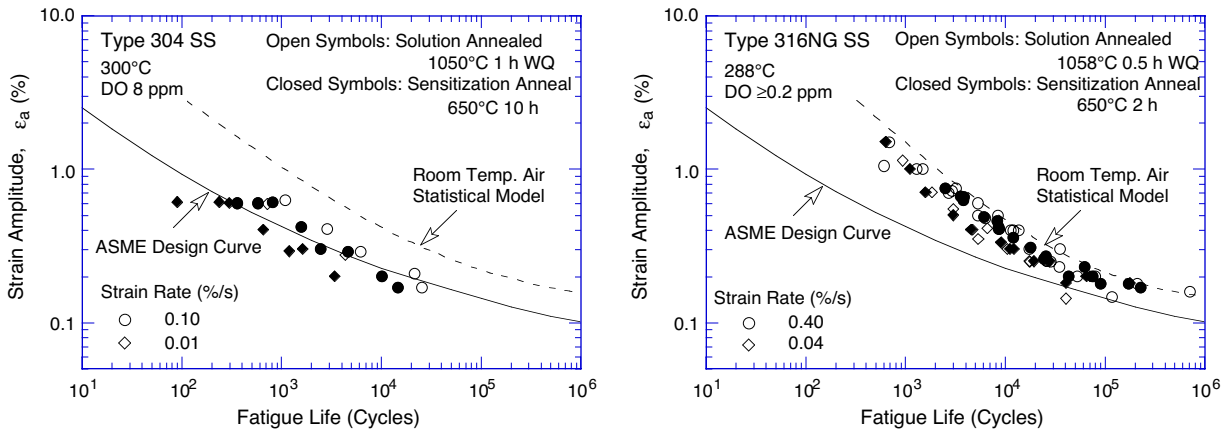

(a) (b)

Figure 16. Effect of sensitization anneal on the fatigue lives of Types (a) 304 and (b) 316NG stainless steel in high–DO water (Refs. 20,26). WQ = water quenched.

is a factor of ≈2 lower than that of the solution–annealed steel, Fig 16a. A sensitization anneal appears to have little or no effect on the fatigue life of Type 316NG SS in high–DO water at 288°C, Fig. 16b.

2.2.7 Flow Rate

It is generally recognized that flow rate most likely has a significant effect on the fatigue life of materials because it may cause differences in local environmental conditions in the enclaves of the microcracks formed during early stages in the fatigue ε–N test. Information about the effects of flow rate on the fatigue life of pressure vessel and piping steels in LWR environments has been rather limited. Recent results indicate that under typical operating conditions for BWRs, environmental effects on the fatigue life of carbon steels are a factor of ≈2 lower at high flow rates (7 m/s) than at low flow rates (0.3 m/s or lower).[35,36] However, the effect of flow rate on the fatigue life of austenitic SSs has not been evaluated. Because the mechanism of fatigue crack initiation in austenitic SSs in LWR environments appears to be different from that in carbon and low–alloy steels, the effect of flow rate on fatigue life may also be different for SSs.

2.2.8 Cast Stainless Steels

Available fatigue ε–N data[3,22,24,32] indicate that in air, the fatigue lives of cast CF–8 and CF–8M SSs are similar to that of wrought austenitic SSs, Fig. 17. It is well known that the Charpy impact and fracture toughness properties of cast SSs are decreased significantly after thermal aging at temperatures between 300 and 450°C.[37–39] As shown in Fig. 18, the cyclic–hardening behavior of cast austenitic SSs is also influenced by thermal aging. At 288°C, cyclic stresses of steels aged for 10,000 h at 400°C are higher than those for unaged material or wrought SSs. Also, strain rate effects on cyclic stress are greater for aged than for unaged steel, i.e., cyclic stresses increase significantly with decreasing strain rate. However, the effect of thermal aging on the fatigue life of these steels cannot be established; thermal aging may or may not affect fatigue life. For example, thermal aging for 25,200 h at 465°C exerted no effect

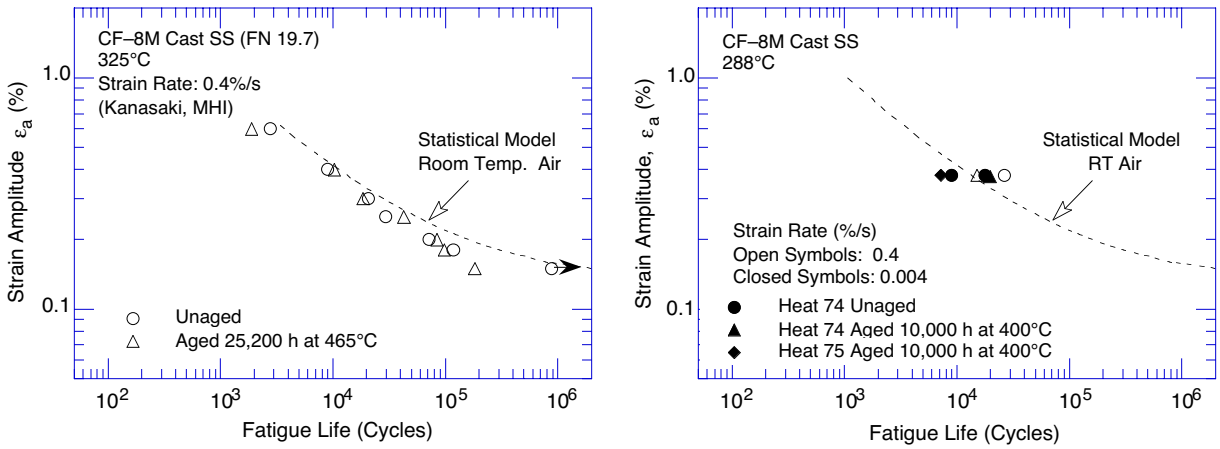

Figure 17. Fatigue strain amplitude–vs.–life data for CF–8M cast SSs in air (Refs. 3,22,24,32)

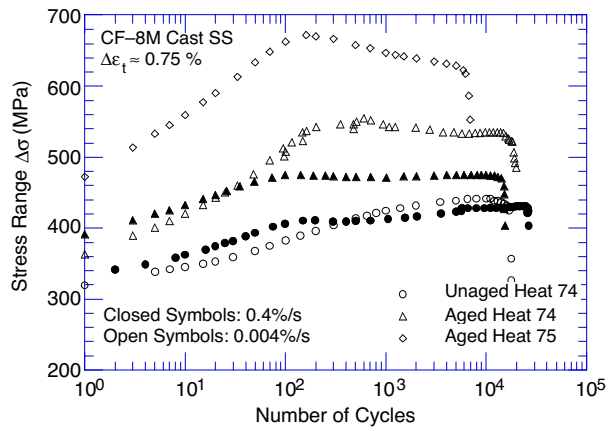

Figure 18.
Effect of strain rate on cyclic–hardening behavior of wrought and cast SSs in air at 288°C (Refs. 3,32)

on the fatigue life of a CF-8M steel in air at 325°C,[22] whereas aging for 10,000 h at 400°C decreased the fatigue life of Heat 74 at 288°C.[30–32] As discussed later, similar behavior is observed in water. These differences may be attributed to microstructural differences that arise from thermal aging temperature. Aging at 400°C results in spinodal decomposition of the ferrite to form Cr–rich regions that very effectively increase tensile strength, whereas, aging at 465°C for extended periods results in the formation of Cr–rich α' particles and overaging.

In LWR coolant environments, the effects of loading and environmental parameters on the fatigue life of cast SSs differ somewhat from those on wrought SSs. The existing fatigue ε–N data[3,22,24,32] indicate that the fatigue lives of cast SSs are comparable to those observed for wrought SSs in low–DO water (Fig. 19). Limited data suggest that the fatigue lives of cast SSs in high–DO water are approximately the same as those in low–DO water.[3] The results also indicate that thermal aging for 10,000 h at 400°C decreases the fatigue lives of CF8M steels.

The reduction in life in LWR environments depends on strain rate (Fig. 20). Effects of strain rate are the same in low– and high–DO water. For unaged material, environmental effects on life do not appear to saturate even at strain rates as low as 0.00001%/s.[22,24] Also, the fatigue lives of these steels are relatively insensitive to changes in ferrite content in the range of 12–28%.[22,24] Existing data are too sparse to define the saturation strain rate for cast

SSs or to establish the dependence of fatigue life on temperature in LWR environments; the effects of strain rate and temperature are assumed to be similar to those for wrought SSs.

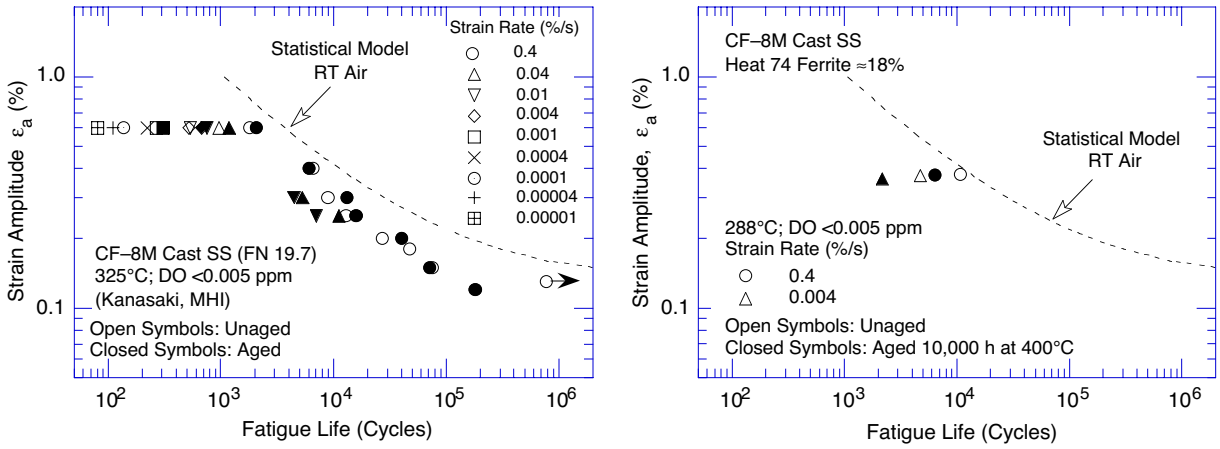

Figure 19. Fatigue strain amplitude–vs.–life data for CF–8M cast SSs in water (Refs. 3,22,24,32)

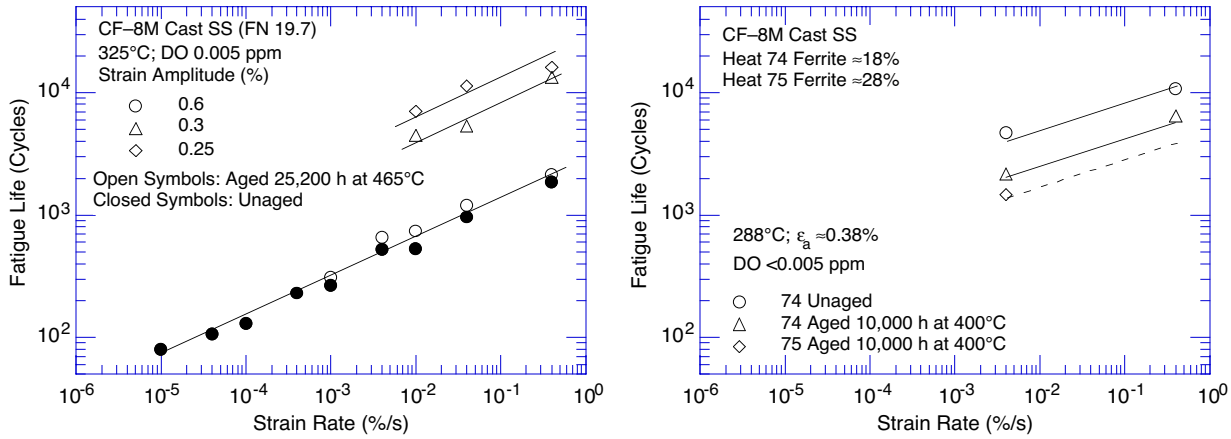

Figure 20. Dependence of fatigue lives of CF–8M cast SSs on strain rate in low–DO water at various strain amplitudes (Refs. 3,22,24,32)

3 Mechanism of Fatigue Crack Initiation

3.1 Formation of Engineering–Size Cracks

The formation of surface cracks and their growth to an "engineering" size (3 mm deep) constitute the fatigue life of a material, which is represented by the fatigue ε–N curves. Fatigue life has conventionally been divided into two stages: initiation, expressed as the cycles required to form microcracks on the surface; and propagation, expressed as cycles required to propagate the surface cracks to engineering size. During cyclic loading of smooth test specimens, surface cracks 10 µm or longer form quite early in life (i.e., <10% of life) at surface irregularities or discontinuities either already in existence or produced by slip bands, grain boundaries, second–phase particles, etc.[5,40–44] Consequently, fatigue life may be considered to be composed entirely of propagation of cracks from 10 to 3000 µm long.[45]

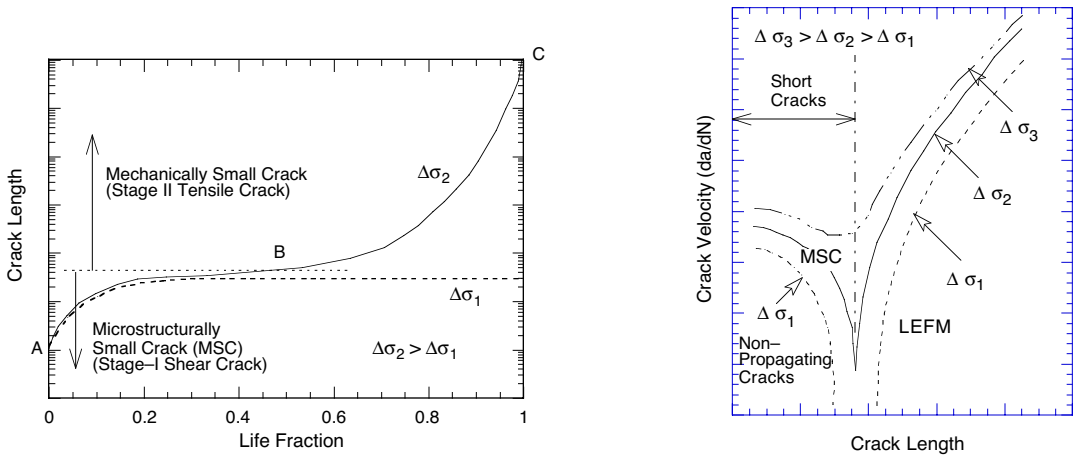

(a) (b)

Figure 21. Schematic illustration of (a) growth of short cracks in smooth specimens as a function of fatigue life fraction and (b) crack velocity as a function of crack length. LEFM = linear elastic fracture mechanics

A schematic illustration of the two stages, i.e., initiation and propagation, of fatigue life is shown in Fig. 21. The initiation stage involves growth of microstructurally small cracks (MSCs), characterized by decelerating crack growth (Region AB in Fig. 21a). The propagation stage involves growth of mechanically small cracks, characterized by accelerating crack growth (Region BC in Fig. 21a). The growth of MSCs is very sensitive to microstructure.[41,42] Fatigue cracks greater than the critical length of MSCs show little or no influence of microstructure, and are termed mechanically small cracks. Mechanically small cracks correspond to Stage II (tensile) cracks, which are characterized by striated crack growth, with a fracture surface normal to the maximum principal stress.

Once a microcrack forms on the surface, it continues to grow along its slip plane as a Mode II (shear) crack in Stage I growth (orientation of the crack is usually at 45° to the stress axis). At low strain amplitudes, a Stage I crack may extend across several grain diameters before the increasing stress intensity of the crack promotes slip on systems other than the primary slip system. A dislocation cell structure normally forms at the crack tip. Because slip is no longer confined to planes at 45° to the stress axis, the crack begins to propagate as a

Mode I (tensile) crack, normal to the stress axis in Stage II growth. At high strain amplitudes, the stress intensity is quite large, and the crack propagates entirely by the Stage II process. Stage II continues until the crack reaches engineering size (≈3 mm deep).

Various criteria have been used to define the crack length for transition from MSC to mechanically small crack; they may be related to the plastic zone size, crack–length–vs.–fatigue–life curve, Weibull distribution of the cumulative probability of fracture, stress–range–vs.–crack–length curve, or grain size. These criteria, summarized in Ref. 6, indicate that the transition crack length is a function of applied stress and microstructure of the material; actual values may range from 150 to 250 µm.

At low stress levels, e.g., $\Delta\sigma_1$ in Fig. 21b, the transition from MSC growth to accelerating crack growth does not occur. This circumstance represents the fatigue limit for the smooth specimen. Although cracks can form below the fatigue limit, they can grow to engineering size only at stresses greater than the fatigue limit. However, cracks larger than the transition crack length, either preexisting, e.g., defects in welded samples, or those created by growth of MSCs at high stresses, can grow at stress levels below the fatigue limit, and their growth can be estimated from linear–elastic or elastic–plastic fracture mechanics. The characterization and understanding of both the initiation stage and propagation stage are important for accurate estimates of the fatigue lives of structural materials.

3.2 Growth of Small Cracks in LWR Environments

The reduction in fatigue life of structural materials in LWR coolant environments has often been attributed to easy crack formation. Measurements of crack frequency, i.e., number of cracks per unit length of the specimen gauge surface, indicate that, under similar loading conditions, the number of cracks in specimens tested in air and low–DO water are comparable, although fatigue life is significantly lower in low–DO water. For Type 316NG SS tested at 288°C, ≈0.375% strain amplitude, and 0.005%/s strain rate, the number of cracks (longer than 20 µm) along a 7–mm gauge length was 16, 14, and 8 in air, simulated PWR (low–DO) water, and high–DO water, respectively.[30] If reduction in life is caused by easy crack formation, specimens tested in water should contain more cracks. Also, as discussed in Section 3.1 above, several studies indicate that fatigue cracks, 10 µm or longer, form quite early in life, i.e., <10% of life. Therefore, at most, easy crack formation can decrease fatigue life by 10%. The reduction in fatigue life in LWR coolant environments most likely arises from an increase in crack growth rates (CGRs) during one or both of the initiation stage (i.e., growth of MSCs), and the propagation stage (i.e., growth of mechanically small cracks).

The enhancement of CGRs in pressure vessel and piping steels in LWR environments has been attributed to either slip oxidation/dissolution[46] or hydrogen–induced cracking[47] mechanisms. The slip dissolution model requires that the surface oxide film is thermodynamically stable to ensure that a crack will propagate with a high aspect ratio without degrading into a blunt pit. A strain increment occurs to rupture that film, thereby exposing the underlying matrix to the environment (Fig. 22). Once the passive oxide film is ruptured, crack extension is controlled by dissolution of freshly exposed surfaces and by the oxidation characteristics.

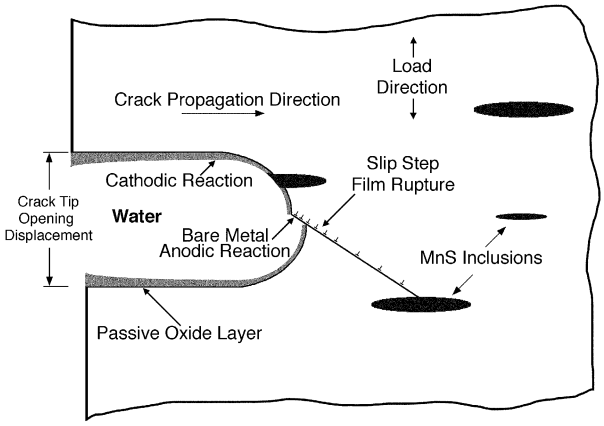

Figure 22.
Schematic illustration of film rupture/slip dissolution process

Hydrogen–induced cracking is explained as follows. Hydrogen produced by the oxidation reaction at or near the crack tip is partly absorbed into the metal. The absorbed hydrogen diffuses ahead of the crack tip, interacts with inclusions, and leads to the formation of cleavage cracks at the inclusion/matrix interface. Linkage of the cleavage cracks leads to discontinuous crack extension in addition to extension caused by mechanical fatigue. Other hydrogen–induced fracture processes may also enhance growth rates in LWR environments. For example, hydrogen can cause localized crack tip plasticity by reducing the stress required for dislocation motion. Both slip oxidation/dissolution and hydrogen–induced cracking mechanisms depend on the rates of oxide rupture, passivation, and liquid diffusion. Therefore, it is often difficult to differentiate between the two processes or to establish their relative contribution to crack growth in LWR environments.

Studies on crack initiation in smooth fatigue specimens indicate that although the growth rates of mechanically small cracks are greater in water than in air, the decrease in fatigue lives of austenitic SSs in LWR environments is caused predominantly by the effects of the environment on the growth of MSCs.[48] Growth of the largest crack in austenitic SSs with fatigue cycles, in air and water environments, is shown in Fig. 23. In the figure, the crack length for the test in air at 288°C and 0.75% strain range was measured only near the end of the test. The data obtained by Orbtlik et al.[43] for Type 316L SS in air at 25°C and ≈0.2% strain range were used to estimate the crack growth in air at 0.75% strain range. Studies on carbon and low-alloy steels[41,42,49] indicate that the fatigue crack size at various life fractions is independent of strain range, strain rate, and temperature; consequently, the depth of the

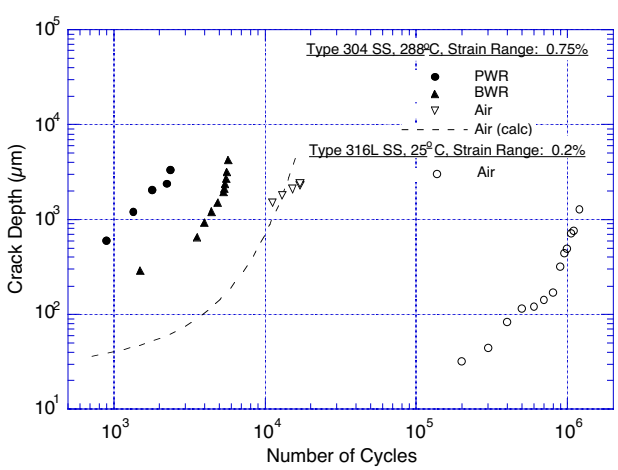

Figure 23.
Depth of largest crack plotted as a function of fatigue cycles for austenitic stainless steels in air and water (Ref. 48)

largest crack at various life fractions is approximately the same at 0.75 and 0.2% strain ranges. The curve for the test in air at 0.75% (shown as a dash line in Fig. 23) was calculated from the best-fit equation of the experimental data for Type 316L SS at 0.2% strain range; the estimated crack lengths at 0.75% strain range show very good agreement with the measured values. The results show that at the same number of cycles, the crack length is longer in low–DO water (PWR) than in air, e.g., after 1500 cycles the crack length in air, high-DO water (BWR), and PWR water is ≈40, 300, and 1100 µm, respectively. The growth of cracks during the initiation stage, i.e., growth of MSCs, is enhanced in water; fatigue cycles needed to form a 500–µm crack are a factor of ≈12 lower in low–DO water than in air. Figure 23 shows that the number of cycles required to produce a 500–µm crack is 800, 3000, and 9,000 in low–DO (PWR), high-DO (BWR), and air environments, respectively; thus the number of cycles is more than a factor of 10 lower in low–DO water than in air.

The CGRs during the propagation stage, i.e., growth of mechanically small cracks, in air and water environments are plotted as a function of crack length in Fig. 24; they were calculated from the best fit of the data in Fig. 23. The CGRs in high–DO water for the specimen with a 24–h soak period (closed circles in Fig. 24) were determined from measurements of fatigue striations. The CGRs are a factor of 2–6 higher in water than in air. Growth rates in PWR water or high–DO water with a 24–h soak period are higher than those in high–DO water with a 120–h soak period. At a crack length of ≈1000 µm, the CGRs in air, high–DO water, and low–DO environment are 0.30, 0.64, and 1.05 µm/cycle, respectively. For the 0.75% strain range and 0.004%/s strain rate, these values correspond to growth rates of $\approx 1.6 \times 10^{-9}$, 3.4×10^{-9}, and 5.6×10^{-9} m/s in air, high–DO water, and low–DO water, respectively. Growth rates are a factor of 3.5 greater in low–DO water than in air.

The existing fatigue crack growth (da/dN) data obtained from fracture–mechanics tests on compact tension (CT) specimens of wrought and cast SSs in LWR environments have been compiled by Shack and Kassner.[50] The results indicate significant enhancement of CGRs in high–DO water; at CGRs of $<10^{-10}$ m/s in air, the rates in BWR normal water chemistry (NWC)

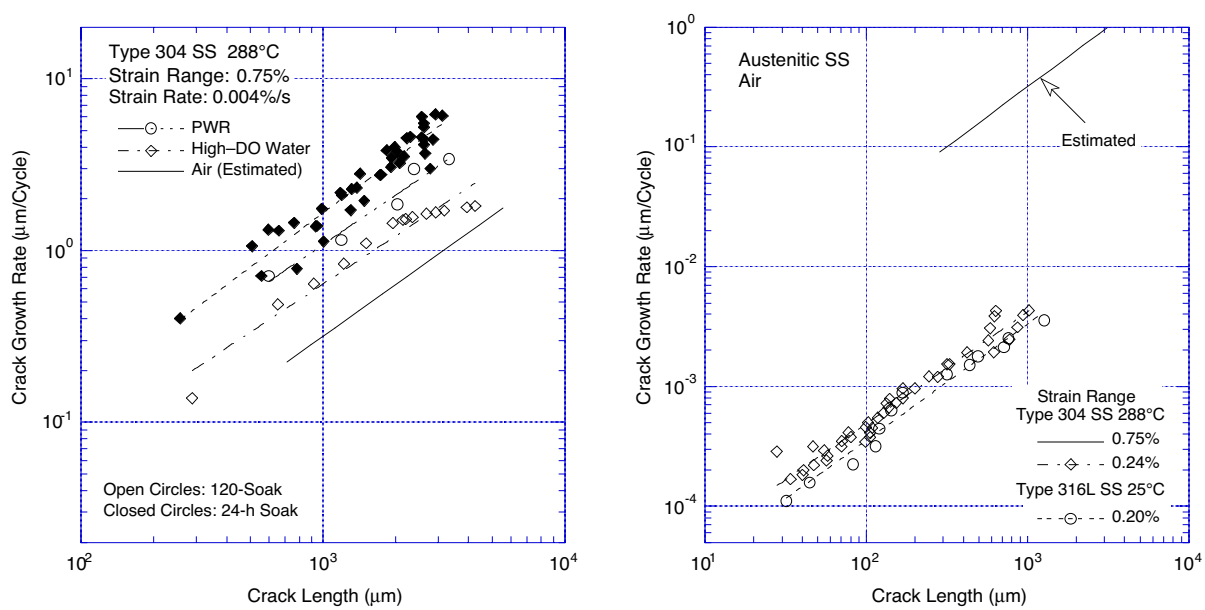

Figure 24. Crack growth rates plotted as a function of crack length for austenitic stainless steels in air and water environments (Refs. 43,48)

conditions exceed the air curve in the ASME Code by a factor of ≈20–30. The experimental CGRs for Type 316NG and sensitized Type 304 SS in high–DO water and those predicted in air for the same mechanical loading conditions are plotted in Fig. 25. The CGRs in air, $\dot{a}_{air}$ (m/s), were determined from the current ASME Section XI correlation at 288°C given by

$$\dot{a}_{air} = 3.43 \times 10^{-12}\, S(R)\, \Delta K^{3.3}/T_R, \tag{11}$$

where function S(R) is expressed as

$$\begin{aligned} S(R) &= 1.0 && R < 0 \\ S(R) &= 1.0 + 1.8R && 0 < R < 0.79 \\ S(R) &= -43.35 + 57.97R, && 0.79 < R < 1.0, \end{aligned} \tag{12}$$

and T_R is the rise time (s) of the loading waveform, R is the load ratio (K_{min}/K_{max}), and ΔK is $K_{max} - K_{min}$. The CGR in water [$\dot{a}_{env}$ (m/s)] with 0.2 ppm DO (i.e., BWR NWC) is expressed in terms of the CGR in air ($\dot{a}_{air}$) by the relationship

$$\dot{a}_{env} = \dot{a}_{air} + 4.5 \times 10^{-5} (\dot{a}_{air})^{0.5}. \tag{13}$$

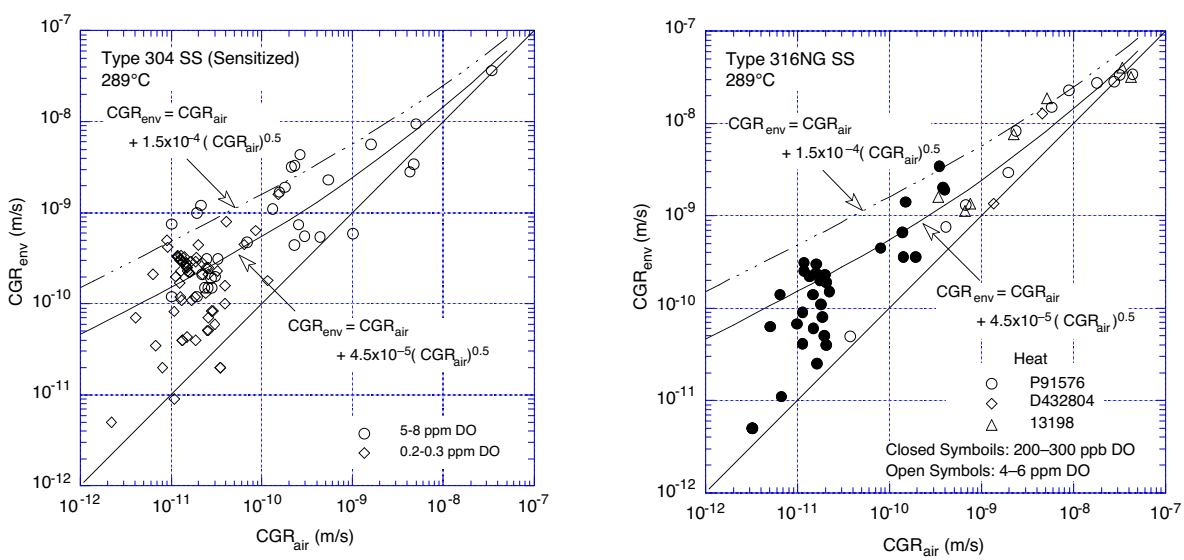

Figure 25. Corrosion fatigue data for Type 316NG and sensitized Type 304 SS in high–DO water at 289°C (Refs. 50)

The CGR data from fracture–mechanics tests in low–DO PWR environments are sparse, particularly at rates that are $<10^{-9}$ m/s. At high CGRs, the observed enhancement in both low– and high–DO environments is relatively small, and the magnitude of the enhancement under the same loading conditions is comparable in the two environments. Until further data become available at low CGRs in simulated PWR water, Shack and Kassner[50] recommend that the environmental enhancement represented by Eq. 13 for 0.2 ppm DO water should also be considered for PWR environments.

The CGRs determined from fatigue ε–N tests in water and air environments at 289°C are plotted in Fig. 26. The rates in high–DO and low–DO (PWR) water represent the measured values shown as open diamonds and circles, respectively, in Fig. 24. The CGRs in air for the

same loading conditions (i.e., the same crack length) were determined from the estimated rates in air, shown by solid line in Fig. 24. The results from fatigue ε–N tests show good agreement with the data obtained from fracture–mechanics tests. The CGRs in high–DO water are consistent with the trend predicted from Eq. 13, the rates in low–DO water are slightly higher. However, the large reductions in fatigue life of austenitic SSs in PWR environments cannot be explained entirely on the basis of enhanced CGRs during the propagation stage, i.e., growth of mechanically small cracks. For example, the CGRs in low–DO water are a factor of 1.6 greater than those in high–DO water, but the fatigue life is a factor of ≈4 lower in low–DO water than in high–DO water. As shown in Fig. 24, the decrease in fatigue lives of austenitic SSs in PWR environments is caused predominantly by the effects of environment on the growth of MSCs.

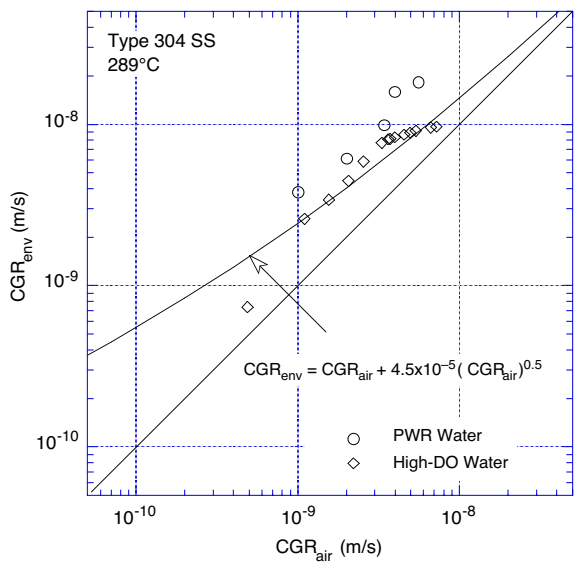

Figure 26.
Crack growth rate data for Type 304 SS determined from fatigue ε–N tests in PWR and high–DO water at 289°C

Equation 13 indicates that environmental effects increase with decreasing CGRs; under loading conditions that correspond to $>10^{-8}$ m/s growth rates in air, mechanical fatigue controls crack advance, and the contribution of environment or corrosion fatigue is insignificant. Because CGRs increase with increasing strain range (Fig. 24), the contribution of corrosion fatigue to crack initiation is likely to decrease with increasing strain range.

It should also be noted that, if enhanced CGRs alone were responsible for the environmentally assisted decrease in fatigue life of materials in LWR environments, environmental effects on the fatigue lives of Alloy 600 and austenitic SSs in LWR environments should be comparable. In air, the fatigue ε–N behavior of Alloy 600 is comparable to that of austenitic SSs.[2] Fatigue CGR data indicate that the enhancement of CGRs of Alloy 600 and austenitic SSs in LWR environments is also comparable.[51] However, the fatigue ε–N behaviors of Alloy 600 and austenitic SSs in water differ significantly; only moderate effects of environment are observed for Alloy 600 and its weld both in low–DO* and high–DO[9] water. For example, the fatigue life of Alloy 600 weld metal in water with <0.005 ppm DO at 325°C and 0.6% strain amplitude decreased by a factor of ≈2.5 when the strain rate was decreased from 0.4 to 0.001%/s. Under similar environmental and loading conditions, the fatigue life of

* H. Kanasaki, Mitsubishi Heavy Industries, Ltd., Fatigue Life of Stainless Steels and Alloy 600 in PWR Primary Water, presented at PVRC Autumn Meeting of the Working Group on S–N Data, October 7–9, 1996, Columbus, OH.

austenitic SSs is decreased by a factor of ≈10. Additional tests on Alloy 600 in low–DO water should be conducted to verify these results.

Studies on crack initiation in carbon and low–alloy steels yield similar results; the decrease in fatigue life in LWR environments is caused primarily by the effects of environment on the growth of cracks that are <100 µm deep.[5,42] Metallographic evaluation of the specimens indicates that the growth of MSCs in carbon and low–alloy steels occurs predominantly by the slip oxidation/dissolution process.[5] However, for SSs, fatigue lives are lower in low–DO water than in high–DO water; such results are difficult to reconcile in terms of the slip oxidation/dissolution mechanism. The reduction in fatigue life of austenitic SSs in low–DO environments is most likely caused by other mechanisms, such as hydrogen–enhanced crack growth.

3.3 Fracture Morphology

A detailed metallographic examination of fatigue test specimens was performed to investigate the role of LWR environments on the formation and growth of fatigue cracks. Fatigue cracks on the gauge surfaces and along longitudinal sections of Type 304 SS tested in air and water environments at 288°C are shown in Fig. 27, and fatigue cracks along longitudinal sections of Type 316NG SS in air and water environments are shown in Fig. 28.

The crack morphology of the specimen surface is somewhat different in air or high–DO water than in low–DO water. For Type 304 SS, fatigue cracks are always straight and normal to the stress axis in low–DO water, whereas in air or high–DO water, they follow certain crystallographic features (Fig. 27). However, the morphology of crack growth into the material is similar in both air and water. Fatigue cracks appear to grow predominantly as Mode I tensile cracks normal to the stress axis; only a few small shear cracks were observed in Type 304 SS specimens.[30,31]

Some differences in the growth of fatigue cracks in air and water environments are observed for Type 316NG. Figure 28 shows that in Type 316NG SS, fatigue cracks appear to grow entirely as Mode I tensile cracks normal to the stress axis in a low–DO PWR environment (<10 ppb DO), and as Mode II shear cracks ≈45° to the stress axis in air and high–DO water. Slip lines or strain lines are also visible in the specimens tested in air or high–DO water. This difference, however, may be due to the different fatigue lives of these specimens. Because fatigue life is longer in air than in low–DO water, shear cracks and slip or strain lines in air may form late during fatigue life. The lives of specimens tested in PWR water under the same loading conditions are much shorter and do not show strain lines.

The fracture morphology of austenitic SSs in air or LWR environment does not differ significantly; during Stage II growth, well–defined fatigue striations are observed in air and water.[3,30] Figure 29 shows photomicrographs of the fracture surfaces of Type 304 and 316NG SS specimens tested at 288°C in air, high–DO water, and a low–DO PWR environment after chemical cleaning and at approximately the same crack length. All specimens show fatigue striations; the spacing between striations is larger in low–DO water than in air. The striation spacings in air and water environments show very good agreement with macroscopic crack growth rates. The presence of well–defined striations suggests that mechanical factors, and not the slip dissolution/oxidation process, are important. Fatigue striations should not be observed if crack growth is enhanced by the slip dissolution/oxidation process.

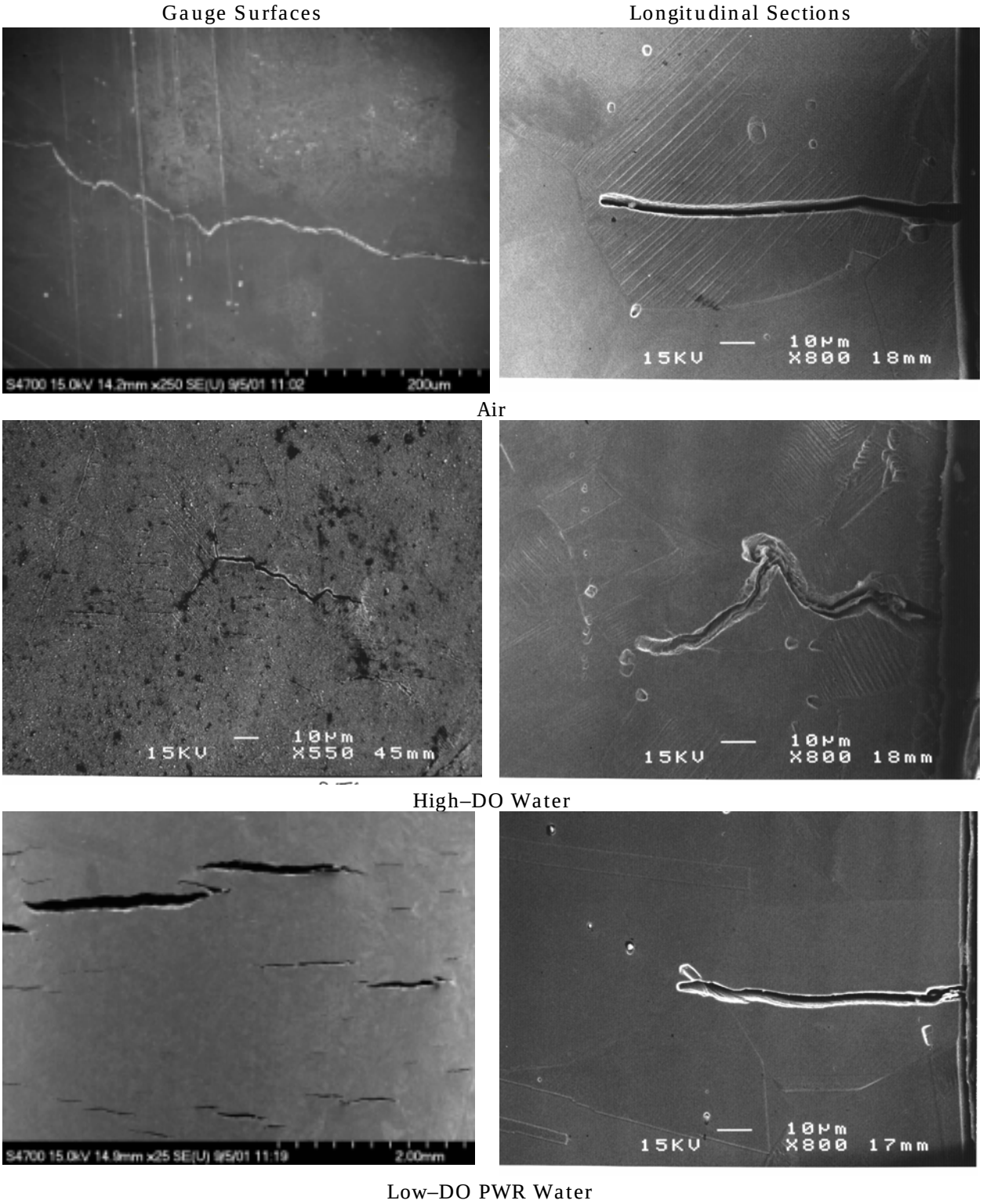

Figure 27. Photomicrographs of fatigue cracks on gauge surfaces and along longitudinal sections of Type 304 stainless steel tested in air, high–DO water, and low–DO simulated PWR environment at 288°C, ≈0.75% strain range, and 0.004%/s strain rate

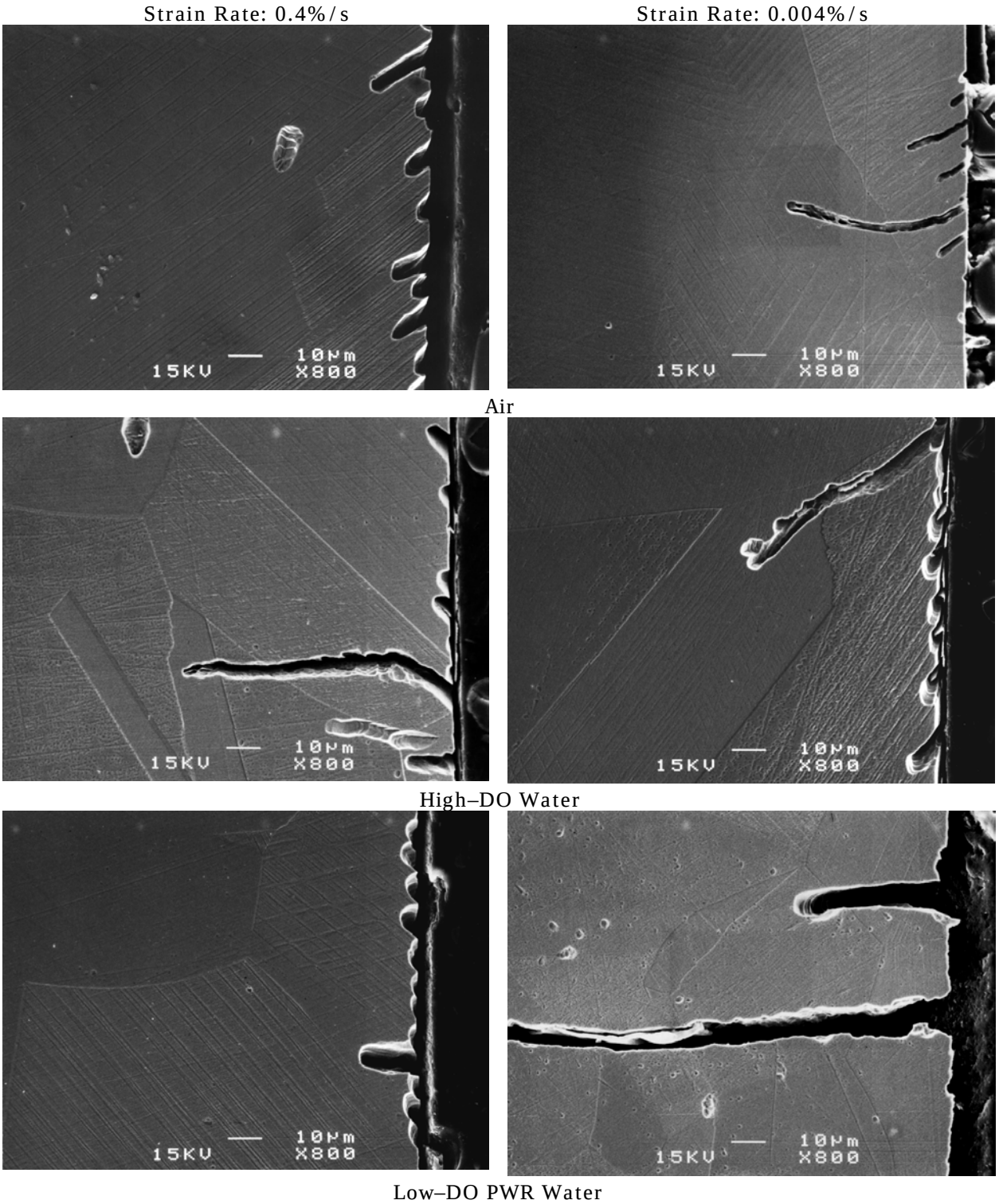

Figure 28. Photomicrographs of surface cracks along longitudinal sections of Type 316NG stainless steel at 288°C, ≈0.75% strain range, and two strain rates in air, high–DO water, and low–DO simulated PWR environment

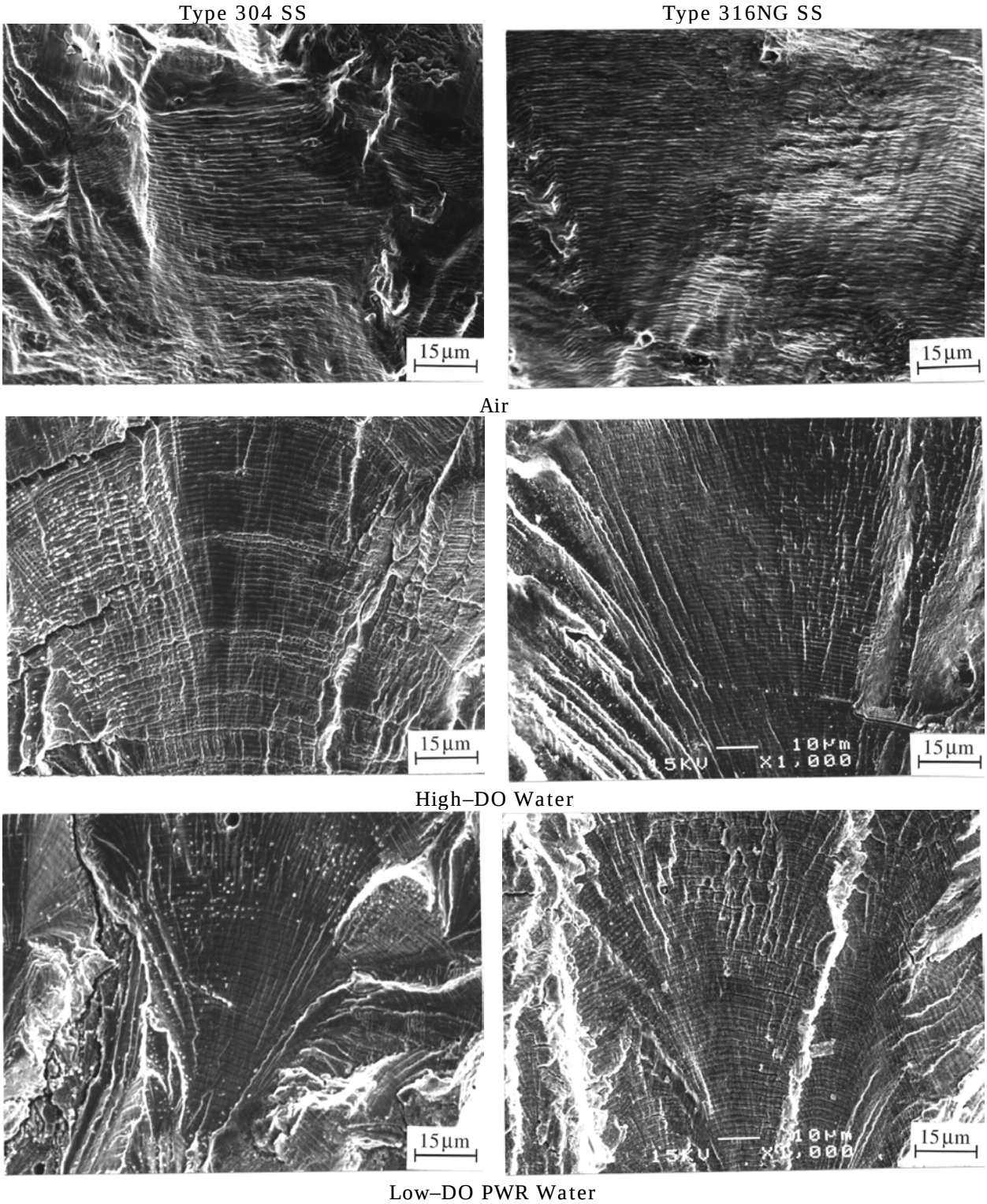

Figure 29. Photomicrographs of fracture surfaces of Types 304 and 316NG SS specimens tested at 288°C, ≈0.75% strain range, and 0.004%/s strain rate in air, high–DO water, and low–DO simulated PWR water

3.4 Surface Oxide Film

The characteristics of the surface oxide films that form on austenitic SSs in LWR coolant environments can influence the mechanism and kinetics of corrosion processes and thereby influence the initiation stage, i.e., the growth of MSCs. Photomicrographs of the gauge surfaces of Type 316NG specimens tested in air, simulated PWR water, and high–DO water are shown in Figs. 30 and 31. Austenitic SSs exposed to LWR environments develop an oxide film that consists of two layers; a fine–grained, tightly–adherent, chromium–rich inner layer, and a crystalline, nickel–rich outer layer composed of large and intermediate–size particles. The inner layer forms by solid–state growth, whereas the crystalline outer layer forms by precipitation or deposition from the solution. A schematic representation of the surface oxide film is shown in Fig. 32.

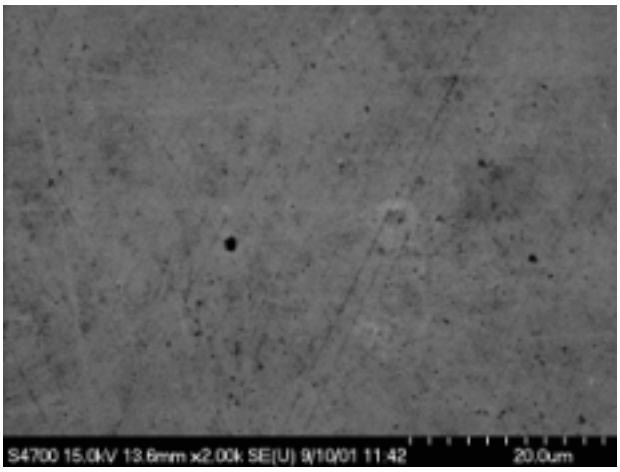

(a)

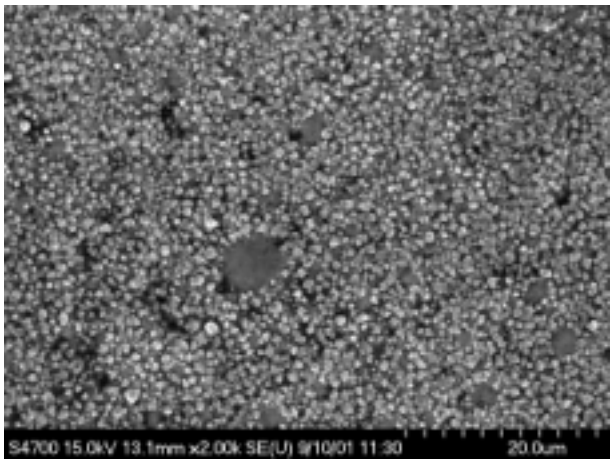

(b)

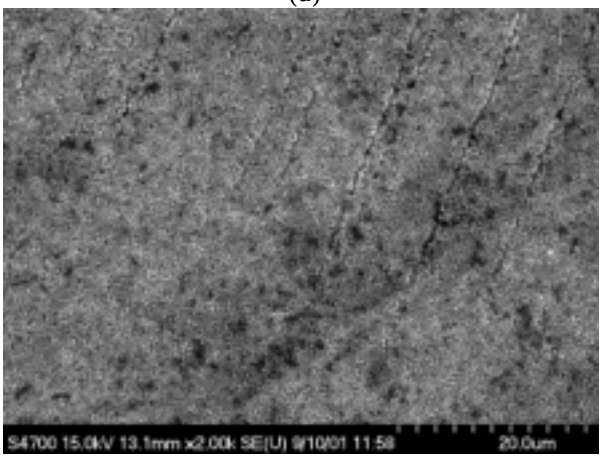

(c)

Figure 30.
Photomicrographs of gauge surfaces of Type 316NG SS specimens tested in (a) air, (b) simulated PWR water, and (c) high–DO water (Refs. 30,31)

Several studies have characterized the oxide films that form on austenitic SSs in LWR environments.[52–58] The inner layer consists of chromium–rich spinel $Ni_xCr_yFe_{3-x-y}O_4$ with nonstoichiometric composition; the actual composition of spinels varies with environmental conditions. Da Cunha Belo et al.[56] determined that the inner layer formed on Type 316L SS in a PWR environment at 350°C consists of mixed chromium oxides (Cr_2O_3 + $FeCr_2O_4$) and Fe_3O_4. Nakayama and Oshida[58] characterized the oxide film on SS exposed to high–DO (8 ppm) water at 300°C as chiefly composed of $NiO{\cdot}(Cr,Fe)_2O_3$ and/or $NiFe_2O_4$, which may be

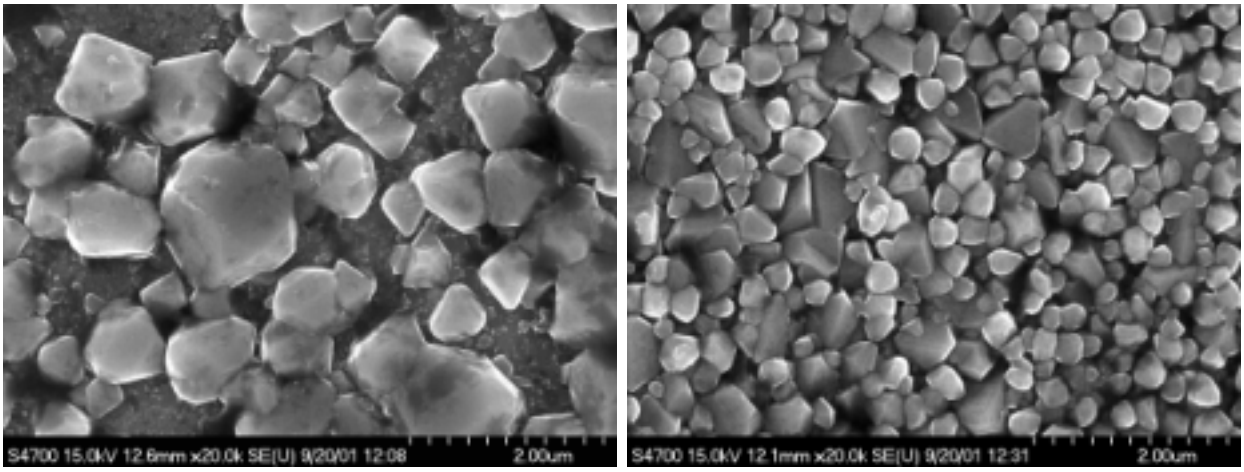

(a) (b)

Figure 31. Higher–magnification photomicrographs of oxide films that formed on Type 316NG stainless steel in (a) simulated PWR water and (b) high–DO water

formed by a solid reaction between NiO and $(Cr,Fe)_2O_3$ or α–Fe_2O_3. Kim[52,53] identified the $FeCr_2O_4$ spinel chromite (or $Fe_xCr_{3-x}O_4$), along with $NiFe_2O_4$, in the inner layer formed on Types 304 and 316 SS exposed at 288°C under conditions of NWC or hydrogen water chemistry (HWC). Kim also noted that the inner oxide layer formed in a NWC BWR environment contains a lower concentration of chromium than that formed in a HWC low–DO environment. Such differences have been attributed to chromium oxidation in high–DO water.

The structure and composition of the crystalline outer layer vary with the water chemistry. In BWR environments, the large particles in the outer layer are primarily composed of α—Fe_2O_3 hematite in NWC, and Fe_3O_4 magnetite in HWC.[52,53] The intermediate particles in the outer layer are composed of α—Fe_2O_3 in NWC and $FeCr_2O_4$ in HWC. The structure of the outer layer varies when the water chemistry is cycled between NWC and HWC. In PWR environments, the large particles have been identified as $Ni_{0.75}Fe_{2.25}O_4$ spinel and the intermediate particles as $Ni_{0.75}Fe_{2.25}O_4$ + Fe_3O_4.[56] The possible effect of minor differences in the surface oxide film on fatigue crack initiation is discussed in the next section.

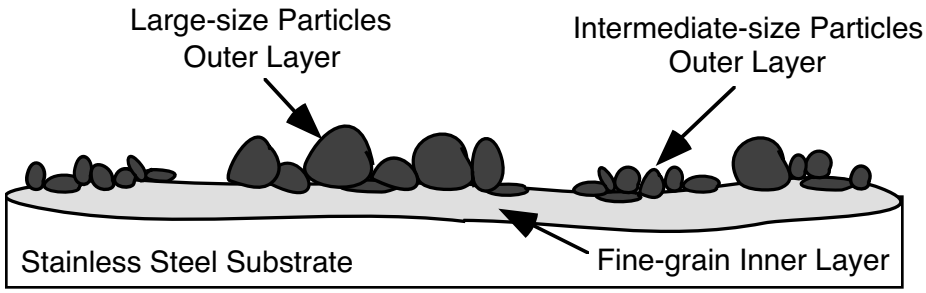

Figure 32. Schematic of the corrosion oxide film formed on austenitic stainless steels in LWR environments

3.5 Exploratory Fatigue Tests

The reduction of fatigue life in high–temperature water has often been attributed to the presence of surface micropits that are formed in high–temperature water and may act as stress raisers and provide preferred sites for the formation of fatigue cracks. In an effort to understand the effects of surface micropits or minor differences in the surface oxide film on fatigue crack initiation, fatigue tests were conducted on Type 316NG (Heat P91576) specimens that were preexposed to either low– or high–DO water and then tested in air or water environments. The results of these tests, and data obtained earlier on this heat and Heat D432804 of Type 316NG SS in air and low–DO water at 288°C, are given in Table 2; the results are plotted in Fig. 33.

Table 2. Fatigue test results for Type 316NG austenitic stainless steel at 288°C and ≈0.5% strain range

Test No.	Dis. Oxygen[a] (ppb)	Dis. Hydrogen (cc/kg)	Li (ppm)	Boron (ppm)	pH at RT	Conduc -tivity[b] (µS/cm)	ECP SS[a] mV (SHE)	Ten. Rate (%/s)	Stress Range (MPa)	Strain Range (%)	Life N_{25} (Cycles)
Heat D432804											
1409	Air Env.	–	–	–	–	–	–	5.0E-1	377.2	0.50	53,144
1410	Air Env.	–	–	–	–	–	–	5.0E-1	377.6	0.50	51,194
1792	Air Env.	–	–	–	–	–	–	5.0E-3	413.4	0.50	35,710
1794	4	23	2	1000	6.4	20.00	–689	5.0E-3	390.9	0.50	7,370
Heat P91576											
1872[c]	Air Env.	–	–	–	–	–	–	4.0E-1	369.3	0.51	48,100
1878[c]	Air Env.	–	–	–	–	–	–	4.0E-3	401.1	0.50	58,300
1879[c]	5	23	–	–	–	0.06	-591	4.0E-3	380.2	0.50	8,310
1880[d]	5	23	–	–	–	0.10	-603	4.0E-3	382.8	0.50	8,420

[a]Measured in effluent.
[b]Measured in feedwater supply tank.
[c]Specimen soaked for 10 days in high–purity water with <5 ppb dissolved oxygen and ≈23 cc/kg dissolved hydrogen.
[d]Specimen soaked for 10 days in high–purity water with ≈500 ppb dissolved oxygen.

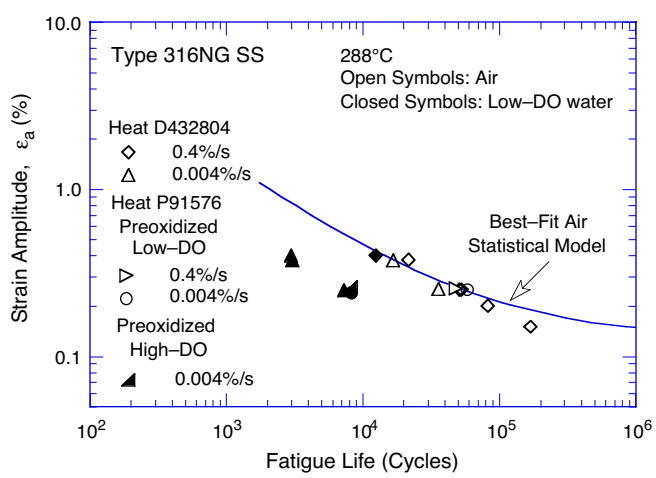

Figure 33.
Effects of environment on formation of fatigue cracks in Type 316NG SS in air and low–DO water environments at 288°C. Preoxidized specimens were exposed for 10 days at 288°C in water that contained either <5 ppb DO and ≈23 cm^3/kg dissolved H_2 or ≈500 ppb DO and no dissolved H_2.

Experimental data given in Table 2 indicate that surface micropits have no effect on the formation of fatigue cracks; the fatigue lives of specimens preoxidized at 288°C in low–DO water and then tested in air are identical to those of unoxidized specimens (Fig. 33). If the presence of micropits was responsible for the reduction in life, the preexposed specimens should show a decrease in life. Also, the fatigue limit of these steels should be lower in water than in air. The fatigue limit of austenitic SSs is approximately the same in water and air

environments. The presence of an oxide film is not a sufficient condition for the environmentally assisted decrease in fatigue lives of materials in LWR environments.

The results also indicate that minor differences in the composition or structure of the surface oxide film also have no effect on the fatigue life of SSs in low–DO water. The fatigue lives of specimens preoxidized in high– or low–DO water and then tested in low–DO water are identical.

4 Operating Experience in the Nuclear Power Industry

Experience with operating nuclear power plants worldwide reveals that many failures may be attributed to fatigue; examples include piping components, nozzles, valves, and pumps.[59–63] In most cases, these failures have been associated with thermal loading due to thermal stratification and striping, or with mechanical loading due to vibratory loading. The thermal stratification is caused by the injection of low–flow, relatively cold feedwater during plant startup, hot standby, and variations below 20% of full power, whereas thermal striping is caused by rapid, localized fluctuations of the interface between hot and cold feedwater. Significant thermal loading due to flow stratification or mixing was not included in the original design basis analyses. Furthermore, the effect of thermal loading may also have been aggravated by corrosion due to a high–temperature aqueous environment.

The mechanism of cracking in feedwater nozzles and piping has been attributed to corrosion fatigue[64,65] or strain–induced corrosion cracking (SICC).[66] Case histories, as well as identification of conditions that lead to SICC of low–alloy steels in LWR systems, have been summarized by Hickling and Blind.[67] A review of significant occurrences of corrosion fatigue damage and failures in various nuclear power plant systems has been presented in an Electric Power Research Institute (EPRI) report.[68] Also, an assessment of the U.S. experience related to PWR primary system leaks observed during the period 1985 through 1996 has been presented by Shah et al.[69]

Hirschberg et al. summarized the operating experience with thermal fatigue of nonisolable piping connected to a PWR reactor coolant system (RCS).[70] Significant cracking has occurred in nonisolable sections of the safety injection system and the piping of a residual–heat removal (RHR) system connected to the PWR coolant system.[71,72] At Farley, cracking occurred in the heat–affected zone of the weld between the first elbow and the horizontal pipe, ≈0.9 m from the cold–leg nozzle of the RCS. At Tihange, the crack was located in the base metal of an elbow, ≈0.6 m from the RCS hot–leg nozzle. At the Genkai plant, cracking occurred in the RHR suction line at the weld between the first elbow downstream of the hot–leg nozzle and the horizontal pipe section. Cracking due to thermal fatigue has also occurred in the safety injection system at the Dampierre 1 and 2 plants, and in the chemical and volume control system (CVCS) of the Obrigheim plant. In all cases, thermal cycling was caused by interaction of hot RCS fluid from turbulent penetration at the top of the pipe, and cold valve leakage fluid that had stratified at the bottom of the pipe. At Genkai, the valve internals alternately shrank and expanded, causing periodic leakage of hot fluid through the stem packing and leak–off line into the elbow.

Thermal stratification, however, can occur even in the absence of valve leakage. Fatigue monitoring indicates that numerous plants measured thermal–stratification cycling in the RHR suction line because the turbulence that penetrated the hot–leg fluid extended into the horizontal pipe section and then stratified because of normal convection.[70] For thermal stratification, the length of the vertical pipe section of the RHR suction line must be short enough for the hot fluid to reach the horizontal pipe section, and the horizontal pipe section must be long enough to increase heat losses. A typical temperature gradient of 49°C and temperature gradients as high as 177°C have been measured in some plants.

Nonisolable leaks due to thermal–stratification cycling have also occurred in the drain lines of the reactor coolant loop, excess letdown lines, and makeup/high–pressure injection

lines at Three Mile Island (TMI), Loviisa 2, Mihama, and Oconee plants.[69] A leak in the cold–leg drain line has occurred in the weld between the first elbow downstream of the loop nozzle and the horizontal pipe section at TMI, and in the elbow extrados at Oconee. In both cases, thermal stratification occurred because turbulent penetration of the RCS fluid periodically extended into the horizontal section of the pipe, and heat was lost because the pipe was not insulated. The same mechanism caused a leak in the excess letdown line at Mihama; the difference was that in the Mihama line, which was insulated, stratification occurred because the horizontal section to the isolation valve was very long, and this led to significant heat loss.

Thermal fatigue has caused leaks in a connecting pipe and shell of the regenerative heat exchanger in the CVCS at Tsuruga 2[73,74] and in a 250–mm pipe section of the heat exchanger bypass of the RHR system at Civaux 1.[75] Thermo–hydraulic mock–up tests indicate that at Tsuruga, thermal fatigue has been caused by superposition of low–frequency temperature gradients due to change in flow pattern, and high–frequency fluctuations due to mixing of the bypass flow and main flow.[73,74]

Regulatory evaluation has indicated that thermal–stratification cycling can occur in all PWR surge lines.[76] In PWRs, the pressurizer water is heated to ≈227°C. The hot water, flowing at a very slow rate from the pressurizer through the surge line to the hot–leg piping, rides on a cooler water layer. The thermal gradients between the upper and lower parts of the pipe can be as high as 149°C.

Cracking has also occurred in austenitic SS channel heads in an experimental test loop used for stress corrosion cracking studies in a simulated PWR environment.[77] Cracks were observed in a region that was subjected to temperature fluctuations between 170 and 190°C at a frequency of 0.05 Hz. The cracks were initiated on the inner surface and exhibited a cracking morphology that was essentially transgranular, with fatigue–like striations visible in some regions of the fracture surface. Thermal fatigue, with possible effects of the PWR coolant environment, was considered the root cause of these failures.[77]

In nonisolable pipe sections, cracking due to thermal cycling has generally been termed high–cycle fatigue, i.e., it occurs at stress levels that correspond to allowable fatigue cycles of 10^5 or higher. The current understanding of turbulence penetration can not accurately predict the frequency of thermal cycling. Environmental effects on fatigue crack initiation can be significant in low–DO water at stress levels above the threshold value and at strain rates <0.4%/s.

Lenz et al.[66] showed that in feedwater lines, strain rates are 10^{-3}–10^{-5}%/s due to thermal stratification, and 10^{-1}%/s due to thermal shock, and that thermal stratification is the primary cause of crack initiation due to SICC. Full–scale mock-up tests to generate thermal stratification in a pipe in a laboratory have confirmed the applicability of laboratory data to component behavior.[78,79] Under the conditions of strain rate and strain range that are typical of thermal stratification in these piping systems, the coolant environment is known to have a significant effect on fatigue crack initiation.[6,22,23]

5 Statistical Model

5.1 Least–Squares Fit

The fatigue ε–N data are generally expressed by Eq. 1, which may be rearranged to express fatigue life N in terms of strain amplitude ε_a as

$$\ln(N) = (1/n1)\ln(A1) - (1/n1)\ln(\varepsilon_a - A2), \tag{14}$$

or $$\ln(N) = A - B\ln(\varepsilon_a - C), \tag{15}$$

where A, B, C are coefficients of the model. Additional terms are included in the model to account for environmental effects and improve agreement with the existing fatigue database. Model features that would be counter to known effects are excluded.

The ASTM designation E739, "Standard Practice for Statistical Analysis of Linear or Linearized Stress–Life (ε–N) and Strain–Life (ε–N) Fatigue Data," treats fatigue life N (or the logarithm of the fatigue life) as the dependent variable and the controlled variables, e.g., stress or strain, as the independent variable. The coefficients of a "linear" model are commonly established through least–squares curve–fitting of the data using fatigue life as the dependent variable. An optimization program sets the coefficients to minimize the sum of the square of the residual errors, which are the differences between the predicted and actual values of N or ln(N). However, such an approach may not be adequate to determine the optimum coefficients of a nonlinear expression such as Eq. 15, which includes a term C related to the fatigue limit. The model fails to address the fact that at low ε_a, most of the error in life is due to uncertainty associated with either measurement of stress or strain or variation in threshold strain caused by material variability. A predictive model based on least–squares fit on N or ln(N) is biased for low ε_a; also, runoff data cannot be included.

The statistical models presented earlier in Refs. 3 and 8 were developed by minimizing the sum of squared Cartesian distances from the data points to the predicted curve. For low ε_a, this approach is very close to optimizing the sum of squared errors in predicted ε_a; at high ε_a, it is very close to optimizing the sum of squared errors in predicted life. Also, because the statistical model includes many nonlinear transformations of variables that account for environmental effects on life and because these variables affect various parts of the data, the actual functional form and transformations are partly responsible for minimizing the squares of the errors. The functional forms and transformation for these variables were chosen a priori on the basis of experimental observations and data trends.

5.2 The ANL Statistical Model

5.2.1 Air Environment

The statistical model for austenitic SSs presented in Refs. 3 and 8 assumes that the fatigue life in air is independent of temperature and that strain rate effects occur at temperatures above 250°C. The possible effect of strain rate on life was included in the model on the basis of very limited data. The existing fatigue ε–N data indicate that variation in strain rate in the range of 0.4–0.008%/s has no effect on the fatigue life of austenitic SSs at

temperatures up to 400°C.[34] In the present report, the effects of strain rate on fatigue life have been excluded from the model, and the existing fatigue data in air have been reevaluated to determine the optimum coefficients of the model. Because exclusion of strain rate effects on fatigue life is not likely to influence coefficient C in Eq. 15, the value C = 0.126 was retained from the earlier analysis; new values of coefficients A and B were determined from least–squares analysis of the data to minimize the sum of squared errors in predicted ln(N).

For Types 304 and 316 SS, the model coefficients A and B obtained from a reevaluation of the data did not significantly differ from those obtained earlier; the values from NUREG/CR–5704 were retained. However, different coefficients were obtained for Type 316NG SS because a larger database was used in the present than in the earlier analysis. In air at temperatures up to 400°C, the fatigue data for Types 304 and 316 SS are best represented by

$$\ln(N) = 6.703 - 2.030 \ln(\varepsilon_a - 0.126) \tag{16}$$

and for Type 316NG, by

$$\ln(N) = 7.433 - 1.782 \ln(\varepsilon_a - 0.126). \tag{17}$$

These correlations are recommended for predicted fatigue lives $\leq 10^6$ cycles.

5.2.2 LWR Environments

As more fatigue ε–N data became available, the statistical model for austenitic SSs in LWR environments was updated.[3,6,8] In NUREG/CR–5704, separate correlations were proposed for low– and high–DO levels (< or ≥0.05 ppm), and low and high temperatures (< or ≥200°C).[3] The temperature dependence proposed by the Pressure Vessel Research Council (PVRC) steering committee for cyclic life and environmental effects (CLEE) was adopted in NUREG/CR–6717; environmental effects were considered moderate at temperatures below 180°C and significant above 220°C, and increased linearly between 180 and 220°C.[6] Also, in NUREG/CR–6717, environmental effects were considered moderate for wrought austenitic SSs in high–DO water with ≥0.05 ppm DO; for cast austenitic SSs, environmental effects were considered the same in both low– and high–DO water and equal to those for wrought SSs in low–DO water. The functional forms describing the effects of temperature and DO level on fatigue life have been revised in the present report.

The critical parameters that influence fatigue life and the threshold values of these parameters for environmental effects to be significant have been summarized in the previous section. In LWR environments, the fatigue life of austenitic SSs depends on strain rate, DO level, and temperature. The functional forms for the effects of strain rate and temperature were based on the data trends shown in Figs. 9 and 12, respectively. For both wrought and cast austenitic SSs, the model assumes threshold and saturation values of 0.4 and 0.0004%/s, respectively, for strain rate, and a threshold value of 150°C for temperature.

The influence of DO level on the fatigue life of austenitic SSs is not well understood. The fatigue lives are decreased significantly in low–DO water, whereas in high–DO water they are either comparable or, for some steels, higher than those in low–DO water. The composition or heat treatment of the steel may influence the magnitude of environmental effects on austenitic SSs. For example, in low–DO water, the fatigue life of sensitized Types 304 and 316 SS is the

same as that of solution–annealed steel, whereas, in high–DO water, it is lower for the sensitized steel. Until more data are available to clearly establish the effects of DO level on fatigue life, the effect of DO level on fatigue life is assumed to be the same in low– and high–DO water and for wrought and cast austenitic SSs.

The least–squares fit of the experimental data in water yields a steeper slope for the ε–N curve than the slope of the curve obtained in air, i.e., coefficient B in Eq. 15 is smaller in water than in air. These results indicate that environmental effects are more pronounced at low than at high strain amplitudes. Such behavior is difficult to rationalize in terms of the mechanisms that have been proposed for fatigue crack initiation in LWR environments. Furthermore, different slopes for the ε–N curves in air and water environments would add complexity to the determination of the environmental correction factor F_{en}, discussed later in this paper. In NUREG/CR–5704 and NUREG/CR–6717, the slope of the ε–N curve was assumed to be the same in LWR and air environments.[3,6]

The mechanism of fatigue crack initiation in austenitic SSs in LWR environments has been examined in Section 3. Fatigue crack initiation has been divided into two stages: an initiation stage that involves the growth of microstructurally small cracks (MSCs) (i.e., cracks smaller than ≈200 μm), and a propagation stage that involves the growth of mechanically small cracks. The reduction in fatigue life of these steels is caused primarily by the effects of environment on the growth of MSCs and, to a lesser extent, on enhanced growth rates of mechanically small cracks. Environmental effects on the growth of MSCs may be more pronounced at low strain amplitudes. Such behavior may explain the steep slope for the ε–N curve in water and should be further investigated. Until further data become available to establish the effects of DO level in the water and composition and heat treatment of the steel on the fatigue life of austenitic SSs, the slope of the ε–N curve is assumed to be the same in LWR and air environments.

The existing fatigue ε–N data were reanalyzed to determine the coefficients of the statistical model for austenitic SSs in LWR environments. Certain data sets were excluded from the analysis. For example, because environmental effects are significantly greater on sensitized steels in high–DO water than on solution–annealed steel, the data for sensitized Types 304 and 316 SS in high–DO water were excluded. Also, based on the test results obtained at ANL (Fig. 10a)[6] the data in high–DO (>0.1 ppm) water that were obtained at temperatures >150°C and strain rates <0.4%/s were also excluded from the analysis; for these tests, the environmental conditions may not have been stable.

The model coefficients obtained from a reevaluation of the data did not significantly differ from those reported earlier in NUREG/CR-5704. The results indicate that, in LWR environments, fatigue data for Types 304 and 316 SS are best represented by

$$\ln(N) = 5.768 - 2.030 \ln(\varepsilon_a - 0.126) + T' \dot{\varepsilon}' O' \tag{18}$$

and that of Type 316NG, as

$$\ln(N) = 6.913 - 1.671 \ln(\varepsilon_a - 0.126) + T' \dot{\varepsilon}' O', \tag{19}$$

where T', $\dot{\varepsilon}'$, and O' are transformed temperature, strain rate, and DO, respectively, defined as follows:

$$T' = 0 \qquad (T < 150°C)$$
$$T' = (T - 150)/175 \qquad (150 \le T < 325°C)$$
$$T' = 1 \qquad (T \ge 325°C) \qquad (20)$$

$$\dot{\varepsilon} = 0 \qquad (\dot{\varepsilon} > 0.4\%/s)$$
$$\dot{\varepsilon} = \ln(\dot{\varepsilon}/0.4) \qquad (0.0004 \le \dot{\varepsilon} \le 0.4\%/s)$$
$$\dot{\varepsilon} = \ln(0.0004/0.4) \qquad (\dot{\varepsilon} < 0.0004\%/s) \qquad (21)$$

$$O' = 0.26 \qquad \text{(all DO levels).} \qquad (22)$$

These models are recommended for predicted fatigue lives $\le 10^6$ cycles. Equations 18 and 20–22 should also be used for cast austenitic SSs such as CF-3, CF-8, and CF–8M. As noted earlier, because the influence of DO level on the fatigue life of austenitic SSs is not well understood, these models may be somewhat conservative for some SSs in high–DO water.

5.3 Japanese MITI Guidelines

The guidelines proposed by the Japanese Ministry of International Trade and Industry (MITI), for assessing the decrease in fatigue life in LWR environments, have been presented by Iida et al.[14] The reduction in fatigue life of various pressure vessel and piping steels in LWR environments is expressed in terms of an environmental fatigue life correction factor F_{en}, which is the ratio of the fatigue life in air at ambient temperature to that in water at the service temperature.[10] For austenitic SSs, F_{en} is expressed in terms of strain rate $\dot{\varepsilon}$ (%/s), temperature T (°C), and strain amplitude ε_a (%) as follows,

$$\ln(F_{en}) = 1.233 - P \ln(\dot{\varepsilon}^*/0.4) \qquad (23)$$

where

$$P = 0.04 \qquad (T \le 100°C)$$
$$P = 9.33 \times 10^{-4}\, T - 0.053 \qquad (100 < T < 325°C)$$
$$P = 0.25 \qquad (T \ge 325°C) \qquad (24)$$

$$\dot{\varepsilon}^* = 0.4 \qquad (\dot{\varepsilon} > 0.4\%/s)$$
$$\dot{\varepsilon}^* = \dot{\varepsilon} \qquad (0.0004 \le \dot{\varepsilon} \le 0.4\%/s)$$
$$\dot{\varepsilon}^* = 0.0004 \qquad (\dot{\varepsilon} < 0.0004\%/s). \qquad (25)$$

$$F_{en} = 1 \qquad (\varepsilon_a \le 0.11\%). \qquad (26)$$

To incorporate environmental effects, a fatigue usage for a specific stress cycle, based on the current Code fatigue design curve, is multiplied by the correction factor.

5.4 Model Developed by the Bettis Laboratory

Based on the available fatigue ε–N data, a model has been developed by the Bettis Laboratory.[80] In this model, the Smith–Watson–Topper (SWT) equivalent strain parameter[81] is used to predict the fatigue life of austenitic SSs in LWR environments under prototypical temperatures and loading rates. The model indicates that the fatigue life of Type 304 SS in water depends on the temperature, strain rate, applied strain amplitude, and water oxygen level. For low–DO water, the fatigue life can be reduced by as much as a factor of 13 at high

temperatures and low strain rates. The Bettis model for predicting fatigue life N in LWR environments is of the following form:

$$N = A \cdot \left(\varepsilon_{SWT} - \varepsilon_0\right)^b \cdot \left[P + \left(1 - P\right) \cdot e^{-kZ^m}\right] \tag{27}$$

where A, b, P, k, ε_0, and m are model constants, and the SWT parameter ε_{SWT} is given by

$$\varepsilon_{SWT} = \left(\varepsilon_a\right)^c \cdot \left(\frac{\sigma_{max}}{E}\right)^{1-c}, \tag{28}$$

in which maximum stress σ_{max} is the sum of the cyclic stress amplitude σ_a and mean stress σ_{mean} (i.e., = $\sigma_a + \sigma_{mean}$), E is the elastic modulus, and c is a constant determined from fatigue tests in air, some of which had an imposed mean stress. The effects of temperature T (K) and strain rate $\dot{\varepsilon}$ (s^{-1}) are incorporated into the model by using the Zener–Hollomon parameter Z, given by

$$Z = \dot{\varepsilon} \cdot e^{\frac{Q}{RT}}, \tag{29}$$

where R is the gas constant and Q is the fitted value of the activation energy. The model constants in Eqs. 27–29 were determined from the existing fatigue ε–N data in water.[80] The constant A is given by

$$\ln(A) = -4.010 + 0.438\ \mathrm{Mat} + 1.030\ \mathrm{O2}, \tag{30}$$

where Mat = 1 for Type 316NG SS and = 0 otherwise, and O2 = 1 for high DO water and = 0 otherwise. The values of other constants are as follows:

b = – 2.10
ε_0 = 8.75 x 10^{-4} mm/mm
P = 0.0359
k = 9.65 (low DO)
k = 20.0 (high DO)
Q = 94.56 kJ/mol (22.6 kcal/mol)
m = – 0.187

The cyclic stress amplitude σ_a (MPa) corresponding to a given strain amplitude, ε_a (mm/mm), is obtained from the cyclic stress–vs.–strain curves in air, given by

$$\sigma_a = (175 - 0.342\ T + 7.10 \times 10^{-4}\ T^2) + (24010 - 4.54 \times 10^{-2}\ T^2 + 156\ \sigma_{mean})\ \varepsilon_a, \tag{31}$$

where T is the temperature (°C), and σ_m is the mean stress (MPa). This cyclic stress–strain curve is valid for stresses above the proportional limit. Below the proportional limit, the stress amplitude is simply the product of the elastic modulus and strain amplitude. The fatigue ε–N curve at zero mean stress can be obtained from Eqs. 27–31 by substituting a value of zero for σ_{mean} in Eqs. 28 and 31.

5.5 Comparison of Various Estimation Schemes

The experimental fatigue ε–N data for austenitic SSs in LWR environments and the corresponding fatigue ε–N curves predicted from the Bettis, ANL, and MITI models are shown in Figs. 34–36. The fatigue lives in LWR environments predicted from the MITI model were determined by multiplying the values obtained from the ASME Code mean fatigue curve by F_{en} calculated from Eq. 23. The Code mean curve is given by

$$\ln(N) = 6.954 - 2.0 \ln(\varepsilon_a - 0.167) \tag{32}$$

where N is the fatigue life, and ε_a is the applied strain amplitude (%). The estimated lives from all models are comparable in the low–cycle regime, i.e., fatigue lives $<10^4$ cycles. The fatigue lives estimated from the MITI guidelines show poor agreement with the experimental data at fatigue lives $>10^3$ cycles (Fig. 36), e.g., the estimated lives are longer than those observed experimentally. The poor agreement is primarily due to the difference between the ASME Code mean fatigue curve and the experimental data. Figure 2 shows that the ASME mean curve is

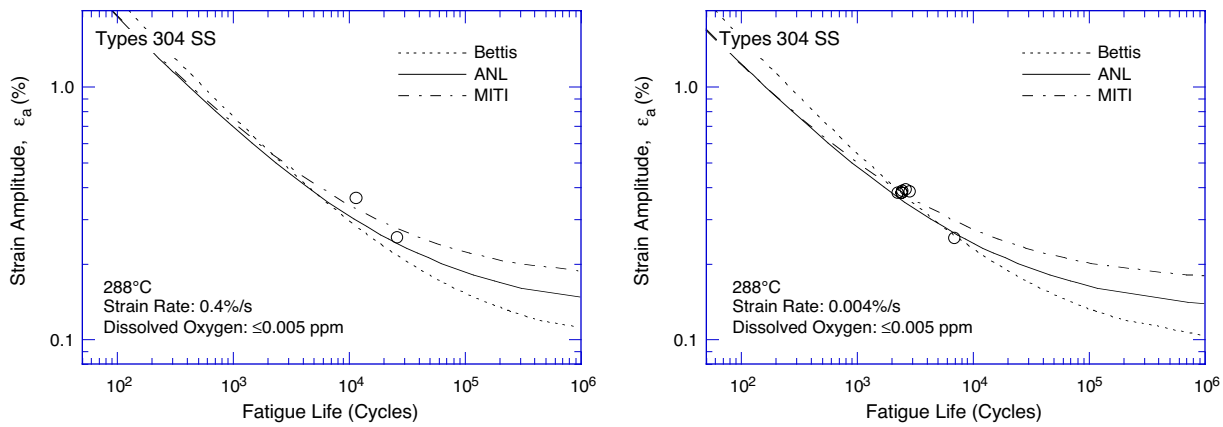

(a) (b)

Figure 34. Experimental and predicted ε–N behavior for Type 304 SS in low–DO water at 289°C and (a) 0.4 and (b) 0.004%/s strain rate

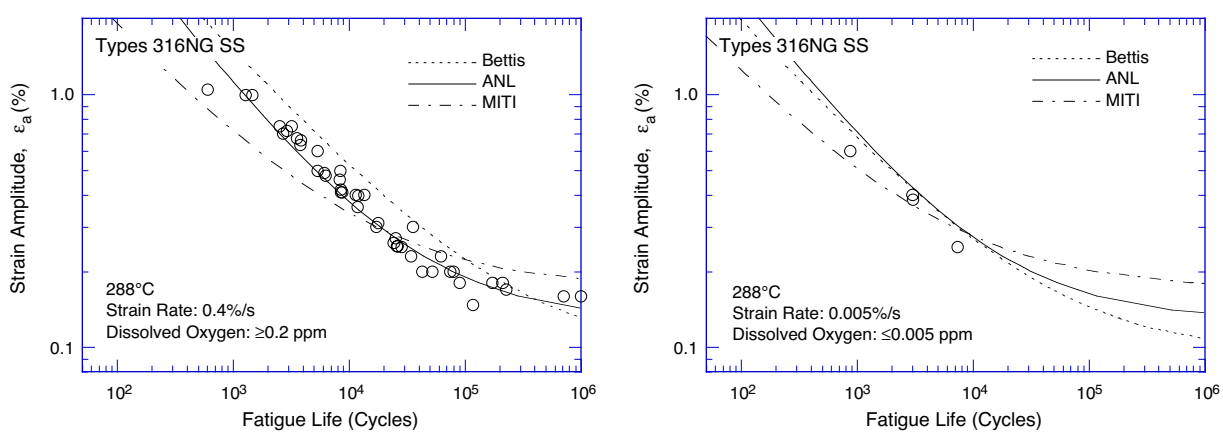

(a) (b)

Figure 35. Experimental and predicted ε–N behavior for Type 316NG SS at 289°C in (a) high–DO water and 0.4%/s strain rate and (b) low–DO water and 0.005%/s strain rate

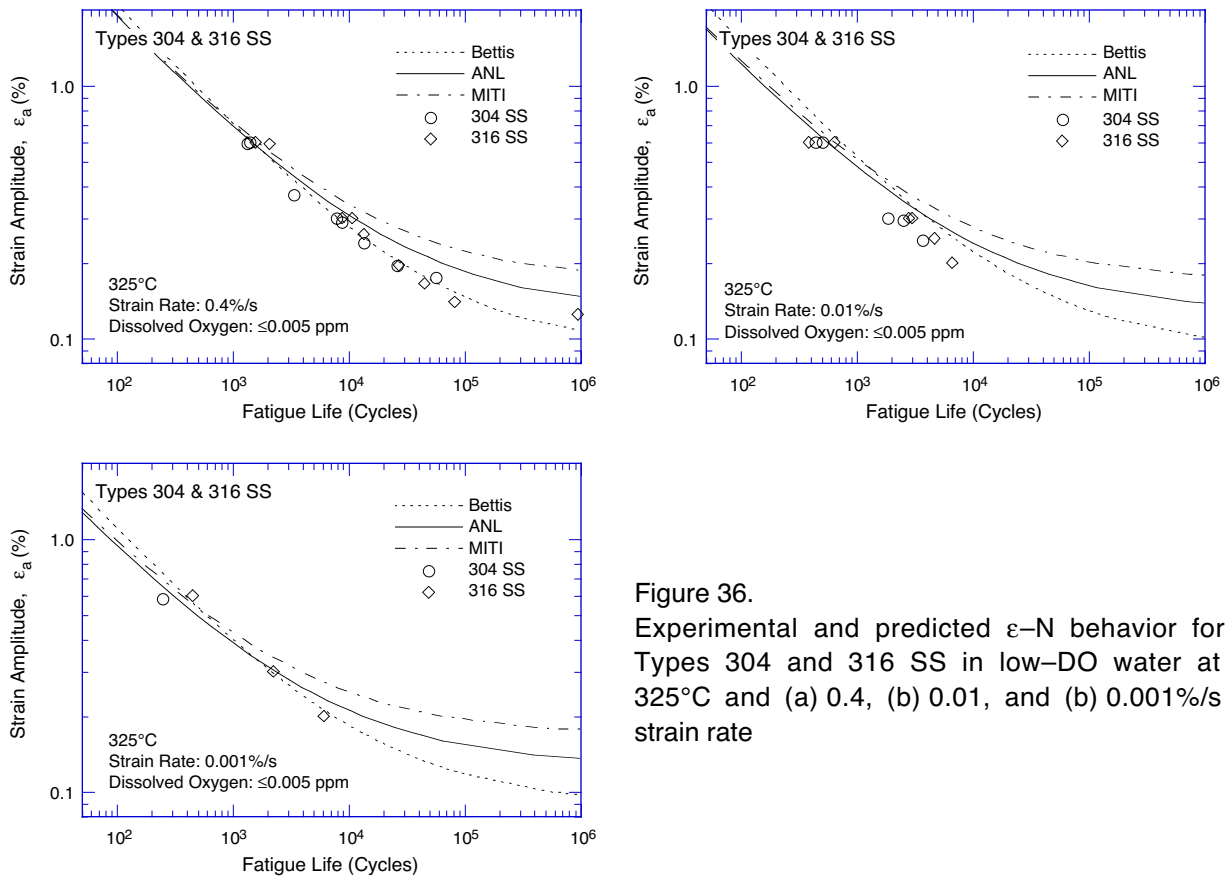

Figure 36.
Experimental and predicted ε–N behavior for Types 304 and 316 SS in low–DO water at 325°C and (a) 0.4, (b) 0.01, and (b) 0.001%/s strain rate

not consistent with the existing fatigue ε–N data for austenitic SSs; at strain amplitudes <0.5%, the mean curve predicts significantly longer fatigue lives than those observed experimentally. Because the fatigue life correction factor F_{en} in the MITI guidelines is applied to fatigue lives determined from the ASME Code curves, estimated fatigue lives at low strain amplitudes (e.g., ≤0.5%) in these guidelines are expected to be longer than those observed experimentally.

In the high–cycle regime, the Bettis model predicts lower lives than the other models. The fatigue ε–N behavior in the high–cycle regime in LWR environments cannot be accurately established because the experimental data are very limited. Exploratory tests in LWR environments indicate that a minimum threshold strain is required for environmentally assisted decrease in the fatigue life of austenitic SSs.[23,25] The threshold strain is comparable to the fatigue limit for the material. In the ANL model, constant C in Eq. 15 (which is related to the fatigue limit) is considered to be the same in air and water environments. In the Bettis model, constant ε_0 in Eq. 27 was determined from the best–fit of existing fatigue ε–N data in LWR environments, which included the results of fatigue tests with mean stress.

The experimentally observed dependence on temperature and strain rate of the fatigue life of austenitic SSs in LWR environments, and that predicted from the Bettis, ANL, and MITI models is shown in Figs. 37 and 38, respectively. Except for the estimates of the MITI model at low strain amplitudes, the fatigue lives predicted from all models show good agreement with the experimental data.

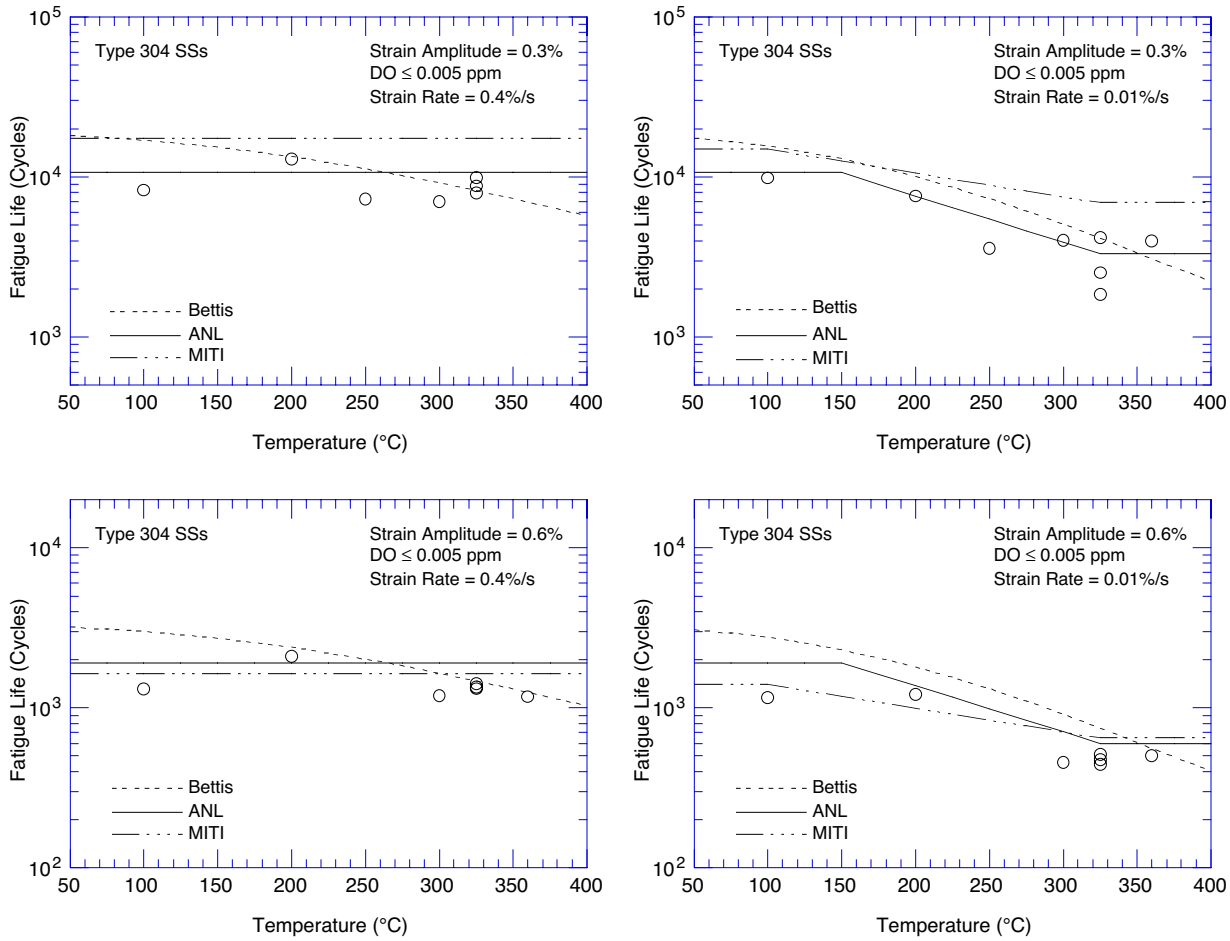

Figure 37. Experimental and predicted change in the fatigue lives of Type 304 SS with temperature in low–DO water at 0.3 and 0.6% strain amplitudes and 0.4 and 0.01%/s strain rates

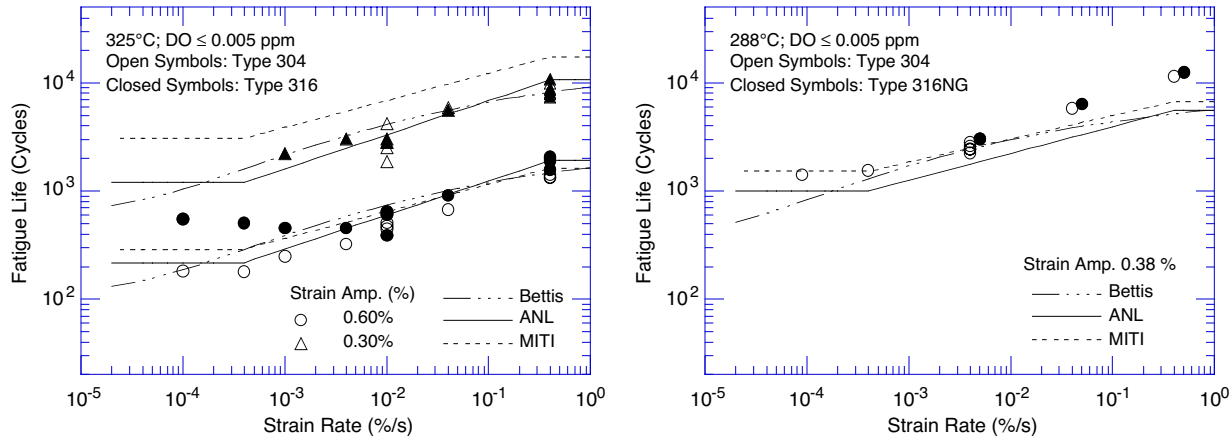

Figure 38. Experimental and predicted change in the fatigue lives of austenitic SS with strain rate in low–DO water at 325°C

6 Incorporating Environmental Effects into Fatigue Evaluations

Two procedures are currently being proposed for incorporating the effects of LWR coolant environments into the ASME Section III fatigue evaluations. Either develop a new set of environmentally adjusted fatigue design curves[3,6,32] or use a fatigue life correction factor F_{en} to adjust the current ASME Code fatigue usage values for environmental effects.[3,6,11–13] For both approaches, the range and bounding values must be defined for key loading and environmental parameters that influence fatigue life. Estimates of fatigue life based on the two approaches may differ because of differences between the ASME mean curves used to develop the current design curves and the best–fit curves to the existing data that are used to develop the environmentally adjusted curves. However, either method provides an acceptable approach to account for environmental effects.

6.1 Fatigue Design Curves

A set of environmentally adjusted fatigue design curves may be developed from the best–fit stress–vs.–life curves to the experimental data in LWR environments by following the procedure that was used to develop the current ASME Code fatigue design curves. The stress–vs.–life curve is obtained from the ε–N curve, e.g., stress amplitude is the product of strain amplitude and elastic modulus. The best–fit experimental curves are first adjusted for the effect of mean stress. The current ASME Code fatigue design curve for austenitic SSs does not include a mean stress correction below 10^6 cycles because, for the current Code mean curve, the fatigue strength at 10^6 cycles is greater than the monotonic yield strength of these steels. However, studies by Wire et al.[82] to establish the effect of mean stress on the fatigue life of Type 304 SS indicate an apparent reduction of up to 26% in strain amplitude in the low– and intermediate–cycle regime (i.e., $<10^6$ cycles) for a mean stress of 138 MPa. Also, the fatigue strength at 10^6 cycles for the best fit of the existing fatigue ε–N data (Eqs. 16 or 18) is lower than the monotonic yield strength of austenitic SSs. The best–fit curve was corrected for mean stress effects with the modified Goodman relationship given by

$$S'_a = S_a\left(\frac{\sigma_u - \sigma_y}{\sigma_u - S_a}\right) \qquad \text{for } S_a < \sigma_y, \tag{33}$$

and

$$S'_a = S_a \qquad \text{for } S_a > \sigma_y, \tag{34}$$

where S'_a is the adjusted value of stress amplitude, and σ_y and σ_u are yield and ultimate strengths of the material, respectively. Equations 33 and 34 assume the maximum possible mean stress and typically give a conservative adjustment for mean stress, at least when environmental effects are not significant. The fatigue design curves are then obtained by lowering the adjusted best–fit curve by a factor of 2 on stress or 20 on cycles, whichever is more conservative, to account for differences and uncertainties in fatigue life that are associated with material and loading conditions.

The new fatigue design curve for austenitic SS in air is shown in Fig. 39, and those in LWR coolant environments at 250, 289, and 325°C, corresponding to strain rates of 0.4, 0.04, 0.004, and a saturation value of 0.0004%/s, are shown in Fig. 40. The new design curves are

based on Eqs. 16 and 18, respectively, for air and water environments. Because the fatigue life of Type 316NG is superior to that of Types 304 or 316 SS at high strain amplitudes, the design curves in Figs. 39 and 40 are somewhat conservative for Type 316NG SS. The results indicate that, in room–temperature air, the current ASME Code design curve for austenitic SSs is nonconservative with respect to the design curve based on the statistical model. The margins between the current Code design curve and the best fit of existing experimental data in air are ≈1.5 on stress and 10–16 on cycles instead of the 2 and 20 originally intended.

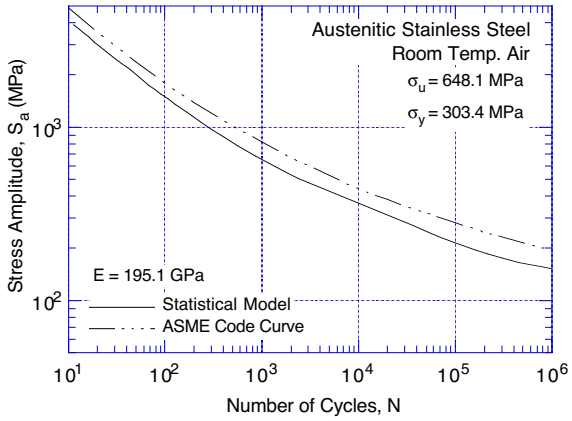

Figure 39.
Fatigue design curves developed from statistical model for austenitic stainless steels in air at room temperature

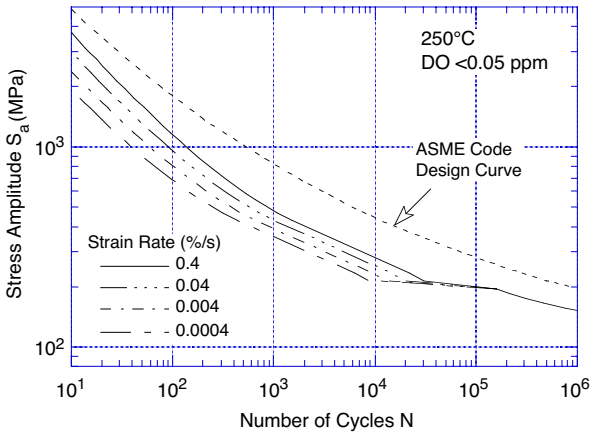

(a)

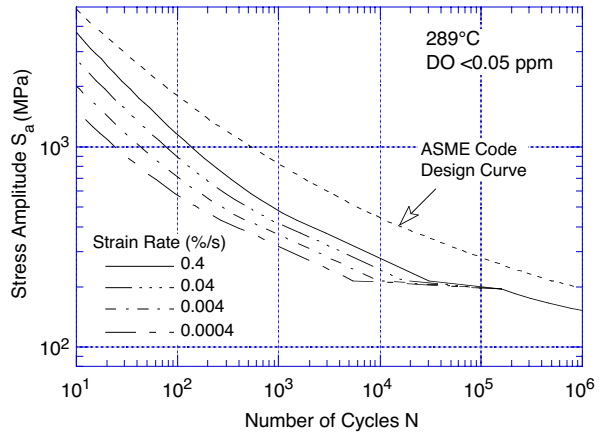

(b)

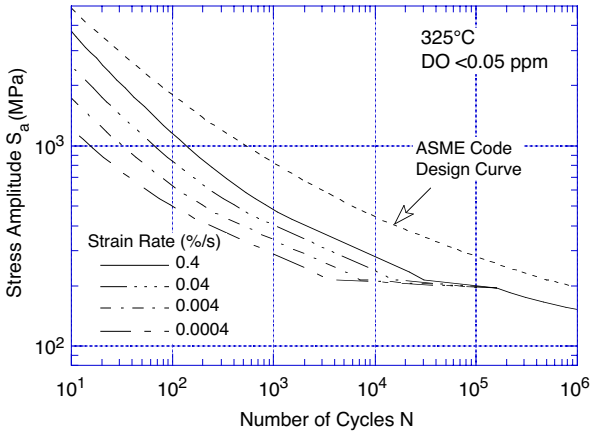

(c)

Figure 40.
Fatigue design curves developed from statistical models for austenitic stainless steels in water with <0.05 ppm DO at (a) 250°C, (b) 289°C, and (c) 325°C

For environmentally adjusted fatigue design curves, a minimum threshold strain is defined, below which environmental effects are modest. The existing fatigue data indicate a threshold strain range of ≈0.32% for austenitic SSs. These values must be adjusted for mean stress effects and variability due to material and experimental scatter. The threshold strain amplitude is decreased by ≈10% to account for mean stress effects and by a factor of 1.5 to account for uncertainties in fatigue life that are associated with material and loading variability. Thus, a threshold strain amplitude of ≈0.1% (stress amplitude of 189 MPa) is obtained for austenitic SSs. The PVRC steering committee for CLEE* has endorsed this threshold value and proposed a ramp for the threshold strain: a lower strain amplitude below which environmental effects are insignificant, a slightly higher strain amplitude above which environmental effects decrease fatigue life, and a ramp between the two values. The two strain amplitudes are 0.10 and 0.11% for austenitic SSs (both wrought and cast).

6.2 Fatigue Life Correction Factor

The effects of reactor coolant environments on fatigue life have also been expressed in terms of a fatigue life correction factor F_{en}, which is the ratio of life in air at room temperature to that in water at the service temperature.[10] A fatigue life correction factor F_{en} can be obtained from the statistical model (Eqs. 16 and 18), where

$$\ln(F_{en}) = \ln(N_{RTair}) - \ln(N_{water}). \tag{35}$$

The fatigue life correction factor for austenitic SSs is given by

$$\ln(F_{en}) = 0.418 - 0.323 \ln(\varepsilon_a - 0.126) - T' \dot{\varepsilon}' O', \tag{36}$$

where the constants T', $\dot{\varepsilon}$', and O' are defined in Eqs. 20–22. Also defined is a strain threshold, shown in Fig. 40, below which environmental effects are modest.

To incorporate environmental effects into the Section III fatigue evaluation, a fatigue usage for a specific stress cycle, based on the current Code fatigue design curve, is multiplied by the correction factor. In Fig. 41, the experimental data adjusted for environmental effects, i.e., the product of experimentally observed fatigue life in LWR environments and F_{en}, are presented with the best–fit ε–N curve in room–temperature air.

The F_{en} correction factor approach (or the EPRI/GE approach) to incorporate environmental effects into the fatigue evaluations has been proposed by Mehta and Gosselin.[11,12] The approach has recently been updated to include the revised statistical models and the PVRC discussions on evaluating environmental fatigue.[13] In the EPRI/GE approach, an "effective" fatigue life correction factor, expressed as $F_{en,eff} = F_{en}/Z$, is also defined, where Z is a factor that represents the perceived conservatism in the ASME Code design curves. The $F_{en,eff}$ approach presumes that all uncertainties have been anticipated and accounted for. The possible conservatism in the current ASME Code design curves is discussed in the next section.

---

*Welding Research Council Progress Report, Vol. LIX No. 5/6, May/June 1999.

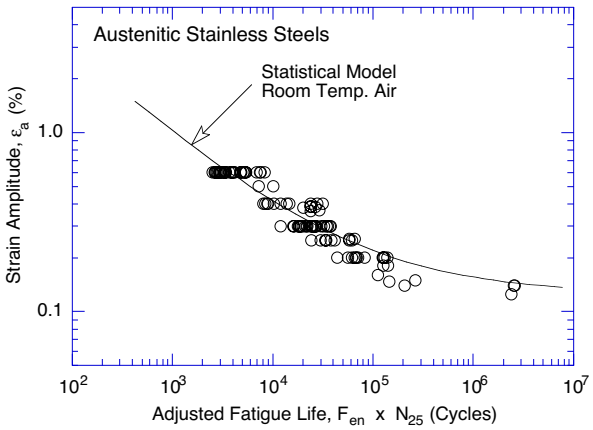

Figure 41.
Experimental data adjusted for environmental effects and best–fit fatigue ε–N curve in room–temperature air for austenitic stainless steels

7 Conservatism in Fatigue Design Curves

The conservatism in the ASME Code fatigue evaluations may arise from (a) the fatigue evaluation procedures and/or (b) the Code fatigue design curves. The overall conservatism in ASME Code fatigue evaluation procedures has been demonstrated in fatigue tests on piping welds and components.[83] In air, the margins between the number of test cycles to failure and the Code allowable number of cycles were 40–310 and 104–510, respectively, for austenitic SS elbows and tees. The margins for girth butt welds were significantly lower at 6–77. In these tests, fatigue life was expressed as the number of cycles for the crack to penetrate through the wall, which ranged in thickness from 6 to 18 mm. The fatigue design curves represent the number of cycles to form a 3–mm–deep crack. Consequently, depending on wall thickness, the actual margins to failure may be lower by a factor of >2.

Deardorff and Smith[84] discussed the types and extent of conservatisms present in the ASME Section III fatigue evaluation procedures and the effects of LWR environments on fatigue margins. The sources of conservatism include design transients that are significantly more severe than those experienced in service, grouping of transients, and simplified elastic–plastic analysis. Environmental effects on two components, the BWR feedwater nozzle/safe end and PWR steam generator feedwater nozzle/safe end, which are known to be affected by severe thermal transients, were also investigated in the study. When environmental effects on fatigue life were not considered, these authors estimated that the ratio of the cumulative usage factors (CUFs) computed with the mean experimental curve for test specimen data to the CUFs computed with the Code fatigue design curve were ≈60 and 90, respectively, for the PWR and BWR nozzles. They estimated the reductions in these margins due to environmental effects to be factors of 5.2 and 4.6 for PWR and BWR nozzles, respectively. Deardorff and Smith[84] argue that, after accounting for environmental effects, there is a factor of 12 and 20 margin on life, respectively, for PWR and BWR nozzles; these factors account for uncertainties due to material variability, surface finish, specimen size, mean stress, and loading history.

Much of the margin arises from the current design procedures, e.g., stress analysis rules, cycle counting, etc., which, as discussed by Deardorff and Smith,[84] are quite conservative. However, the ASME Code permits improved approaches to fatigue evaluations, e.g., finite–element analyses, fatigue monitoring, improved K_e factors, etc.; these can significantly decrease the conservatisms. Fatigue tests conducted on vessels at Southwest Research Institute for the PVRC[85] show that ≈5–mm–deep cracks can form in carbon and low–alloy steels very close to the fatigue cycles predicted by the ASME Code design curve (Fig. 42). The tests were performed in room–temperature water on vessels with a 0.914–m diameter and 19–mm walls. These results demonstrate clearly that when the actual applied stress or strain is known the Code fatigue design curves do not ensure large margins of conservatism.

The ASME Code requirements of a factor of 2 on stress and 20 on cycles were intended to cover several variables that can influence fatigue life. The actual contribution of these variables is not well documented. Although these factors were intended to be somewhat conservative, they should not be considered safety margins. The variables that can affect fatigue life in air and LWR environments can be broadly classified into three groups:

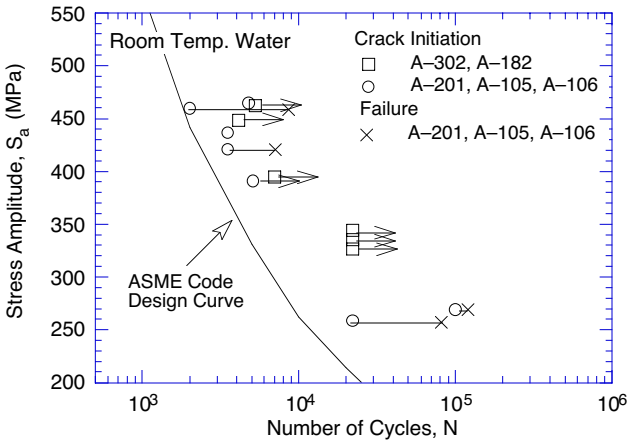

Figure 42.
Fatigue data for carbon and low–alloy steel vessels tested in room–temperature water (Ref. 85)

(a) Material
- (i) Composition
- (ii) Metallurgy: grain size, inclusions, orientation within a forging or plate
- (iii) Processing: cold work, heat treatment
- (iv) Size and geometry
- (v) Surface finish: fabrication surface condition
- (vi) Surface preparation: surface work hardening

(b) Loading
- (i) Strain rate: rise time
- (ii) History: linear damage summation or Miner's rule
- (iii) Mean stress
- (iv) Biaxial effects: constraints

(c) Environment
- (i) Water chemistry: DO, lithium hydroxide, boric acid concentrations
- (ii) Temperature
- (iii) Flow rate

The existing fatigue ε–N database covers an adequate range of material parameters (i–iii), a loading parameter (i), and environment parameters (i and ii); therefore, the variability and uncertainty in fatigue life due to these parameters have been incorporated into the model. The existing data are most likely conservative with respect to the effects of surface preparation because the fatigue ε–N data are obtained for specimens that are free of surface cold work. Fabrication procedures for fatigue test specimens generally follow ASTM guidelines, which require that the final polishing of the specimens avoids surface work hardening. The statistical model does not include the effects of flow rate on the fatigue life; the model is based on tests conducted at relatively low flow rates. Recent results indicate that under the conditions typical of operating BWRs, environmental effects on the fatigue life of carbon and low–alloy steels are a factor of ≈2 lower at high flow rates (7 m/s) than those at very low flow rates (0.3 m/s or lower). The effects of flow rate on the fatigue life of austenitic SSs have not been investigated. Because the mechanism of fatigue crack initiation in LWR environments appears to be different for austenitic SSs than for carbon and low–alloy steels, the effect of flow rate may be different for SSs. Biaxial effects are covered by design procedures and need not be considered in the fatigue design curves.

The contributions of four groups of variables, namely, material variability and data scatter, specimen size and geometry, surface finish, and loading history (Miner's rule), must be considered in developing the fatigue design curves that are applicable to components. Data available in the literature have been reviewed in NUREG/CR–6717 to determine the effect of these variables on the fatigue life of components.[8]

Material Variability and Data Scatter: The results of a rigorous statistical analysis of the fatigue ε–N data[8] indicate that relative to the mean curve, the curve that represents a 5% probability of fatigue cracking is a factor of ≈2.5 lower in life and a factor of 1.4–1.7 lower in strain. Therefore, factors of 2.5 on life and 1.7 on strain provide a 90% confidence for the variations in fatigue life associated with compositional and metallurgical differences, material processing, and experimental scatter.

Size and Geometry: The effect of specimen size on the fatigue life has been investigated for smooth specimens of various diameters in the range of 2–60 mm.[86–89] No intrinsic size effect has been observed for smooth specimens tested in axial loading or plain bending. However, a size effect does occur in specimens tested in rotating bending; the fatigue endurance limit decreases by ≈25% by increasing the specimen size from 2 to 16 mm but does not decrease further with larger sizes.[89] In addition, some effect of size and geometry has been observed on small–scale–vessel tests conducted at the Ecole Polytechnique in conjunction with the large–size–pressure–vessel tests carried out by the Southwest Research Institute.[85] The tests at the Ecole Polytechnique were conducted in room–temperature water on ≈305–mm–inner–diameter, 19–mm–thick shells with nozzles made of machined bar stock. The results indicate that the number of cycles to form a 3–mm–deep crack in a 19–mm–thick shell may be 30–50% lower than those in a small test specimen. Thus, a factor of ≈1.4 on cycles and a factor of ≈1.25 on strain can be used to account for size and geometry.

Surface Finish: Fatigue life is sensitive to surface finish; cracks can initiate at surface irregularities that are normal to the stress axis. The height, spacing, shape, and distribution of surface irregularities are important for crack initiation. The most common measure of roughness is average surface roughness R_a, which is a measure of the height of the irregularities. Investigations of the effects of surface roughness on the low–cycle fatigue of Type 304 SS in air at 593°C indicate that fatigue life decreases as surface roughness increases.[90,91] The effect of roughness on crack initiation $N_i(R)$ is given by

$$N_i(R_q) = 1012\ R_q^{-0.21}, \tag{37}$$

where the RMS value of surface roughness (R_q) is in micrometers. Studies indicate that an R_a of 3 µm (or an R_q of 4 µm) represents the maximum surface roughness for drawing/extrusion, grinding, honing, and polishing processes and a mean value for the roughness range for milling or turning processes.[92] For SSs, an R_q of 4 µm in Eq. 37 (R_q of a smooth polished specimen is ≈0.0075 µm) would decrease fatigue life by a factor of ≈3.[90] A factor of 3 decrease in life corresponds to a factor of ≈1.3 on strain.* A study of the effect of surface finish on fatigue life of carbon steel in room–temperature air showed a factor of 2 decrease in life when R_a is increased from 0.3 to 5.3 µm.[93] These results are consistent with Eq. 37. Fatigue test data on rectangular bars of austenitic SSs under compressive load with differing surface finish indicate

---

* The factor applied on strain (K_S) is obtained from the factor applied on cycles (K_N) by using the relationship $K_S = (K_N)^{0.2326}$.

a factor of ≈1.6 decrease in stress (or strain) in the high–cycle fatigue regime (i.e., $>10^5$ cycles).[75] In the same study, the effect of grinding on the fatigue limit of welds was very large, e.g., a factor of 3–4 decrease in fatigue limit.

In an earlier report,[3] it was argued that, because austenitic SSs develop a corrosion scale in high–temperature water, the effect of surface finish may not be significant in LWR environments. Therefore, the subfactor for surface finish effects may be as low as 1.5 or may be eliminated completely. To check the validity of this argument, fatigue tests were conducted on Type 304 specimens that had been scarred under controlled conditions, in a lathe, with 50–grit sandpaper to produce circumferential scratches. The measured surface roughness of the specimen is shown in Fig. 43. The average surface roughness (R_a) was 1.2 µm, and the RMS value of surface roughness (R_q) was 1.6 µm (61.5 micro–inch). The fatigue tests were conducted in air and low–DO water (i.e., <5 ppb DO and ≈23 cc/kg dissolved hydrogen) at 289°C, 0.25% strain amplitude, fully reversed saw–tooth wave form with 0.004 and 0.4%/s strain rates, respectively, in tension and compression. The results of these tests and data obtained earlier on Type 304 SS are shown in Fig. 44. In both air and low–DO water environments, the fatigue life of scarred specimens is a factor of ≈3 lower than that of smooth specimens. Thus, a factor of 2–3 on cycles is needed to account for the effects of surface finish in both air and water environments.

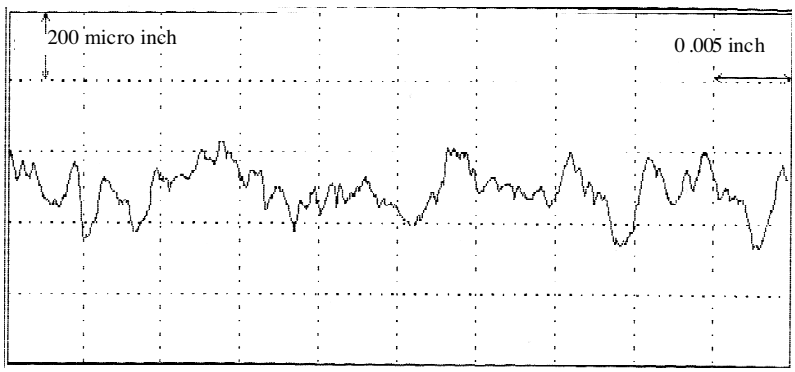

Figure 43. Surface roughness profile of the fatigue test specimen

A PVRC working group has been compiling and evaluating fatigue ε–N data related to the effects of LWR coolant environments on the fatigue lives of pressure boundary materials.[16] One of the tasks in the PVRC activity consisted of defining a set of values for material, loading, and environmental variables that lead to moderate or acceptable effects of environment on fatigue life. A factor of 4 on the ASME mean life was chosen as a working definition of "moderate" or "acceptable" effects of environment, i.e., up to a factor of 4 decrease in fatigue life due to the environment is considered acceptable and does not require further fatigue evaluation. The basis for this criterion was the discussion presented by Cooper[94] regarding the initial scope and intent of the Section III fatigue design procedures. He states that the factor of 20 on life is the product of the following three subfactors:

Scatter of data (minimum to mean)	2.0
Size effect	2.5
Surface finish, atmosphere, etc.	4.0

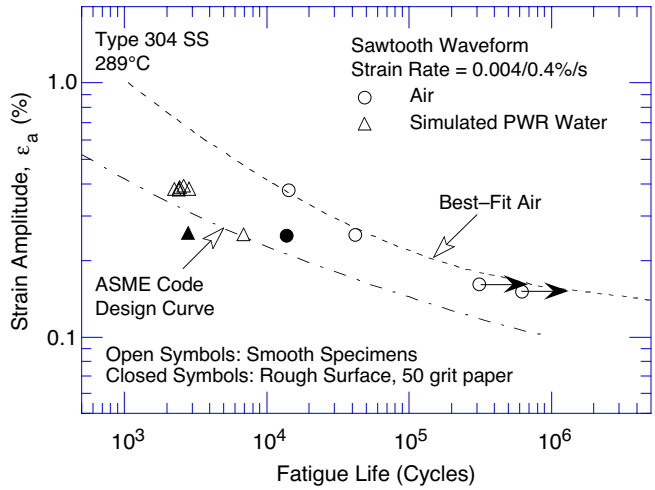

Figure 44.
Effect of surface roughness on fatigue life of Type 304 stainless steel in air and low–DO water at 289°C

The criterion for "acceptable" effects of the environment assumes that the current Code design curve includes a factor of 4 (i.e., the third subfactor listed above) to account for the effects of environment. However, Cooper[94] further states that the term "atmosphere" was intended to reflect the effects of an industrial atmosphere in comparison with an air–conditioned laboratory, not the effects of a specific coolant environment. Furthermore, the third subfactor includes the effect of surface finish on fatigue life. Figure 44 shows that surface finish can decrease the fatigue life of austenitic SSs by a factor of 3 in both air and water environments.

Loading History: The effects of load history during variable amplitude fatigue of smooth specimens are well known.[95–98] The presence of a few cycles at high strain amplitude in a load history causes the fatigue life at smaller strain amplitude to be significantly lower than that at constant amplitude loading. As discussed in Section 3.1, growth of mechanically small cracks can occur at strain levels below the fatigue limit of the material. Studies on fatigue damage in Type 304 SS under complex loading histories[99] indicate that the loading sequence of decreasing strain levels (i.e., high strain level followed by low strain level) is more damaging than that of increasing strain levels. The fatigue life of the steel decreased by a factor of 2–4 under a decreasing–strain sequence. In another study, the fatigue limit of medium carbon steels was lowered even after low–stress high–cycle fatigue; the higher the stress, the greater the decrease in fatigue threshold.[100] In general, the mean fatigue ε–N curves are lowered to account for damaging cycles that occur below the constant–amplitude fatigue limit of the material.[101,102] A factor of 1.5–2.5 on cycles and 1.3–1.6 on strain may be used to incorporate the effects of load histories on fatigue life.

The subfactors that may be used to account for the effects of various material, loading, and environmental variables on fatigue life are summarized in Table 3. A factor of at least 10 on cycles is needed to account for the differences and uncertainties in relating the fatigue lives of laboratory test specimens to those of actual reactor components. The factors on strain primarily account for the variation in the fatigue limit of the material caused by material variability, component size and surface finish, and load history. Because these parameters influence the growth of short cracks (<100 μm), the adjustments on strain to account for the effects of material variability, component size, surface finish, and loading history are typically not cumulative but rather are controlled by the parameter that has the largest effect on life.

Thus, a factor of at least 1.6 on strain is needed to account for the differences and uncertainties in relating the fatigue lives of laboratory test specimens to those of actual reactor components. These results suggest that the current ASME Code requirements of a factor of 2 on stress and 20 on cycle to account for differences and uncertainties in fatigue life that are associated with material and loading conditions are quite reasonable.

Table 3. Factors on cycles and strain to be applied to mean ε–N curve

Parameter	Factor on Life	Factor on Strain
Material variability & experimental scatter	2.5	1.4–1.7
Size effect	1.4	1.25
Surface finish	2.0–3.0	1.6
Loading history	1.5–2.5	1.3–1.6
Total adjustment	10.0–26.0	1.6–1.7

8 Summary

The existing fatigue ε–N data for wrought and cast austenitic SSs in air and LWR environments have been evaluated to establish the effects of material and loading variables, such as steel type, strain amplitude, strain rate, temperature, and DO level in water, on the fatigue lives of these steels.

In air, the fatigue lives of Types 304 and 316 SS are comparable and those of Type 316NG are superior at high strain amplitudes. The fatigue life of austenitic SSs in air is independent of temperature in the range from room temperature to 427°C. Also, variation in strain rate in the range of 0.4–0.008%/s has no effect on the fatigue lives of SSs at temperatures up to 400°C. The fatigue ε–N behavior of cast SSs is similar to that of wrought austenitic SSs.

The fatigue lives of cast and wrought austenitic SSs are decreased in LWR environments; the decrease depends on strain rate, DO level in water, and temperature. A minimum threshold strain is required for environmentally assisted decrease in the fatigue life of SSs, and this strain appears to be independent of material type (weld or base metal) and temperature in the range of 250–325°C. Environmental effects on fatigue life occur primarily during the tensile–loading cycle and at strain levels greater than the threshold value. Strain rate and temperature have a strong effect on fatigue life in LWR environments. Fatigue life decreases logarithmically with decreasing strain rate below 0.4%/s; the effect saturates at 0.0004%/s. Similarly, the fatigue ε–N data suggest a threshold temperature of 150°C; in the range of 150–325°C, logarithm of life decreases linearly with temperature.

The fatigue lives of wrought and cast austenitic SSs are decreased significantly in low–DO (i.e., <0.01 ppm DO) water. However, environmental effects on the fatigue lives of these steels in high–DO water are not well known. In high–DO water the magnitude of environmental effects may be influenced by the composition or heat treatment of the steel. The existing fatigue ε–N data indicate that the fatigue lives of cast SSs are approximately the same in low– and high–DO water and are comparable to those observed for wrought SSs in low–DO water. The fatigue lives of wrought SSs in high–DO water are comparable for some steels and higher for other steels than the lives in low–DO water. Also, environmental effects on fatigue life are greater for sensitized than solution–annealed steels in high–DO water, whereas in low–DO water, a sensitization anneal has no effect on fatigue life.

The mechanism of fatigue crack initiation in austenitic SSs in LWR environments has been examined. Fatigue crack initiation has been divided into two stages: an initiation stage that involves the growth of MSCs (i.e., cracks smaller than ≈200 μm), and a propagation stage that involves the growth of mechanically small cracks. Crack lengths as a function of fatigue cycles have been determined in air and LWR environments. The results indicate that decreases in the fatigue lives of these steels are caused primarily by the effects of the environment on the growth of MSCs and, to a less extent, on enhanced growth rates of mechanically small cracks.

To characterize fracture morphology, fatigue test specimens were examined in detail by metallography. The crack morphology of the specimen surface is different in low–DO water than in air or high–DO water; cracks are always straight and normal to the stress axis in low–DO water, whereas, in air or high–DO water, they follow certain crystallographic features. However, the morphology of crack growth into the material is similar in air and water

environments; during the propagation stage, well–defined fatigue striations are observed in both air and water environments. The differing crack morphology of the surface of the specimens tested in low–DO water indicates that the mechanism of crack initiation is different in the low–DO PWR environment than in air or high–DO water. The presence of well–defined striations indicates that mechanical factors are important; environmentally assisted reduction in the fatigue life of austenitic SSs is most likely caused by mechanisms such as hydrogen–enhanced crack growth.

Austenitic SSs exposed to LWR environments develop a dark, fine–grained, tightly–adherent, chromium–rich inner layer that forms by solid–state growth, and a crystalline nickel–rich outer layer composed of large– and intermediate–size particles that form by precipitation or deposition from the solution. The characteristics of the surface oxide films might influence the mechanism and kinetics of corrosion processes and thereby influence fatigue crack initiation. Exploratory fatigue tests were conducted on austenitic SS specimens that were preexposed to either low– or high–DO water and then tested in air or water environments in an effort to understand the effects of surface micropits or minor differences in the surface oxide on fatigue crack initiation. The results indicate that the presence of a surface oxide film or any difference in the characteristics of the oxide film has no effect on fatigue crack initiation in austenitic SSs in LWR environments.

Statistical models are presented for estimating the fatigue life of austenitic SSs as a function of material, loading, and environmental parameters. Functional form and bounding values of these parameters are based on experimental observations and data trends. The models are recommended for predicted fatigue lives $\leq 10^6$ cycles. The results indicate that the ASME mean curve for SSs is not consistent with the experimental data; the current ASME mean curve is nonconservative.

Two approaches have been proposed for incorporating the effects of LWR environments into ASME Section III fatigue evaluations. Both approaches are based on the best–fit curves to the experimental fatigue ε–N data in LWR environments. In the first approach, environmentally adjusted fatigue design curves are developed by adjusting the best–fit experimental curve for the effect of mean stress and by setting margins of 20 on cycles and 2 on strain to account for the uncertainties in life associated with material and loading conditions. These curves provide allowable cycles for fatigue crack initiation in LWR coolant environments. The second approach considers the effects of reactor coolant environments on fatigue life in terms of an environmental correction factor F_{en}, which is the ratio of fatigue life in air at room temperature to that in water under reactor operating conditions. To incorporate environmental effects into the ASME Code fatigue evaluations, a fatigue usage factor for a specific load set, based on the current Code design curves, is multiplied by the correction factor. Data available in the literature have been reviewed to evaluate the conservatism in the existing ASME Code fatigue design curves. The results suggest that the current ASME Code requirements of a factor of 2 on stress and 20 on life are quite reasonable.

References

1. B. F. Langer, "Design of Pressure Vessels for Low–Cycle Fatigue," ASME J. Basic Eng. 84, 389–402 (1962).

2. C. E. Jaske and W. J. O'Donnell, "Fatigue Design Criteria for Pressure Vessel Alloys," Trans. ASME J. Pressure Vessel Technol. 99, 584–592 (1977).

3. O. K. Chopra, "Effects of LWR Coolant Environments on Fatigue Design Curves of Austenitic Stainless Steels," NUREG/CR–5704, ANL–98/31 (1999).

4. Criteria of Section III of the ASME Boiler and Pressure Vessel Code for Nuclear Vessels, The American Society of Mechanical Engineers, New York (1964).

5. O. K. Chopra and W. J. Shack, "Effects of LWR Coolant Environments on Fatigue Design Curves of Carbon and Low–Alloy Steels," NUREG/CR–6583, ANL–97/18 (March 1998).

6. O. K. Chopra and W. J. Shack, "Environmental Effects on Fatigue Crack Initiation in Piping and Pressure Vessel Steels," NUREG/CR–6717, ANL–00/27 (May 2001).

7. S. Majumdar, O. K. Chopra, and W. J. Shack, "Interim Fatigue Design Curves for Carbon, Low–Alloy, and Austenitic Stainless Steels in LWR Environments," NUREG/CR–5999, ANL–93/3 (1993).

8. J. Keisler, O. K. Chopra, and W. J. Shack, "Fatigue Strain–Life Behavior of Carbon and Low–Alloy Steels, Austenitic Stainless Steels, and Alloy 600 in LWR Environments," NUREG/CR–6335, ANL–95/15 (1995).

9. J. Keisler, O. K. Chopra, and W. J. Shack, "Fatigue Strain–Life Behavior of Carbon and Low–Alloy Steels, Austenitic Stainless Steels, and Alloy 600 in LWR Environments," Nucl. Eng. Des. 167, 129–154 (1996).

10. M. Higuchi and K. Iida, "Fatigue Strength Correction Factors for Carbon and Low–Alloy Steels in Oxygen–Containing High–Temperature Water," Nucl. Eng. Des. 129, 293–306 (1991).

11. H. S. Mehta and S. R. Gosselin, "An Environmental Factor Approach to Account for Reactor Water Effects in Light Water Reactor Pressure Vessel and Piping Fatigue Evaluations," in Fatigue and Fracture Volume 1, PVP Vol. 323, H. S. Mehta, ed., American Society of Mechanical Engineers, New York, pp. 171–185 (1996).

12. H. S. Mehta and S. R. Gosselin, "Environmental Factor Approach to Account for Water Effects in Pressure Vessel and Piping Fatigue Evaluations," Nucl. Eng. Des. 181, 175–197 (1998).

13. H. S. Mehta, "An Update on the EPRI/GE Environmental Fatigue Evaluation Methodology and its Applications," in Probabilistic and Environmental Aspects of Fracture and Fatigues, PVP Vol. 386, S. Rahman, ed., American Society of Mechanical Engineers, New York, pp. 183–193 (1999).

14. K. Iida, T. Bannai, M. Higuchi, K. Tsutsumi, and K. Sakaguchi, "Comparison of Japanese MITI Guideline and Other Methods for Evaluation of Environmental Fatigue Life Reduction," in Pressure Vessel and Piping Codes and Standards, PVP Vol. 419, M. D. Rana, ed., American Society of Mechanical Engineers, New York, pp. 73–81 (2001).

15. A. G. Ware, D. K. Morton, and M. E. Nitzel, "Application of NUREG/CR–5999 Interim Design Curves to Selected Nuclear Power Plant Components," NUREG/CR–6260, INEL–95/0045 (March 1995).

16. W. A. Van Der Sluys and S. Yukawa, "Status of PVRC Evaluation of LWR Coolant Environmental Effects on the S–N Fatigue Properties of Pressure Boundary Materials," in Fatigue and Crack Growth: Environmental Effects, Modeling Studies, and Design Considerations, PVP Vol. 306, S. Yukawa, ed., American Society of Mechanical Engineers, New York, pp. 47–58 (1995).

17. J. B. Conway, R. H. Stentz, and J. T. Berling, "Fatigue, Tensile, and Relaxation Behavior of Stainless Steels," TID–26135, U.S. Atomic Energy Commission, Washington, DC (1975).

18. D. L. Keller, "Progress on LMFBR Cladding, Structural, and Component Materials Studies During July, 1971 through June, 1972, Final Report," Task 32, Battelle–Columbus Laboratories, BMI–1928 (1977).

19. D. A. Hale, S. A. Wilson, E. Kiss, and A. J. Gianuzzi, "Low Cycle Fatigue Evaluation of Primary Piping Materials in a BWR Environment," GEAP–20244, U.S. Nuclear Regulatory Commission (Sept. 1977).

20. M. Fujiwara, T. Endo, and H. Kanasaki, "Strain Rate Effects on the Low–Cycle Fatigue Strength of 304 Stainless Steel in High–Temperature Water Environment; Fatigue Life: Analysis and Prediction," in Proc. Intl. Conf. and Exposition on Fatigue, Corrosion Cracking, Fracture Mechanics, and Failure Analysis, ASM, Metals Park, OH, pp. 309–313 (1986).

21. H. Mimaki, H. Kanasaki, I. Suzuki, M. Koyama, M. Akiyama, T. Okubo, and Y. Mishima, "Material Aging Research Program for PWR Plants," in Aging Management Through Maintenance Management, PVP Vol. 332, I. T. Kisisel, ed., American Society of Mechanical Engineers, New York, pp. 97–105 (1996).

22. H. Kanasaki, R. Umehara, H. Mizuta, and T. Suyama, "Fatigue Lives of Stainless Steels in PWR Primary Water," Trans. 14th Intl. Conf. on Structural Mechanics in Reactor Technology (SMiRT 14), Lyon, France, pp. 473–483 (1997).

23. H. Kanasaki, R. Umehara, H. Mizuta, and T. Suyama, "Effects of Strain Rate and Temperature Change on the Fatigue Life of Stainless Steel in PWR Primary Water," Trans. 14th Intl. Conf. on Structural Mechanics in Reactor Technology (SMiRT 14), Lyon, France, pp. 485–493 (1997).

24. K. Tsutsumi, H. Kanasaki, T. Umakoshi, T. Nakamura, S. Urata, H. Mizuta, and S. Nomoto, “Fatigue Life Reduction in PWR Water Environment for Stainless Steels,” in Assessment Methodologies for Preventing Failure: Service Experience and Environmental Considerations, PVP Vol. 410-2, R. Mohan, ed., American Society of Mechanical Engineers, New York, pp. 23–34 (2000).

25. K. Tsutsumi, T. Dodo, H. Kanasaki, S. Nomoto, Y. Minami, and T. Nakamura, “Fatigue Behavior of Stainless Steel under Conditions of Changing Strain Rate in PWR Primary Water,” in Pressure Vessel and Piping Codes and Standards, PVP Vol. 419, M. D. Rana, ed., American Society of Mechanical Engineers, New York, pp. 135–141 (2001).

26. M. Higuchi and K. Iida, “Reduction in Low–Cycle Fatigue Life of Austenitic Stainless Steels in High–Temperature Water,” in Pressure Vessel and Piping Codes and Standards, PVP Vol. 353, D. P. Jones, B. R. Newton, W. J. O'Donnell, R. Vecchio, G. A. Antaki, D. Bhavani, N. G. Cofie, and G. L. Hollinger, eds., American Society of Mechanical Engineers, New York, pp. 79–86 (1997).

27. M. Higuchi, K. Iida, and K. Sakaguchi, “Effects of Strain Rate Fluctuation and Strain Holding on Fatigue Life Reduction for LWR Structural Steels in Simulated PWR Water,” in Pressure Vessel and Piping Codes and Standards, PVP Vol. 419, M. D. Rana, ed., American Society of Mechanical Engineers, New York, pp. 143–152 (2001).

28. M. Hayashi, “Thermal Fatigue Strength of Type 304 Stainless Steel in Simulated BWR Environment,” Nucl. Eng. Des. 184, 135–144 (1998).

29. M. Hayashi, K. Enomoto, T. Saito, and T. Miyagawa, “Development of Thermal Fatigue Testing with BWR Water Environment and Thermal Fatigue Strength of Austenitic Stainless Steels,” Nucl. Eng. Des. 184, 113–122 (1998).

30. O. K. Chopra and D. J. Gavenda, “Effects of LWR Coolant Environments on Fatigue Lives of Austenitic Stainless Steels,” in Pressure Vessel and Piping Codes and Standards, PVP Vol. 353, D. P. Jones, B. R. Newton, W. J. O'Donnell, R. Vecchio, G. A. Antaki, D. Bhavani, N. G. Cofie, and G. L. Hollinger, eds., American Society of Mechanical Engineers, New York, pp. 87–97 (1997).

31. O. K. Chopra and D. J. Gavenda, “Effects of LWR Coolant Environments on Fatigue Lives of Austenitic Stainless Steels,” J. Pressure Vessel Technol. 120, 116–121 (1998).

32. O. K. Chopra and J. L. Smith, “Estimation of Fatigue Strain–Life Curves for Austenitic Stainless Steels in Light Water Reactor Environments,” in Fatigue, Environmental Factors, and New Materials, PVP Vol. 374, H. S. Mehta, R. W. Swindeman, J. A. Todd, S. Yukawa, M. Zako, W. H. Bamford, M. Higuchi, E. Jones, H. Nickel, and S. Rahman, eds., American Society of Mechanical Engineers, New York, pp. 249–259 (1998).

33. O. K. Chopra and J. Muscara, “Effects of Light Water Reactor Coolant Environments on Fatigue Crack Initiation in Piping and Pressure Vessel Steels,” in Proc. 8th Intl. Conf. on Nuclear Engineering, 2.08 LWR Materials Issue, Paper 8300, American Society of Mechanical Engineers, New York (2000).

34. C. Amzallag, P. Rabbe, G. Gallet, and H. –P. Lieurade, “Influence des Conditions de Sollicitation Sur le Comportement en Fatigue Oligocyclique D'aciers Inoxydables Austénitiques,” Memoires Scientifiques Revue Metallurgie Mars, pp. 161–173 (1978).

35. A. Hirano, M. Yamamoto, K. Sakaguchi, K. Iida, and T. Shoji, “Effects of Water Flow Rate on Fatigue Life of Carbon Steel in High–Temperature Pure Water Environment,” in Assessment Methodologies for Predicting Failure: Service Experience and Environmental Considerations, PVP Vol. 410–2, R. Mohan, ed., American Society of Mechanical Engineers, New York, pp. 13–18 (2000).

36. E. Lenz, N. Wieling, and H. Muenster, “Influence of Variation of Flow Rates and Temperature on the Cyclic Crack Growth Rate under BWR Conditions,” in Environmental Degradation of Materials in Nuclear Power Systems – Water Reactors, The Metallurgical Society, Warrendale, PA (1988).

37. G. Slama, P. Petrequin, and T. Mager, “Effect of Aging on Mechanical Properties of Austenitic Stainless Steel Castings and Welds,” in Assuring Structural Integrity of Steel Reactor Pressure Boundary Components, SMiRT Post Conference Seminar 6, Monterey, CA, 1983.

38. O. K. Chopra, “Estimation of Fracture Toughness of Cast Stainless Steels During Thermal Aging in LWR Systems,” NUREG/CR–4513, ANL–93/22 (August 1994).

39. O. K. Chopra, “Effect of Thermal Aging on Mechanical Properties of Cast Stainless Steels,” in Proc. of the 2nd Int. Conf. on Heat–Resistant Materials, K. Natesan, P. Ganesan, and G. Lai, eds., ASM International, Materials Park, OH, pp. 479–485 (1995).

40. K. J Miller, “Initiation and Growth Rates of Short Fatigue Cracks,” Fundamentals of Deformation and Fracture, Eshelby Memorial Symposium, Cambridge University Press, Cambridge, U.K., pp. 477–500 (1985).

41. K. Tokaji, T. Ogawa, and S. Osaka, “The Growth of Microstructurally Small Fatigue Cracks in a Ferrite–Pearlite Steel,” Fatigue Fract. Eng. Mater. Struct. 11, 311–342 (1988).

42. D. J. Gavenda, P. R. Luebbers, and O. K. Chopra, “Crack Initiation and Crack Growth Behavior of Carbon and Low–Alloy Steels,” Fatigue and Fracture 1, Vol. 350, S. Rahman, K. K. Yoon, S. Bhandari, R. Warke, and J. M. Bloom, eds., American Society of Mechanical Engineers, New York, pp. 243–255 (1997).

43. K. Obrtlik, J. Polák, M. Hájek, and A. Vasek, “Short Fatigue Crack Behaviour in 316L Stainless Steel,” Intl. J. Fatigue 19, 471–475 (1997).

44. S. G. Sundara Raman, D. Argence, and A. Pineau, “High Temperature Short Fatigue Crack Behaviour in a Stainless Steel,” Fatigue Fract. Eng. Mater. Struct. 20, 1015–1031 (1997).

45. K. J. Miller, “Damage in Fatigue: A New Outlook,” in International Pressure Vessels and Piping Codes and Standards: Volume 1 – Current Applications, PVP Vol. 313–1, K. R. Rao and Y. Asada, eds., American Society of Mechanical Engineers, New York, pp. 191–192 (1995).

46. F. P. Ford, “Overview of Collaborative Research into the Mechanisms of Environmentally Controlled Cracking in the Low Alloy Pressure Vessel Steel/Water System,” Proc. 2nd Int. Atomic Energy Agency Specialists' Meeting on Subcritical Crack Growth, NUREG/CP–0067, MEA–2090, Vol. 2, pp. 3–71 (1986).

47. H. Hänninen, K. Törrönen, and W. H. Cullen, “Comparison of Proposed Cyclic Crack Growth Mechanisms of Low Alloy Steels in LWR Environments,” Proc. 2nd Int. Atomic Energy Agency Specialists' Meeting on Subcritical Crack Growth, NUREG/CP–0067, MEA–2090, Vol. 2, pp. 73–97 (1986).

48. J. L. Smith, and O. K. Chopra, “Crack Initiation in Smooth Fatigue Specimens of Austenitic Stainless Steel in Light Water Reactor Environments,” in Operations, Applications, and Components – 1999, PVP Vol. 395, I. T. Kisisel, ed., American Society of Mechanical Engineers, New York, pp. 235–242 (1999).

49. C. M. Suh, R. Yuuki, and H. Kitagawa, “Fatigue Microcracks in a Low Carbon Steel,” Fatigue Fract. Eng. Mater. Struct. 8, 193-203 (1985).

50. W. J. Shack and T. F. Kassner, “Review of Environmental Effects on Fatigue Crack Growth of Austenitic Stainless Steels,” NUREG/CR–6176, ANL–94/1 (May 1994).

51. O. K. Chopra, W. K. Soppet, and W. J. Shack, “Effects of Alloy Chemistry, Cold Work, and Water Chemistry on Corrosion Fatigue and Stress Corrosion Cracking of Nickel Alloys and Welds,” NUREG/CR–6721, ANL–01/07 (April 2001).

52. Y. J. Kim, “Characterization of the Oxide Film Formed on Type 316 Stainless Steel in 288°C Water in Cyclic Normal and Hydrogen Water Chemistries,” Corrosion 51 (11), 849–860 (1995).

53. Y. J. Kim, “Analysis of Oxide Film Formed on Type 304 Stainless Steel in 288°C Water Containing Oxygen, Hydrogen, and Hydrogen Peroxide,” Corrosion 55 (1), 81–88 (1999).

54. R. L. Tapping, R. D. Davidson, E. McAlpine, and D. H. Lister, “The Composition and Morphology of Oxide Films Formed on Type 304 Stainless Steel in Lithiated High–Temperature Water,” Corrosion Sci. 26 (8), 563–576 (1986).

55. D. H. Lister, R. D. Davidson, and E. McAlpine, “The Mechanism and Kinetics of Corrosion Product Release from Stainless Steel in Lithiated High–Temperature Water,” Corrosion Sci. 27 (2), 113–140 (1987).

56. M. Da Cunha Belo, M. Walls, N. E. Hakiki, J. Corset, E. Picquenard, G. Sagon, and D. Neol, “Composition, Structure and Properties of the Oxide Films Formed on the Stainless Steel 316L in a Primary Type PWR Environment,” Corrosion Sci. 40 (2/3), 447–463 (1998).

57. B. Stellwag, “The Mechanism of Oxide Film Formation on Austenitic Stainless Steels in High–Temperature Water,” Corrosion Sci. 40 (2/3), 337–370 (1998).

58. T. Nakayama and Y. Oshida, “Identification of the Initial Oxide Films on 18–8 Stainless Steel in High–Temperature Water,” Corrosion NACE 24 (10), 336–337 (1968).

59. K. Kussmaul, R. Rintamaa, J. Jansky, M. Kemppainen, and K. Törrönen, "On the Mechanism of Environmental Cracking Introduced by Cyclic Thermal Loading," in IAEA Specialists Meeting Corrosion and Stress Corrosion of Steel Pressure Boundary Components and Steam Turbines, VTT Symp. 43, Espoo, Finland, pp. 195–243 (1983).

60. K. Iida, "A Review of Fatigue Failures in LWR Plants in Japan," Nucl. Eng. Des. 138, 297–312 (1992).

61. NRC IE Bulletin No. 79–13, "Cracking in Feedwater System Piping," U.S. Nuclear Regulatory Commission, Washington, DC (June 25, 1979).

62. NRC Information Notice 93–20, "Thermal Fatigue Cracking of Feedwater Piping to Steam Generators," U.S. Nuclear Regulatory Commission, Washington, DC (March 24, 1993).

63. K. Kussmaul, D. Blind, and J. Jansky, "Formation and Growth of Cracking in Feed Water Pipes and RPV Nozzles," Nucl. Eng. Des. 81, 105–119 (1984).

64. H. Watanabe, "Boiling Water Reactor Feedwater Nozzle/Sparger, Final Report," NEDO–21821–A, General Electric Co., San Jose, CA (1980).

65. B. M. Gordon, D. E. Delwiche, and G. M. Gordon, "Service Experience of BWR Pressure Vessels," in Performance and Evaluation of Light Water Reactor Pressure Vessels, PVP Vol.–119, American Society of Mechanical Engineers, New York, pp. 9–17 (1987).

66. E. Lenz, B. Stellwag, and N. Wieling, "The Influence of Strain–Induced Corrosion Cracking on the Crack Initiation in Low–Alloy Steels in HT–Water – A Relation Between Monotonic and Cyclic Crack Initiation Behavior," in IAEA Specialists Meeting Corrosion and Stress Corrosion of Steel Pressure Boundary Components and Steam Turbines, VTT Symp. 43, Espoo, Finland, pp. 243–267 (1983).

67. J. Hickling and D. Blind, "Strain–Induced Corrosion Cracking of Low–Alloy Steels in LWR Systems – Case Histories and Identification of Conditions Leading to Susceptibility," Nucl. Eng. Des. 91, 305–330 (1986).

68. R. B. Dooley, and R. S. Pathania, "Corrosion Fatigue of Water Touched Pressure Retaining Components in Power Plants," EPRI TR–106696, Electric Power Research Institute, Palo Alto, CA (1997).

69. V. N. Shah, M. B. Sattison, C. L. Atwood, A. G. Ware, G. M. Grant, and R. S. Hartley, "Assessment of Pressurized Water Reactor Primary System Leaks," NUREG/CR–6582, INEEL/EXT–97–01068 (Dec. 1998).

70. P. Hirschberg, A. F. Deardorff, and J. Carey, "Operating Experience Regarding Thermal Fatigue of Unisolable Piping Connected to PWR Reactor Coolant Systems," Int. Conf. on Fatigue of Reactor Components, Napa, CA, July 31–August 2, 2000.

71. NRC Information Notice 88–01, "Safety Injection Pipe Failure," U.S. Nuclear Regulatory Commission, Washington, DC (Jan. 27, 1988).

72. NRC Bulletin No. 88–08, “Thermal Stresses in Piping Connected to Reactor Coolant Systems,” U.S. Nuclear Regulatory Commission, Washington, DC (June 22; Suppl. 1, June 24; Suppl. 2, Aug. 4, 1988; Suppl. 3, April 1989).

73. T. Sakai, “Leakage from CVCS Pipe of Regenerative Heat Exchanger Induced by High–Cycle Thermal Fatigue at Tsuruga Nuclear Power Station Unit 2,” Int. Conf. on Fatigue of Reactor Components, Napa, CA, July 31–August 2, 2000.

74. T. Hoshino, T. Ueno, T. Aoki, and Y. Kutomi, Leakage from CVCS Pipe of Regenerative Heat Exchanger Induced by High–Cycle Thermal Fatigue at Tsuruga Nuclear Power Station Unit 2, in Proc. 8th Intl. Conf. on Nuclear Engineering, 1.01 Operational Experience/Root Cause Failure Analysis, Paper 8615, American Society of Mechanical Engineers, New York (2000).

75. C. Faidy, T. Le Courtois, E. de Fraguier, J–A Leduff, A. Lefrancois, and J. Dechelotte, Thermal Fatigue in French RHR System, Int. Conf. on Fatigue of Reactor Components, Napa, CA, July 31–August 2, 2000.

76. NRC Bulletin No. 88–11, Pressurizer Surge Line Thermal Stratification, U.S. Nuclear Regulatory Commission, Washington, DC (Dec. 20, 1988).

77. J. Daret, J. M. Boursier, and J. M. Olive, Cracking of Stainless Steel Channel Heads in a Primary Water Experimental Loop, in Proc. Tenth Intl. Symp. on Environmental Degradation of Materials in Nuclear Power Systems – Water Reactors, NACE International, Houston, TX (2001).

78. J.–M. Stephan and J. C. Masson, Auxiliary Feedwater Line Stratification and Coufast Simulation, Int. Conf. on Fatigue of Reactor Components, Napa, CA, July 31–August 2, 2000.

79. E. Lenz, A. Liebert, and N. Wieling, Thermal Stratification Tests to Confirm the Applicability of Laboratory Data on Strain–Induced Corrosion Cracking to Component Behavior, in 3rd IAEA Specialists Meeting on Sub–Critical Crack Growth, Moscow, pp. 67–91 (1990).

80. T. R. Leax, Statistical Models of Mean Stress and Water Environment Effects on the Fatigue Behavior of 304 Stainless Steel, in Probabilistic and Environmental Aspects of Fracture and Fatigues, PVP Vol. 386, S. Rahman, ed., American Society of Mechanical Engineers, New York, pp. 229–239 (1999).

81. K. N. Smith, P. Watson, and T. H. Topper, A Stress–Strain Function for the Fatigue of Metals, J. Materials, JMLSA 5 (4), 767–778 (1970).

82. G. L. Wire, T. R. Leax, and J. T. Kandra, Mean Stress and Environmental Effects on Fatigue in Type 304 Stainless Steel, in Probabilistic and Environmental Aspects of Fracture and Fatigues, PVP Vol. 386, S. Rahman, ed., American Society of Mechanical Engineers, New York, pp. 213–228 (1999).

83. M. E. Mayfield, E. C. Rodabaugh, and R. J. Eiber, A Comparison of Fatigue Test Data on Piping with the ASME Code Fatigue Evaluation Procedure, ASME Paper 79–PVP–92, American Society of Mechanical Engineers, New York (1979).

84. A. F. Deardorff and J. K. Smith, Evaluation of Conservatisms and Environmental Effects in ASME Code, Section III, Class 1 Fatigue Analysis, SAND94–0187, prepared by Structural Integrity Associates, San Jose, CA, under contract to Sandia National Laboratories, Albuquerque, NM (1994).

85. L. F. Kooistra, E. A. Lange, and A. G. Pickett, Full–Size Pressure Vessel Testing and Its Application to Design, J. Eng. Power 86, 419–428 (1964).

86. R. E. Peterson, Fatigue Tests of Small Specimens with Particular Reference to Size Effect, Trans. Amer. Soc. Steel Testing 18, 1041–1053 (1930).

87. D. Morkovin and H. F. Moore, Third Progress Report on the Effect of Size of Specimen on Fatigue Strength of Three Types of Steel, Proc. Amer. Soc. Test. Mater. 44, 137–158 (1944).

88. C. E. Philips and R. B. Heywood, The Size Effect in Fatigue of Plain and Notched Steel Specimens Loaded Under Reversed Direct Stress, Proc. Inst. Mech. Eng. 165, 113–124 (1951).

89. C. Massonnet, The Effect of Size, Shape, and Grain Size on the Fatigue Strength of Medium Carbon Steel, Proc. Amer. Soc. Test. Mater. 56, 954–978 (1956).

90. P. S. Maiya and D. E. Busch, Effect of Surface Roughness on Low–Cycle Fatigue Behavior of Type 304 Stainless Steel, Met. Trans. 6A, 1761–1766 (1975).

91. P. S. Maiya, Effect of Surface Roughness and Strain Range on Low–Cycle Fatigue Behavior of Type 304 Stainless Steel, Scripta Metall. 9, 1277–1282 (1975).

92. K. J. Stout, Surface Roughness – Measurement, Interpretation, and Significance of Data, Mater. Eng. 2, 287–295 (1981).

93. K. Iida, A Study of Surface Finish Effect Factor in ASME B&PV Code Section III, in Pressure Vessel Technology, Vol. 2, L. Cengdian and R. W. Nichols, eds., Pergamon Press, New York, pp. 727–734 (1989).

94. W. E. Cooper, The Initial Scope and Intent of the Section III Fatigue Design Procedure, in Welding Research Council, Inc., Technical Information from Workshop on Cyclic Life and Environmental Effects in Nuclear Applications, Clearwater, Florida, January 20–21, 1992.

95. M. A. Pompetzki, T. H. Topper, and D. L. DuQuesnay, The Effect of Compressive Underloads and Tensile Overloads on Fatigue Damage Accumulation in SAE 1045 Steel, Int. J. Fatigue 12 (3), 207–213 (1990).

96. A. Conle and T. H. Topper, Evaluation of Small Cycle Omission Criteria for Shortening of Fatigue Service Histories, Int. J. Fatigue 1, 23–28 (1979).

97. A. Conle and T. H. Topper, Overstrain Effects During Variable Amplitude Service History Testing, Int. J. Fatigue 2, 130–136 (1980).

98. Li Nian and Du Bai–Ping, Effect of Monotonic and Cyclic Prestrain on the Fatigue Threshold in Medium–Carbon Steels, Int. J. Fatigue 14 (1), 41–44 (1992).

99. M. J. Manjoine, Fatigue Damage Models for Annealed Type 304 Stainless Steel under Complex Strain Histories, Trans. 6th Intl. Conf. on Structural Mechanics in Reactor Technology (SMiRT), Vol. L, 8/1, North–Holland Publishing Co., pp. 1–13 (1981).

100. Li Nian and Du Bai–Ping, The Effect of Low–Stress High–Cycle Fatigue on the Microstructure and Fatigue Threshold of a 40Cr Steel, Int. J. Fatigue 17 (1), 43–48 (1995).

101. E. Haibach and D. Schutz, Fatigue Life Evaluation with Particular Attention to Local Strain and Stress Time Histories, Proc. Inst. Mech. Eng. (1974).

102. D. J. Dowdell, H. H. E. Leipholz, and T. H. Topper, The Modified Life Law Applied to SAE–1045 Steel, Int. J. Fract. 31, 29–36 (1986).

NRC FORM 335
(2-89)
NRCM 1102,
3201, 3202

U. S. NUCLEAR REGULATORY COMMISSION

BIBLIOGRAPHIC DATA SHEET

(See instructions on the reverse)

1. REPORT NUMBER
(Assigned by NRC. Add Vol., Supp., Rev., and Addendum Numbers, if any.)

NUREG/CR- 6787
ANL-01/25

2. TITLE AND SUBTITLE

Mechanism and Estimation of Fatigue Crack Initiation in Austenitic Stainless Steels in LWR Environments

3. DATE REPORT PUBLISHED

MONTH	YEAR
August	2002

4. FIN OR GRANT NUMBER
Y6388

5. AUTHOR(S)

O. K. Chopra

6. TYPE OF REPORT
Technical

7. PERIOD COVERED *(Inclusive Dates)*

8. PERFORMING ORGANIZATION – NAME AND ADDRESS *(If NRC, provide Division, Office or Region, U.S. Nuclear Regulatory Commission, and mailing address; if contractor, provide name and mailing address.)*

Argonne National Laboratory
9700 South Cass Avenue
Argonne, IL 60439

9. SPONSORING ORGANIZATION – NAME AND ADDRESS *(If NRC, type "Same as above": if contractor, provide NRC Division, Office or Region, U.S. Nuclear Regulatory Commission, and mailing address.)*

Division of Engineering Technology
Office of Nuclear Regulatory Research
U.S. Nuclear Regulatory Commission
Washington, DC 20555-0001

10. SUPPLEMENTARY NOTES

J. Muscara, NRC Project Manager

11. ABSTRACT (200 words or less)

The ASME Boiler and Pressure Vessel Code provides rules for the construction of nuclear power plant components. Figures I-9.1 through I-9.6 of Appendix I to Section III of the Code specify fatigue design curves for structural materials. However, the effects of light water reactor (LWR) coolant environments are not explicitly addressed by the Code design curves. Existing fatigue strain-vs.-life (ε-N) data illustrate potentially significant effects of LWR coolant environments on the fatigue resistance of pressure vessel and piping steels. This report provides an overview of fatigue crack initiation in austenitic stainless steels in LWR coolant environments. The existing fatigue ε-N data have been evaluated to establish the effects of key material, loading, and environmental parameters (such as steel type, strain range, strain rate, temperature, dissolved-oxygen level in water, and flow rate) on the fatigue lives of these steels. Statistical models are presented for estimating the fatigue ε-N curves for austenitic stainless steels as a function of the material, loading, and environmental parameters. Two methods for incorporating environmental effects into the ASME Code fatigue evaluations are presented. The influence of reactor environments on the mechanism of fatigue crack initiation in these steels is also discussed.

12. KEY WORDS/DESCRIPTORS *(List words or phrases that will assist researchers in locating this report.)*

Fatigue Strain-Life Curves
Fatigue Design Curves
Fatigue Crack Initiation
LWR Environment
Austenitic Stainless Steels
Cast Austenitic Stainless Steels

13. AVAILABILITY STATEMENT
Unlimited

14. SECURITY CLASSIFICATION
(This Page)
Unclassified
(This Report)
Unclassified

15. NUMBER OF PAGES

16. PRICE

NRC FORM 335 (2-89)